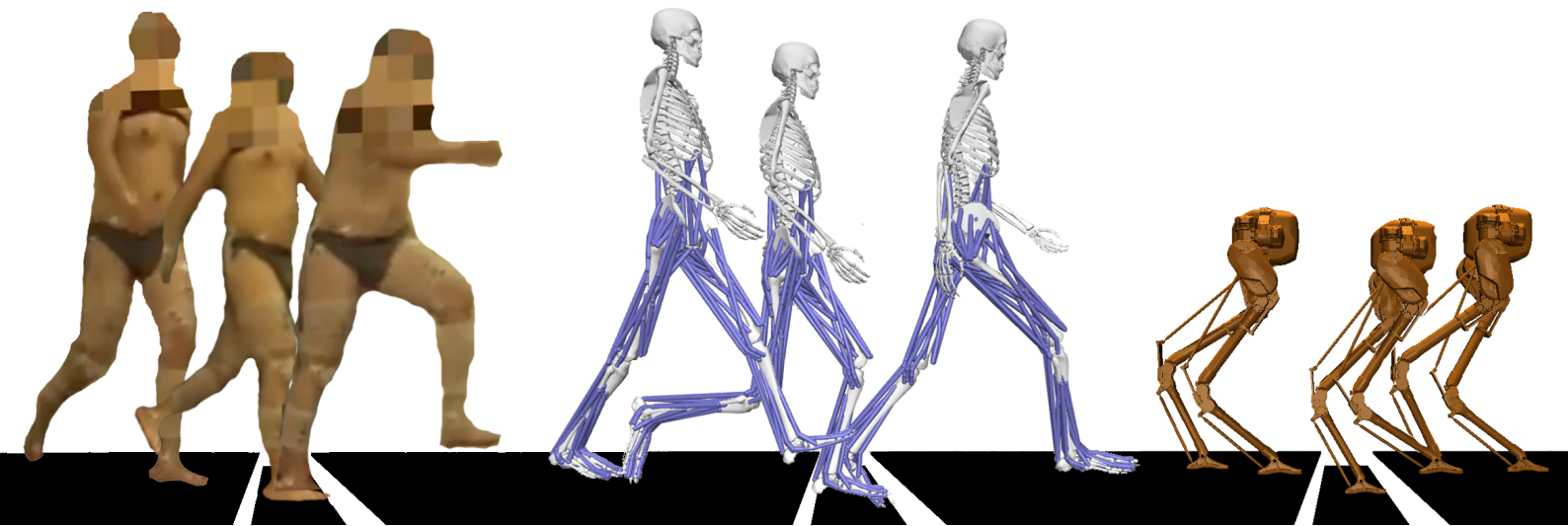


FROM HUMAN WALKING TO BIPEDAL ROBOT LOCOMOTION: REFLEX INSPIRED COMPENSATION ON EXPECTED AND UNEXPECTED DOWNSTEPS



In partial fulfillment of the requirements for the degree of
Master of Science in Mechanical Engineering

by

Joris Petrus Martinus Verhagen

under the supervision of

Dr. Xiaobin Xiong (Caltech)

Dr. Ajay Seth (TU Delft)

Prof. Aaron Ames (Caltech)

April 2022


TU Delft

Caltech

ABSTRACT

Humans and other biological bipedal walkers are extraordinarily agile and robust. This is especially apparent when certain features of the environment are unknown such as unexpected downsteps (for example, suddenly walking off the side-walk or not expecting the last stair when descending). Humans can negotiate these downsteps—both expected and unexpected—with remarkable agility and ease. The contributions from active compensation, passive dynamics, and reflexes that humans employ to overcome these downsteps are however not inherently present in bipedal robots. This motivates us to assess whether externally observed behavior can be used to achieve the same capabilities in bipedal robots. One of the challenges with this proposal is the morphological differences between humans and robots. Taking the bipedal robot Cassie as an example, these differences predominantly constitute to overall- and segment mass, leg morphology, and a lack of an upper body. The observed behavior from the human should subsequently be scaled to represent an appropriate nominal and compensatory behavior of the robot.

This thesis aims to systematically study the translation of this human behavior to bipedal walking robots, regardless of the morphology of the walkers. We start from human experimental data where nominal walking, expected downstep, and unexpected downstep trials were conducted. The human data is analyzed from the perspective of a reduced-order representation of the human. The reduced-order representation encodes the center of mass dynamics and contact forces. An equivalent reduced-order model is used to represent the bipedal robot, which allows for the translation of the nominal walking and downstep behaviors between human and robot. The morphological differences between the human and the robot are therefore resolved by realizing dynamically equivalent behavior which is embedded into the full-order dynamics of a bipedal robot via optimization-based controllers. The results demonstrate traversing expected and unexpected downsteps in simulation on the underactuated 3D walking robot Cassie.

ACKNOWLEDGEMENTS

My thesis has been a fascinating adventure, and multiple people deserve my gratitude. First, I would like to thank my advisor, Assistant Professor Ajay Seth, for his mentorship and support in combining my interests with his expertise. Secondly, I want to thank my daily supervisor, Dr. Xiaobin Xiong. Upon my arrival at Caltech, he guided me in becoming intrinsically familiar with the field of bipedal robotics, and working alongside his vast expertise in the things that fascinate us, has been invaluable. I would also like to sincerely thank Professor Aaron Ames, not only for opening up his lab to me as a visiting student but also for taking the time to give me advice and presenting me with new insights along the way.

I would also like to thank many members of the AMBER lab, specifically Min Dai, Ryan Cosner, and Meagan Tucker. Not only did these people provide me with many insightful discussions, but they have also made me feel right at home at a place on the other side of the world. From TU Darmstadt's Lauflabor Lab, I want to thank Dr. Guoping Zhao for his openness to collaborate and for sharing many of his insights during my entire thesis.

Lastly, I want to thank my family and friends for their support and their encouragement to pursue my dream of bipedal robotics research.

Contents

1	INTRODUCTION	1
1.1	Perspectives On Realizing Robotic Walking	1
1.2	Scope Of The Thesis	2
1.3	Structure	3
2	PRELIMINARIES	4
2.1	Bipedal Walking	4
2.1.1	Human Walking	4
2.1.2	Robotic Walking	5
2.2	Mathematical Models of Bipedal Robots	7
2.2.1	Holonomic Constraints and Ground Contact	7
2.2.2	Impact Mapping	10
2.3	Feedback Control of Nonlinear Systems	11
2.3.1	Feedback Linearization	11
2.3.2	Control Lyapunov Functions	12
2.3.3	Task Space Control	13
3	HUMAN WALKING ON DOWNSTEPS	15
3.1	Data Collection	15
3.2	Kinematics and Kinetics Analysis	16
3.3	Human Data Interpolation	19
4	HUMAN WALKING MODEL REDUCTION	21
4.1	The Actuated Spring-Loaded Inverted Pendulum Model	22
4.2	Reduced Order Model Fitting	23
4.3	Reduced Order Model Walking Realization	24
4.3.1	Vertical CoM Tracking	24
4.3.2	Contact Force Embedding	25
4.3.3	Horizontal stabilization	26
4.3.4	Control Structure	27
4.4	Results	28
5	ROBOT WALKING SYNTHESIS	31
5.1	Output Definitions	31
5.2	Human Inspired Trajectory Synthesis	31
6	3D ROBOTIC WALKING REALIZATION	34
6.1	The Bipedal Robot Cassie	34
6.2	2D Prototyping	35
6.3	Robot Walking Output Construction	37
6.3.1	Force Embedding	37
6.3.2	Swing Foot Trajectory Construction	38
6.4	Contact Force Embedded Task Space Control	38
7	RESULTS	41
7.1	3D Cassie Downstep Navigation	41
7.2	Energy Efficiency	43
8	DISCUSSION	45
8.1	Human Walking	45
8.2	Reduced Order Model Walking	45
8.3	3D Robotic Walking	45
9	CONCLUSION	47
9.1	Future Work	47

9.1.1	Vertical Center Of Mass Dynamics	47
9.1.2	Systems With Non-Trivial Compliance	48
9.1.3	3D Fully Actuated Walking	48
9.1.4	Follow-The-Leader	48
A	CONTRIBUTIONS	49
B	HUMAN EXPERIMENTS	59
C	ACTUATED SPRING LOADED INVERTED PENDULUM MODEL	60
D	BACKSTEPPING BARRIER FUNCTION RESULTS	61
E	3D ROBOT WALKING CONTROL	63

List of Figures

Figure 1.1	Human measurement data to a skeletal model to realizing locomotion on Cassie	2
Figure 2.1	Different phases for the nominal human walking gait	5
Figure 2.2	Examples of <i>historic</i> bipedal robots	6
Figure 2.3	Examples of <i>modern</i> bipedal robots	6
Figure 2.4	Different phases for the nominal Cassie walking gait	7
Figure 2.5	Foot contact wrench for a general foot and Cassie	9
Figure 3.1	The experiment setup for data collection of human walking .	16
Figure 3.2	Gait tiles of the human subject in OpenSim walking over an expected 10 cm downstep	17
Figure 3.3	Gait tiles of the human subject in OpenSim walking over an expected 10 cm downstep	17
Figure 3.4	Average vertical CoM position and vertical GRF for flat-ground, expected, and unexpected downsteps	18
Figure 3.5	The angular momentum around the contact point for walking on flat-ground, expected, and unexpected downsteps . . .	18
Figure 3.6	The desired vertical CoM trajectory and the GRF in SSP parameterized by time and the downstep height for expected downsteps	20
Figure 3.7	The desired vertical CoM trajectory and the GRF in SSP parameterized by time and the downstep height for unexpected downsteps	20
Figure 4.1	Inverted Pendulum and Spring-Loaded Inverted Pendulum reduced order models for walking	22
Figure 4.2	actuated Spring-Loaded Inverted Pendulum model in SSP and DSP	22
Figure 4.3	Abstraction of the human kinematics and kinetics towards the reduced order aSLIP model of walking	24
Figure 4.4	Embedding of the measured ground reaction forces on the walker	26
Figure 4.5	H-LIP walking on flat terrain and on a slope.	27
Figure 4.6	Simulation results of the aSLIP walking over an expected downstep with 10 centimeter depth	28
Figure 4.7	Simulation results of the aSLIP walking over an unexpected downstep with 10 centimeter depth	29
Figure 4.8	Trajectory generation and control structure of the BBF walking realization.	30
Figure 5.1	Phase portraits of the CoM kinematics of the human and the robot.	33
Figure 6.1	The underactuated and compliant Cassie biped.	34
Figure 6.2	The compliant and actuated sagittal joints and the degrees of freedom of the Cassie biped.	35
Figure 6.3	Bézier polynomials of the smooth transition and vertical swing foot trajectories.	39
Figure 6.4	Trajectory generation and control structure of the 3D walking realization on Cassie.	40

Figure 7.1	Period-1 and Period-2 orbits of 3D walking for expected and unexpected downsteps with 10cm depth	41
Figure 7.2	Simulation results of 3D walking for Cassie over an expected downstep with 10cm depth	42
Figure 7.3	Simulation results of 3D walking for Cassie over an unexpected downstep with 10cm depth	43
Figure B.1	Motion capture markers on the human subject and the perturbation platform.	59
Figure D.1	The desired vertical CoM trajectory and the GRF in SSP parameterized by time and the downstep height for expected downsteps for Cassie	61
Figure D.2	The desired vertical CoM trajectory and the GRF in SSP parameterized by time and the downstep height for unexpected downsteps for Cassie	61
Figure D.3	Simulation results of the aSLIP walking over an expected downstep with 10cm depth	62
Figure D.4	Simulation results of the aSLIP walking over an unexpected downstep with 10cm depth	62

List of Tables

Table 5.1	Walking parameters from human data and Cassie from the human-to-robot walking synthesis.	33
Table 6.1	Bézier polynomial coefficients for nominal walking and compensatory steps.	38
Table 7.1	Supplied power and Cost of Transport of canonical H-LIP walking and human synthesized SLIP walking.	44

The field of bipedal robotics has experienced tremendous progress in the last decades. Realizations have grown from conservative fully-actuated walking to agile and versatile dynamic walking with compliance and underactuation. However, even in fully known environments, the agility and robustness of mechanical bipeds has not matched their biological counterparts. We argue that this is due to a lack of online motion planning, an absence of reflex-like control, and disadvantageous passive dynamics, which biological systems employ to overcome disturbances. The robustness and adaptiveness can most notably be seen when considering significant unexpected changes in stepping height. For example, the running gait of a guinea fowl over expected and unexpected downsteps [1] highlights the advantageous reflexive behavior and passive properties of the leg. These allow the birds to, contrary to intuition, be more successful in navigating unexpected downsteps compared to expected downsteps. These downstep scenarios have received great attention in human running [2; 3] and walking [4; 5; 6; 7; 8; 9] which focus on a muscular-level and whole-body-level analysis of the human compensatory gait. While there have been efforts to achieve similar downstep behavior in the context of robotic running [10; 11], they have yet to be realized on walking robots with different morphologies. Therefore, this thesis aims to translate the deliberate and reflexive behavior present in humans to morphologically different bipedal robots.

1.1 PERSPECTIVES ON REALIZING ROBOTIC WALKING

The nonlinear control and biomechanics communities have traditionally pursued the study of bipedal robot locomotion from different perspectives. The control theorist is mainly concerned with realizing stable and robust locomotion with formal guarantees—even if the resulting walking does not directly share commonality with human walking. Methods such as offline trajectory optimization with Hybrid Zero Dynamics [12; 13], closed-form reduced-order model stepping methods [14; 15; 16], offline reduced-order model gait generation [17], and Model-Predictive Control [18; 19; 20] all require a varying degree of model knowledge and have been successfully utilized to achieve a varying degree of dynamic walking behaviors experimentally on underactuated robots. The biomechanist typically focuses on the methods of actuation and activation [21; 22; 23] and human morphology [24; 25]. Although formal notions of *biologically-inspired walking* [26; 27] and walking imitation on morphologically similar bipeds [28] exist, the intersection of these distinct fields has received less focus than expected from the significant similarities between analyzing biological bipedal locomotion and realizing robotic bipedal locomotion. These methods are in contrast to the work presented in this thesis, where we are especially interested in employing human data for realizing bipedal robot walking on morphologically different bipeds. Additionally, while there have been approaches to benchmarking human likeness [29; 25] it has not yet been addressed how to achieve human-like behaviors on walking robots.

Existing methods of traversing significant expected and unexpected changes in ground height have been realized with finite-state machines and offline trajectory optimization [30; 31], flexible gait adaptations from offline optimization [32], heuristic rules [33] or relied on the underlying robustness of the controller [34; 35]. How-

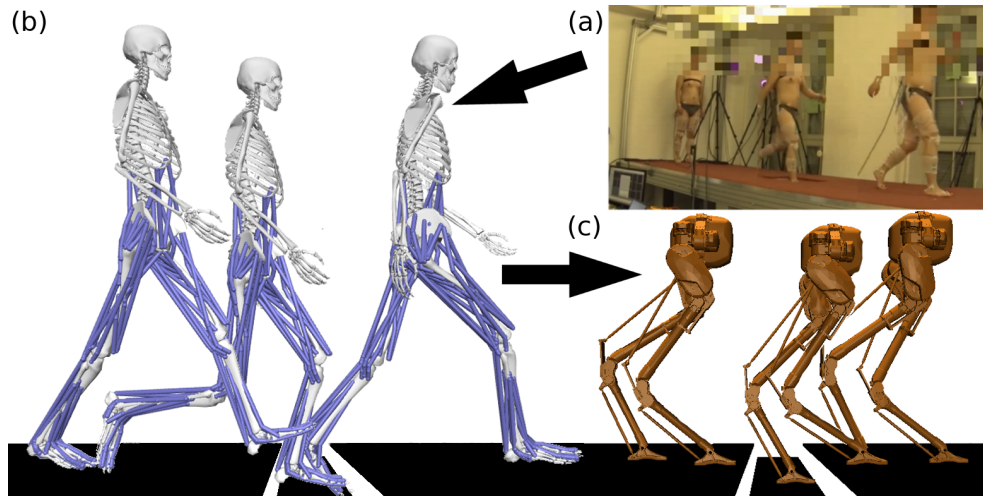


Figure 1.1: The human measurement data (a) mapped to a representative skeletal model of the test subject in OpenSim (b), towards realizing walking over the same downsteps on Cassie (c). Changes occur in step-time, step-length, forward walking velocity, desired contact forces, and vertical CoM trajectories.

ever, observations from biological walkers have not yet informed morphologically different bipedal robots in the traversal of unexpected changes to the ground height.

1.2 SCOPE OF THE THESIS

This thesis presents a method for translating downstep behaviors, both expected and unexpected, from humans to walking robots. We consider specifically the 3D bipedal robot Cassie [36], which is substantially morphologically different from a human. To achieve this, we first collect data from human walking downsteps and abstract this behavior to a reduced-order model (RoM) that captures the essential components of this behavior: the kinematics of the Center of Mass (CoM) and the ground reaction forces (GRF). We then realize a stable nominal and downstep walking realization of this RoM via the actuated Spring-Loaded Inverted Pendulum (aSLIP) model. We stabilize the vertical state and realize force-embedding with the Backstepping-Barrier Function framework [37] and stabilize the horizontal state via step-size adaptation of the Hybrid Linear Inverted Pendulum (H-LIP) using its linear Step-to-Step (S2S) dynamics [35]. For the 3D implementation, we assume a rigid model of the biped where the output dynamics are stabilized using a Task-Space Controller (TSC), and force-embedding is realized as a linear constraint. The result of this approach is downstep behaviors on the 3D model of Cassie in simulation. We, therefore, can start from human data for downstepping and, through a principled abstraction of the key elements of locomotion, arrive at robotic downstepping regardless of morphological similarities. Figure 1.1 gives a schematic overview of this translation. Human motion capture measurement data is presented in a musculoskeletal model [38] after which Center of Mass and Ground Reaction Forces are dynamically scaled towards a reduced-order representation of Cassie. This realizes 3D walking over expected and unexpected downsteps for different downstep heights.

This thesis will subsequently demonstrate that the human nominal and compensatory gait data can introduce desirable compensatory behavior on morphologically different bipedal walkers. It is furthermore argued that this principled abstraction of key elements of nominal and downstep locomotion and scaling towards morphologically different bipeds can be widely applicable to *follow-the-leader* scenarios,

where the robot observes humans traversing the environment and infers information for its own motion planning, to overcome a wide variety of walking environments by informed mimicking of the human on an equivalent Reduced-order Model level.

1.3 STRUCTURE

The structure of this thesis is as follows. First, in Chapter 2 we will address preliminary theory on principles of human and robot locomotion. In Chapter 3 we describe the human downstep experiments, data abstraction, and corresponding data analysis. Chapter 4 uses the human locomotion data, coupled with a RoM analysis, to generate walking on SLIP models. We describe the human-to-robot motion synthesis in Chapter 5 which is embedded onto the full-order dynamics of 3D robot in Chapter 6. We describe the main contribution of this thesis, 3D walking on Cassie for flat-ground, expected, and unexpected downsteps, in Chapter 7. We conclude the thesis with a discussion and conclusion in Chapter 8 and 9 respectively.

2 | PRELIMINARIES

This chapter will introduce background theory on biological and bipedal robot locomotion. First, we introduce the principles of bipedal walking in biology and its relation to bipedal walking in robotics. We introduce how we can mathematically model bipedal robots and how they can be controlled using nonlinear control methods.

2.1 BIPEDAL WALKING

Bipedal locomotion addresses a complex yet straightforward task: to transport oneself from the current position to the desired position. This task is most often performed by either walking or running. Walking consists of an inverted pendulum-like (IP) gait where the body of the walker vaults over a stance leg. The walking gait consists of alternating single support phases (SSP), where one leg is in contact with the ground, and double support phases (DSP), where both legs are in contact with the ground. Running consists of alternations of SSP and in-air phases. With an eye to the day-to-day operation of both humans and bipedal robots, we specifically consider the walking gait in this thesis.

2.1.1 Human Walking

This section will consider the nominal walking of humans and describe some of its core characteristics. Downstep walking (which is the focus of this thesis) is explicitly addressed in Chapter 3.

A macro-analysis of human walking concerns two significant theories. First popularized is the *six determinants of gait* theory [39] which proposes that a set of six kinematic features¹ reduce the sagittal and coronal displacement of the CoM. It is assumed that displacing the CoM in directions that are not necessary for enabling a forward motion is energetically costly and subsequently reduced by the inner walking mechanisms and muscular control of the human. Conversely, the *inverted pendulum* theory [40; 41] proposes that having the CoM travel over the stance leg in a constant-length pendulum fashion is more energetically efficient. These theories are subsequently in conflict, yet both theories have merit [42]. The *six determinants of gait* theory explains the step-to-step impact but fails to address the energy conservation. The theory of *dynamic walking* [42] has shown the validity of the *inverted pendulum* theory for energy conservation and *six determinants of gait* for CoM redirection.

In human walking, additional phases within SSP and DSP can be identified. After the initial contact with the ground at heel-strike, the heel is a momentary rotation point. This heel-roll, also known as the contact phase, starts at the Loading Response (\mathcal{D}_{LR}) and occurs until the foot is fully in contact with the ground (Opposite Toe-Off). This introduces the Early Stance (\mathcal{D}_{ES}), the first half of the SSP, which

¹ The six determinants of gait; 1: Pelvic rotation, 2: Pelvic obliquity (unconfirmed contribution), 3: Knee flexion during stance (not significantly contributing), 4: Foot rockers, 5: ankle muscles, 6: Narrowing walking base

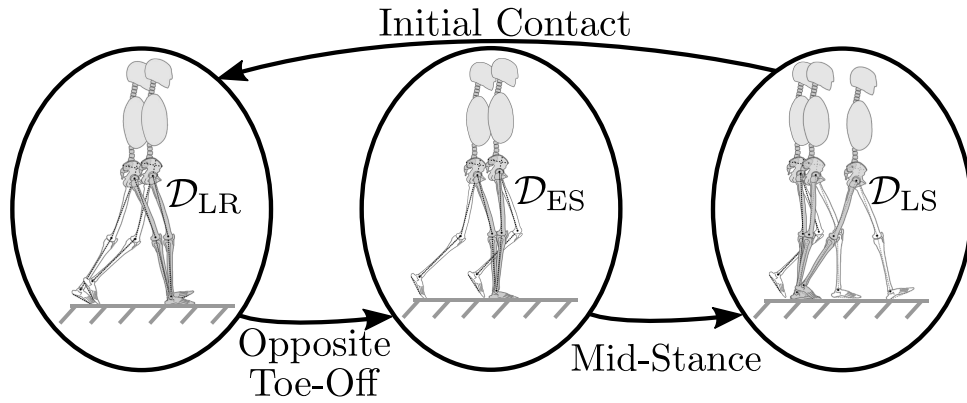


Figure 2.1: Different phases for the nominal human walking gait, consisting of the Loading Response \mathcal{D}_{LR} , Early Stance \mathcal{D}_{ES} , and Late Stance \mathcal{D}_{LS}

transitions into the Late Stance phase (\mathcal{D}_{LS}), the second half of the SSP, by the Mid-Stance event. The Late Stance starts the heel lift from the ground while the sole and toes remain in contact. This specific roll phase is identified as the toe-roll or propulsive phase. The stance phase subsequently consists of two underactuated (in the sagittal plane) roll phases and a fully actuated (in the sagittal plane) flat-footed phase². For bipedal robotics, the introduction of these additional underactuated phases could lead to an increase in energy efficiency [24]. Figure 2.1 displays the phases of human walking.

Although foot-roll phases in bipedal robotics have had many implementations, especially when intending to realize bio-inspired walking gaits [43; 44; 45; 27], this exceeds the current capabilities of Cassie. Subsequently, and with the goal to generalize the implementation to any walking platform, in this thesis, only flat-footed walking is realized on the robot. However, this results in a displacement of the horizontal CoM that cannot be realized due to the changes in foot size and location of the Center of Pressure (CoP). We address this difficulty in Chapter 5.

The full dynamics of the human are challenging to analyze during a nominal and a compensatory walking motion, yet the human gait is well-described by so-called Reduced Order Models (RoMs), or template models. We will see in Chapter 4 that the full-order dynamics of the human during nominal and compensatory gait can be abstracted towards the actuated Spring-Loaded Inverted Pendulum Model (aSLIP), that facilitates a more straightforward comparison between the observed walking motion of the human and the desired walking motion of the bipedal robot.

2.1.2 Robotic Walking

Bipedal human walking and bipedal robotic walking understandably have significant similarities. In both cases, the walker moves via two feet that alternate in contact with the ground, and the feet are extended and retracted via joint-level actuation. Most common robotic bipeds are humanoids, named after their comparative morphology to the human, yet, early mechanisms of locomotion such as McGeer’s passive dynamic walker [46] take a much more fundamental approach to the design of (in this case passive) walking mechanisms. Figure 2.2 shows some representative examples of historic bipeds that paved the way toward the current *state-of-the-art* of bipedal robotics.

² One could regard the human as overactuated as there are more actuators (muscles) than degrees of freedom for many of the joints. However, underactuated is stated because the contact point between ground and foot during the roll phases is not actuated, and subsequently, there are more degrees of freedom than actuated joints.

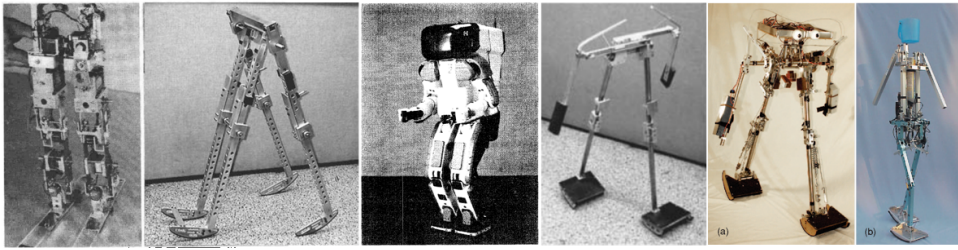


Figure 2.2: Examples of *historic* bipedal robots (from left to right): Biper-3 [54], McGeer's Passive Dynamic Walker [46], Honda Humanoid Robot [50], Cornell Passive Biped [47], Cornell Biped [55], and Denise [49]

As the field progressed, the bipedal robots, and their motion planning and control, changed from passive [46; 47], minimally actuated [48; 49], or statically stable [50] bipeds towards actuated dynamically stable realizations (although it could be stated that the understanding shown in these earlier passive and minimally actuated implementations is often lost). Figure 2.3 illustrates examples of modern bipeds where Cassie, the robot considered in this thesis, is shown in the center.

Cassie is capable of unsupported walking in 3D. The physical model additionally has structural compliance via knee and heel leaf springs, and is underactuated in the coronal plane. We assume underactuation in the sagittal plane by not using the ankle torque for the following reasons; the ankle actuation is weak (the maximum available torque is 10% of the knee- and hip-motors' maximum available torque), and ankle underactuation is a particular case of fully actuated walking. Fully actuated walking is therefore always realizable with the methods discussed here by including an additional trackable output of the horizontal CoM position.

Unlike Atlas by Boston Dynamics [51], most bipedal robots are actuated by conventional electrical torque motors. The potential similarities in pneumatic and muscular actuation, for bipedal robots such as Pneumat-BB [52] and the human, are outside of the scope of this thesis; readers are referred to [53]. Although bipedal robots that are morphologically similar to humans allow a more straightforward human-to-robot motion synthesis, the focus on morphologically different bipeds in this thesis allows generalizability between the human and any bipedal robot. The phases under consideration are SSP and DSP (flat-footed walking), without foot-roll occurrences that are apparent in the human gait. Figure 2.4 shows the alternation of the considered walking phases of Cassie.



Figure 2.3: Examples of *modern* bipedal robots (from left to right): ATRIAS [34], DURUS [44], Cassie [36], Atlas [51], Valkyrie [56], and Digit [36]. ATRIAS, DURUS, Cassie, and Digit all have structural compliance in their designs.

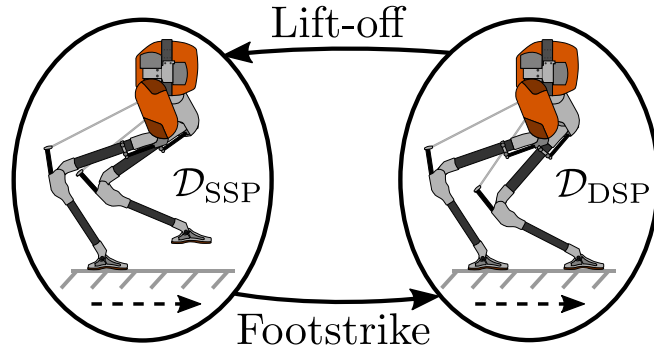


Figure 2.4: Different phases for the nominal Cassie walking gait, consisting of Double Support Phase (DSP) and Single Support Phase (SSP). The walking direction is indicated with the dotted arrow and highlights that Cassie has inverted knees.

2.2 MATHEMATICAL MODELS OF BIPEDAL ROBOTS

A (rigid) bipedal robot is a series of links, possibly with loops, that are either connected to the ground by one foot, two feet, or no feet. This first leads to the definition of the dynamical model of a biped as a floating body where foot contact is enforced using holonomic constraints. While this thesis considers Agility Robotics's Cassie biped, which has compliant joints, we first assume a general rigid biped. We write down the potential and kinetic energy of the model, which can be encapsulated by the Lagrangian

$$L(q, \dot{q}) = E_{\text{kin}}(q, \dot{q}) - E_{\text{pot}}(q), \quad (2.1)$$

where $E_{\text{kin}}(q, \dot{q})$ is the kinetic energy, $E_{\text{pot}}(q)$ is the potential energy, and q is the set of generalized coordinates of the robot $q = [q_j^T, p_b^T, \phi_b^T]^T \in SE(3) \times \mathbb{R}^n$ with $q_j \in \mathbb{R}^n$ the body coordinates of the robot and $p_b \in \mathbb{R}^3$ and $\phi_b \in SO(3)$ the position and orientation of the base in a fixed world frame respectively. After applying the method of Lagrange, we can write the dynamical model of the free-floating biped as

$$D(q)\ddot{q} + H(q, \dot{q}) = Bu, \quad (2.2)$$

where $D(q)$ is the inertia matrix, $H(q, \dot{q})$ is the Coriolis and gravity terms grouped into a single vector $H(q, \dot{q}) = C(q, \dot{q})\dot{q} + G(q)$, B is the actuation matrix³, and $u \in \mathbb{R}^m$ is the vector of actuator torques applied between two links of the biped. At this point, the model of the biped in Equation (2.2) assumes no contact with the ground surface.

2.2.1 Holonomic Constraints and Ground Contact

To describe the behavior in SSP or DSP, we need to realize ground contact for the model in Equation (2.2) and add holonomic constraints of one or two feet respectively that constrain the movement of the feet. For 3D walking, we wish to ensure at all times that

- the horizontal contact forces remain within the friction cone to prevent slippage (dry friction is represented by the *Amontons-Coulomb* model),
- the vertical contact force remains positive (the ground exerts a positive, upwards force) as the ground is assumed non-sticky and the foot should refrain from lifting from the ground,

³ As Cassie contains rotational torque actuators and the generalized coordinates are similarly of joint rotations, B is constant.

- the moments around the horizontal axes should be limited such that no rotation around the edges of the feet occur.

We write these constraints respectively as

$$\begin{cases} 0 < F_{st}^{fz} \\ -\frac{\mu}{\sqrt{2}}F_{st}^{fz} < F_{st}^{fx} < \frac{\mu}{\sqrt{2}}F_{st}^{fz} \\ -\frac{\mu}{\sqrt{2}}F_{st}^{fz} < F_{st}^{fy} < \frac{\mu}{\sqrt{2}}F_{st}^{fz}, \\ -w_b F_{st}^{fz} < F_{st}^{mx} < w_a F_{st}^{fz} \\ -l_b F_{st}^{fz} < F_{st}^{my} < l_a F_{st}^{fz} \end{cases}, \quad (2.3)$$

where F_{st}^i indicates a force or moment of the ground contact wrench

$$F_{st} = \begin{bmatrix} F_{st}^{fx} & F_{st}^{fy} & F_{st}^{fz} & F_{st}^{mx} & F_{st}^{my} & F_{st}^{mz} \end{bmatrix}, \quad (2.4)$$

as fz indicates a force in the z -direction, mx indicates a moment around the x -axis, and w_a, w_b, l_a , and l_b are defined by the geometry of the foot according to Figure 2.5. The moment around the z -axis would prevent rotation, yet this constraint depends on the unknown force distribution on the surface of the foot and is therefore often neglected. The third and fourth constraints in Equation (2.3) are known as the *Zero Moment Point (ZMP)* constraints [57] and prevent the foot from rotating around its edges during flat-footed standing or walking. The roll phases apparent in human walking from Chapter 2.1.1 intentionally violate these constraints. We will see that the ground contact constraints in Equation (2.3) are affine⁴ in the holonomic forces which themselves are either decision variables in the Quadratic Program (QP) Controller or affine in the control torques u . Subsequently, in both scenarios the ground contact constraints can be enforced via a linear constraint on the decision variables of the QP. As for the first case, we can write the ground contact constraint specifically for the line-segment foot of Cassie as

$$\underbrace{\begin{bmatrix} 0 & 0 & -1 & 0 & 0 \\ 1 & 0 & -\frac{\mu}{\sqrt{2}} & 0 & 0 \\ -1 & 0 & -\frac{\mu}{\sqrt{2}} & 0 & 0 \\ 0 & 1 & -\frac{\mu}{\sqrt{2}} & 0 & 0 \\ 0 & -1 & -\frac{\mu}{\sqrt{2}} & 0 & 0 \\ 0 & 0 & -l_a & 0 & 1 \\ 0 & 0 & -l_b & 0 & -1 \\ 0 & 0 & -l_a\mu & 1 & 0 \\ 0 & 0 & -l_b\mu & -1 & 0 \end{bmatrix}}_{A_{GRF}} \underbrace{\begin{bmatrix} F_{st}^{fx} \\ F_{st}^{fy} \\ F_{st}^{fz} \\ F_{st}^{mx} \\ F_{st}^{my} \\ F_{st}^{mz} \end{bmatrix}}_{F_{GRF}} \leq 0_{[9 \times 1]}, \quad (2.5)$$

where, due to the line-segment feet assumption of Cassie as shown in Figure 2.5, the moment around the x -axis is zero and $0_{[9 \times 1]}$ indicates a column array with zeros of size nine.

In the second scenario, the feet in contact with the ground can be ensured static by constraining its kinematics according to

⁴ An affine control system is defined as a control system in which the control input appears linearly in the equations, e.g. when considering the form $y = Ax + b$, the system is said to be affine in x

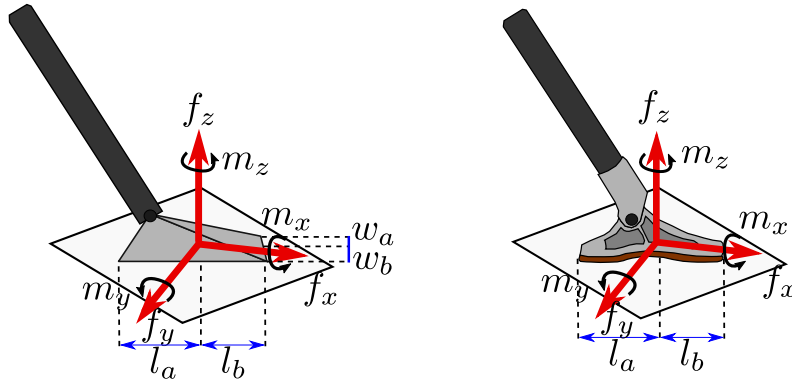


Figure 2.5: The ground exerts a wrench on a general foot and the line-segment foot design of Cassie. Due to this line-segment representation, no moment around the x-axis is exerted. The reference frame is located at an arbitrary point on the foot.

$$\begin{aligned}
 c_i &= p_i = 0, \\
 \frac{\partial p_i}{\partial q} \dot{q} &= J_i \dot{q} = 0, \\
 \frac{\partial p_i}{\partial q} \ddot{q} + \frac{\partial \frac{\partial p_i}{\partial q}}{\partial t} \dot{q} &= J_i \ddot{q} + \dot{J}_i \dot{q} = 0,
 \end{aligned} \tag{2.6}$$

where c_i and p_i indicate a constraint and the position of i , some part of the biped in consideration (e.g. the mid-foot, heel, or toe). For SSP, we define the constraint matrix for a single foot according to Equation (2.6) but consider not only the position of the mid-foot but also the rotation of the foot, defined via a simplified foot-pitch $p_{\text{heel},i}^z - p_{\text{toe},i}^z$. In DSP we consider these constraints for both feet as shown in Equation (2.7). Additionally, if we wish to consider a rigid model (as opposed to the compliance presented in the knee and tarsus springs of Cassie) we can apply joint-level holonomic constraints which we can denote by $\phi_{\text{jointlevel}}$. Details on the inherent compliance of Cassie are presented in Chapter 6 yet for now we combine all the holonomic constraints as

$$c_{\text{SSP}} = \begin{bmatrix} p_{\text{midfoot},i}^x \\ p_{\text{midfoot},i}^z \\ p_{\text{heel},i}^z - p_{\text{toe},i}^z \\ \phi_{\text{jointlevel}} \end{bmatrix} \quad c_{\text{DSP}} = \begin{bmatrix} p_{\text{midfoot},i}^x \\ p_{\text{midfoot},i}^z \\ p_{\text{heel},i}^z - p_{\text{toe},i}^z \\ p_{\text{midfoot},j}^x \\ p_{\text{midfoot},j}^z \\ p_{\text{heel},i}^z - p_{\text{toe},j}^z \\ \phi_{\text{jointlevel}} \end{bmatrix}, \tag{2.7}$$

from which we straightforwardly define the Jacobian $J_{\text{hol}}(q)$ and time-derivative of the Jacobian $\dot{J}_{\text{hol}}(q, \dot{q})$. Now, let us define the holonomic forces which are explicitly dependent and affine in the control torques u . For simplicity, we drop any dependencies on q or \dot{q} . The projection of the inertia matrix into the holonomic constraints can be written as

$$M = J_{\text{hol}} D J_{\text{hol}}^T, \tag{2.8}$$

and the holonomic forces are obtained according to

$$F_{\text{hol}} = \underbrace{-M^{-1}(J_{\text{hol}} D^{-1} F_{\text{vec}} + \dot{J}_{\text{hol}} \dot{q})}_{f_F} + \underbrace{-M^{-1} J_{\text{hol}} B}_{g_F} u. \tag{2.9}$$

The ground contact wrench is therefore directly obtained via the projection of the holonomic constraints upon the equations of motion. This ground contact wrench

is affine in the control torques u . The equations of motion with the holonomic constraints can then be obtained in a familiar affine form

$$\ddot{q} = \underbrace{D^{-1}(F_{vec} + J_{hol}^T f_F)}_{f_{\ddot{q}}} + \underbrace{D^{-1}(B + J_{hol}^T g_F)}_{g_{\ddot{q}}} u, \quad (2.10)$$

where $f_{\ddot{q}}$ and $g_{\ddot{q}}$ represent the autonomous and controlled parts of the differential equation. The state space form can be presented as

$$\dot{x} = \underbrace{\begin{bmatrix} \dot{q} \\ f_{\ddot{q}} \end{bmatrix}}_{f(x)} + \underbrace{\begin{bmatrix} 0^{n \times m} \\ g_{\ddot{q}} \end{bmatrix}}_{g(x)} u, \quad (2.11)$$

where $x = [q \ \dot{q}]^T \in \mathcal{X} \subseteq \mathbb{R}^n$ is the set of states, $u \in \mathcal{U} \subseteq \mathbb{R}^m$ is the control input, and f and g are locally Lipschitz continuous functions.

2.2.2 Impact Mapping

It is now possible to forward integrate equations of motion of the model for a given phase (SSP or DSP) and compute control torques that realize desired behavior for a single phase. However, a feature of bipedal walking is the switching of ground contact with either one or two feet, and the dynamics of the biped are subsequently governed by equations of motion of their respective phases. The switching behavior from SSP to DSP and DSP to SSP can be described by detecting intersections with a switching surface and mapping the state with a reset map Δ . The transitions from SSP to DSP and from DSP to SSP are respectively detected by the switching surfaces

$$\begin{aligned} S_{SSP \rightarrow DSP} &= \{x_1 \in \mathcal{X}_1 \mid p_{\text{swing foot}}^z(x_1) = 0, \dot{p}_{\text{swing foot}}^z(x_1) < 0\}, \\ S_{DSP \rightarrow SSP} &= \{x_2 \in \mathcal{X}_2 \mid F_{\text{stance foot}}^z(x_2) = 0, \dot{F}_{\text{stance foot}}^z(x_2) < 0\}, \end{aligned} \quad (2.12)$$

where x_i is the state in domain i , p_k^z is the vertical position of body k with respect to the stance foot, and F_k^z is the vertical ground reaction force of body k . The switching surfaces indicates that the SSP event takes place when the swing foot reaches zero height with a negative velocity, and that the DSP event takes place when the GRF of the stance foot reaches zero force with a negative time derivative. Based on the assumption that the both legs remain flat footed and in its current position during the transition from SSP to DSP, we can constrain this on a velocity level according to

$$p_{imp}(q) = 0 \quad \longrightarrow \quad \frac{\partial p_{imp}(q)}{\partial q} \dot{q}^+ = J_{imp}(q) \dot{q}^+ = 0, \quad (2.13)$$

where p_{imp} indicates the constrained position before and after the impact. Combining this with a rigid impact model [58], which introduces a contact impulse into the dynamic model. By integrating this over over the impact duration, we can obtain the impact equation

$$D(q^-)(\dot{q}^+ - \dot{q}^-) = J_{imp}(q)^T F_{imp}, \quad (2.14)$$

The post-impact configuration constraint in Equation (2.13) can be combined with the impact equation to obtain the post-impact velocities \dot{q}^+ and the impulsive forces F_{imp} . The two equations result in the linear system with a square and invertible matrix according to

$$\begin{bmatrix} D & -J^T \\ J & 0 \end{bmatrix} \begin{bmatrix} \dot{q}^+ \\ F_{imp} \end{bmatrix} = \begin{bmatrix} D\dot{q}^- \\ 0 \end{bmatrix}. \quad (2.15)$$

The transition from DSP to SSP is smooth and might only involve a relabeling matrix R , mapping the joints of the right leg to the left leg and vice-versa, to use the symmetry of the walker.

2.3 FEEDBACK CONTROL OF NONLINEAR SYSTEMS

The control of bipedal robotic locomotion is a complex task. In general, the challenges lay in the nonlinearities of the system, the hybrid nature of the dynamics, and the potential underactuation of the biped from point-foot walking [59] or compliance [60]. We can define the system as a Hybrid Control System

$$HC = \Sigma = (\Gamma, \mathcal{X}, \mathcal{U}, \mathcal{S}, \Delta, \mathcal{F}), \quad (2.16)$$

in which Γ is a directed graph indicating the alternation between walking phases (see Figure 2.1 and 2.4), \mathcal{X} is the state manifold which is an open connected subset of \mathbb{R}^n , \mathcal{U} is the actuator manifold which is an open connected subset of \mathbb{R}^m , \mathcal{S} is the switching surface from Equation (2.12), and \mathcal{F} is the flow on the state manifold \mathcal{X} according to Equation (2.10). For clarity, considering a single phase and disregarding the hybrid nature of the system, the resulting non-hybrid Control System can be written as

$$C = \Sigma_i = (\mathcal{X}_i, \mathcal{U}_i, \mathcal{F}_i). \quad (2.17)$$

Different methods exist to compute the required control signal for these control systems. First, we will explain Feedback Linearization, which yields convergence in the output dynamics using a closed-form solution. This method is used extensively in the tracking of offline optimized gaits with, for example, Hybrid Zero Dynamics [12; 13; 27; 61]. This method will be used in the Backstepping Barrier Function (BBF) framework [37] for RoM walking in Chapter 4. Afterward, we will explain the optimization-based (Rapidly) Exponentially Stable Control Lyapunov Function ((R)ES-CLF) [62; 63] which is a convex quadratic program (QP) formulation that yields *theoretical* guaranteed exponential convergence in the output dynamics of the system. The RES-CLF will find application in the BBF framework in Chapter 4. Lastly, we will address the Task-Space Controller QP, which, although without formal guarantees, can stabilize output dynamics and has some advantages compared to the CLF-QP regarding the implementation. Subsequently, the TSC is utilized in the 2D and 3D Cassie walking simulations. Other control methods such as (Partial) Hybrid Zero Dynamics [12; 27], and high-level control with biologically inspired musculoskeletal walking and reflex control walking [64; 65] are outside of the scope of this thesis and, as such, will not be explicitly addressed in this section, but more on these topics can be read in [53].

2.3.1 Feedback Linearization

Feedback linearization is a straightforward yet powerful approach toward controlling nonlinear systems. It relies on two operations; a nonlinear change of the coordinates and a nonlinear state feedback [66]. This results in a transformation of the nonlinear system into a linear system through the change in coordinates and the closed-form computed control input. With regards to bipedal robot control, feedback linearization is closely tied with the notion of Hybrid Zero Dynamics [12; 13]. Furthermore, human-inspired walking with HZD is realized in [27] where the trajectories of the joint angles from the nominal human gait are also used in the cost function of the offline gait optimization.

Considering the dynamical system of the form in Equation (2.2), we define a system that is to track desired outputs

$$y(x) = y^a(x) - y^d(x), \quad (2.18)$$

where $y^a : \mathcal{X} \rightarrow \mathbb{R}^m$ indicates the actual outputs, and $y^d : \mathbb{R} \times \mathbb{R}^a \rightarrow \mathbb{R}^m$ indicates the desired outputs. Assuming that the outputs have vector relative degree k^5 (RDk)

⁵ Vector Relative Degree is defined as the number of differentiations needed to take on the output to have it directly be affected by the control input.

we can define the derivatives of the outputs along the controlled and autonomous part of the state equations

$$y^k(x) = L_f^k y(x) + L_g L_f^{k-1} y(x) u, \quad (2.19)$$

where $L_f y(x)$ denotes the Lie derivative of $y(x)$ along the vector field of $f(x)$ and $L_g L_f^{k-1} y(x)$ is the decoupling matrix which is invertible. Subsequently, if the system is feedback linearizable, we can directly compute the control signal

$$u(x) = (L_g L_f^{k-1} y(x))^{-1} (-L_f^k y(x) + v) \iff y^k = v, \quad (2.20)$$

where v is the auxiliary feedback control signal. If the feedback linearized control signal is applied to the system in Equation (2.2) for relative degree 2 outputs, y_2 , we obtain a linear system for the output dynamics

$$\dot{\eta} = \begin{bmatrix} \dot{y}_2 \\ \dot{y}_2 \end{bmatrix} = \begin{bmatrix} 0 & I \\ 0 & 0 \end{bmatrix} \eta + \begin{bmatrix} 0 & 0 \\ 0 & I \end{bmatrix} v = F\eta + Gv. \quad (2.21)$$

As we wish to control the actual outputs towards the desired outputs, we can define a choice of the auxiliary feedback control signal v as

$$v = \dot{y}_2 = -K_P y_2 - K_D \dot{y}_2, \quad (2.22)$$

where K_P and K_D are the proportional and derivative control gains. Although this controller yields convergence to $\eta \rightarrow 0$, it cannot leverage the natural dynamics of the system and cannot incorporate actuator and feasibility constraints. Subsequently, a solution from feedback linearization is not necessarily valid. For offline gait trajectories, where actuator constraints can be included in the offline whole-body trajectory optimization, these constraints are assumed to be satisfied during nominal walking. Although feedback linearization cannot incorporate actuator and feasibility constraints, it is still a powerful tool and will be used in the Backstepping Barrier Function controller for stabilizing the underactuated RoM.

2.3.2 Control Lyapunov Functions

Given the shortcomings of feedback linearization with regards to an inability to leverage the natural dynamics of the system and the incorporation of actuator and feasibility constraints from Chapter 2.2.1, other optimization-based control methods are used in the control of bipedal robots. The Exponentially Stable Control Lyapunov Function (ES-CLF) [62] and the Rapidly Exponentially Stable Control Lyapunov Function (RES-CLF) [63] frameworks are methods of achieving *theoretically* guaranteed convergence and stability in the output dynamics of a controlled system. The framework relies on a *Control Lyapunov Function*⁶ $V(\eta) : \mathbb{R}^m \rightarrow \mathbb{R}$. Consider the Lyapunov Function

$$V(\eta) = \eta^T P \eta, \quad (2.23)$$

where P is from the solution of the continuous-time algebraic Riccati equation

$$F^T P + P F - P G G^T P + Q = 0, \quad (2.24)$$

where $Q = Q^T > 0$ and $P = P^T > 0$. The derivative of Equation 2.23 is defined as

$$\dot{V}(\eta, v) = L_F V(\eta) + L_G V(\eta) v, \quad (2.25)$$

where the Lie derivatives of V along the vector fields of F and G are defined as

$$L_F V(\eta) = \eta^T (F^T P + P F) \eta, \quad (2.26)$$

$$L_G V(\eta) = 2\eta^T P G, \quad (2.27)$$

⁶ The Lyapunov function conditions apply: continuously differentiable, positive definite, and radially unboundedness

which follows straightforwardly from Equations (2.21) and (2.23). With our desire to realize exponential convergence, a constraint on the CLF can be formulated that guarantees that the derivative of the output dynamics imposes a minimum rate of decrease in $V(\eta)$. Subsequently, if there exists some constant λ (convergence rate) such that

$$\dot{V}(\eta, v) + \lambda V(\eta) \leq 0, \quad (2.28)$$

then the Lyapunov function $V(\eta)$ is said to be an ES-CLF and any η is exponentially stabilizable to zero. This formulation is a convex optimization problem that can be solved in real-time. The constraint in Equation (2.28) leads to an optimization-based control law formulation

$$\min_u \|u\|^2 \quad (2.29)$$

$$\text{s.t. } L_f V(x) + L_g V(x)u + \lambda V(x) \leq 0 \quad (\text{ES-CLF})$$

$$u_{\min} \leq u \leq u_{\max}. \quad (\text{torque limit})$$

In practice, additional constraints are introduced to ensure a feasible solution on the biped. The collection of these constraints can make the ES-CLF QP infeasible. To ensure that at least an approximately optimal solution exists, we introduce a slack variable δ that allows relaxation of the ES-CLF constraint. If we additionally introduce the constraints for bipedal walking from Chapter 2.2.1, we obtain the complete ES-CLF QP formulation

$$\min_{u, F_h, \dot{q}} \|u\|^2 + p\delta^2 \quad (2.30)$$

$$\text{s.t. } D\dot{q} + C = J_h^T F_h + Bu \quad (\text{EOM})$$

$$L_f V(x) + L_g V(x)u + \lambda V(x) \leq \delta \quad (\text{ES-CLF})$$

$$J_h \dot{q} + \dot{J}_h q = 0 \quad (\text{holonomic})$$

$$u_{\min} \leq u \leq u_{\max} \quad (\text{torque limit})$$

$$A_{\text{GRF}} F_{\text{GRF}} \leq 0, \quad (\text{friction cone})$$

where p weights the relaxation of the CLF constraint with respect to the actuation. As long as the slack variable δ is not too large for too long, approximate exponential convergence can be achieved in practice.

2.3.3 Task Space Control

Another approach to track desired output trajectories on nonlinear systems is Task Space Control (TSC)⁷. As the CLF constraint is relaxed in practice with an additional decision/slack variable δ , the TSC and the CLF-QP can obtain identical performance [35]. However, an advantage of the TSC is the decreased number of tuning parameters and a more intuitive gain tuning.

If we again consider $RD1$ and $RD2$ outputs for an affine control system, we can define affine relationships for the derivative of the outputs w.r.t. the control input as well

$$\begin{aligned} \dot{Y}_1 &= \underbrace{J_i}_{A_1} \dot{q} + \underbrace{\dot{J}_i q - \dot{Y}_1^d}_{b_1} \\ \dot{Y}_2 &= \underbrace{J_j}_{A_2} \dot{q} + \underbrace{\dot{J}_j q - \dot{Y}_2^d}_{b_2}, \end{aligned} \quad (2.31)$$

which can be combined in a system according to

$$\ddot{Y} = \mathbf{A}u + \mathbf{b} = \begin{bmatrix} A_1 \\ A_2 \end{bmatrix} u + \begin{bmatrix} b_1 \\ b_2 \end{bmatrix}, \quad (2.32)$$

⁷ Task Space Control is also known in the literature as whole-body control and operational space control.

which indicate the actual accelerations of the output. For *RD1* and *RD2* outputs, we can then define the desired accelerations that stabilize the system with the use of *P* and *PD* control respectively and ensure that the outputs stabilize themselves according to a second order system. According to the definition of a second-order system, the first time derivative of *RD1* outputs is affine in the control input, so we use a Proportional gain. The second time derivative of *RD2* outputs is affine in the control input so we use a Proportional and a Derivative gain.

$$\ddot{\mathbf{Y}}^d = \begin{bmatrix} \dot{Y}_1^d \\ \dot{Y}_2^d \end{bmatrix} = \begin{bmatrix} -K_{p,1}Y_1 \\ -K_{p,2}Y_2 - K_{d,2}\dot{Y}_2 \end{bmatrix}. \quad (2.33)$$

As we now have an expression for the actual and the desired output of the system in terms of PD control, we can minimize the error between the two and formulate a Quadratic Program (QP) to find the optimal applied torques subjected to feasibility constraints

$$\begin{aligned} \min_{u, F_h, \dot{q}} \quad & \|\ddot{\mathbf{Y}} - \ddot{\mathbf{Y}}^d\|^2 & (2.34) \\ \text{s.t.} \quad & D\ddot{q} + C = J_h^T F_h + Bu & (\text{EOM}) \\ & J_h\dot{q} + \dot{J}_h\dot{q} = 0 & (\text{holonomic}) \\ & u_{\min} \leq u \leq u_{\max} & (\text{torque limit}) \\ & A_{\text{GRF}}F_{\text{GRF}} \leq 0. & (\text{friction cone}) \end{aligned}$$

Additional constraints such as contact force embedding to ensure kinematic similarity between the human and the robot will be addressed in later chapters.

The background information on bipedal walking, robot modeling, and nonlinear control allows us to continue with our human walking analysis and implementations of robotic walking on reduced-order models and full-order 3D walkers.

3

HUMAN WALKING ON DOWNSTEPS

Many bipedal walkers in nature prove themselves as versatile, efficient, and robust in a wide variety of environments. This robustness is most apparent in the ability to overcome unexpected perturbations in the ground surface height, and the biomechanics community has analyzed this behavior in much detail. The initial inspiration of this thesis [1] highlights the extraordinary capabilities of the guinea fowl when running over unexpected downsteps (similar to those considered in this thesis). The observation that guinea fowls are more successful in traversing unexpected downsteps than expected downsteps seems counter-intuitive and reveals the extraordinary reflex behavior and passive (or uncontrolled) dynamics of the system. These properties have advanced over millennia of evolution but are not apparent in bipedal robotics. On the contrary; the passive dynamics of a bipedal robot are often not explicitly taken into account in the design and control. It could therefore be beneficial to map this reflexive behavior and resulting passive dynamics explicitly onto bipeds.

We will address human behavior when walking over expected and unexpected downsteps in this chapter. This scenario has been researched at a muscular-reflex level [5; 6; 7] and whole-body level [67; 68; 9; 8]. Pre-impact reflexes during unexpected downsteps, such as those in the stance ankle [6], are difficult to analyze and even more difficult to map to morphologically different bipeds (especially the ones that are not driven by muscle-like actuation). In this chapter, we will perform an analysis of the CoM behavior and the resultant GRFs. Additionally, we will consider the angular momentum around the stance leg as an important metric for stability. We will first explain the measurement setup and the experimental trials, then we will perform the analysis of the CoM, GRFs, and the angular momentum around the stance leg. We will finalize with measurement data processing to be applicable towards RoM walking in Chapter 4. The morphological differences between the human and the robot prevent the applicability of a joint-level analysis that has been addressed in literature [67; 9; 8].

3.1 DATA COLLECTION

To understand the human response to walking over expected and unexpected downsteps, we analyzed experiments conducted at the Lauflabor lab at Technische Universität Darmstadt. Human subjects walked on a platform 2 meters wide and 6 meters long shown in Figure 3.1. A variable height walking platform is located at the center of the platform, which can quickly control the vertical position of a single step-tile using electric motors, as shown in Appendix B. Three force plates are present: before (9287C, Kistler, Switzerland), on (9260AA, Kistler, Switzerland), and after (9287C, Kistler, Switzerland) the variable height platform. These force plates measure the ground reaction forces at 1 kHz. Full body movement is recorded by a motion capture system (Qualisys, Sweden) consisting of 26 markers and 16 cameras that run at 240 Hz. Eight trials are conducted for each downstep height at 0.0 cm, -2.5 cm, -5.0 cm, -7.5 cm, and -10.0 cm for both expected- and unexpected situations. For the unexpected trials, the downstep platform is lowered when the swing foot is approaching the ground, which is detected by the interruption of a laser beam.

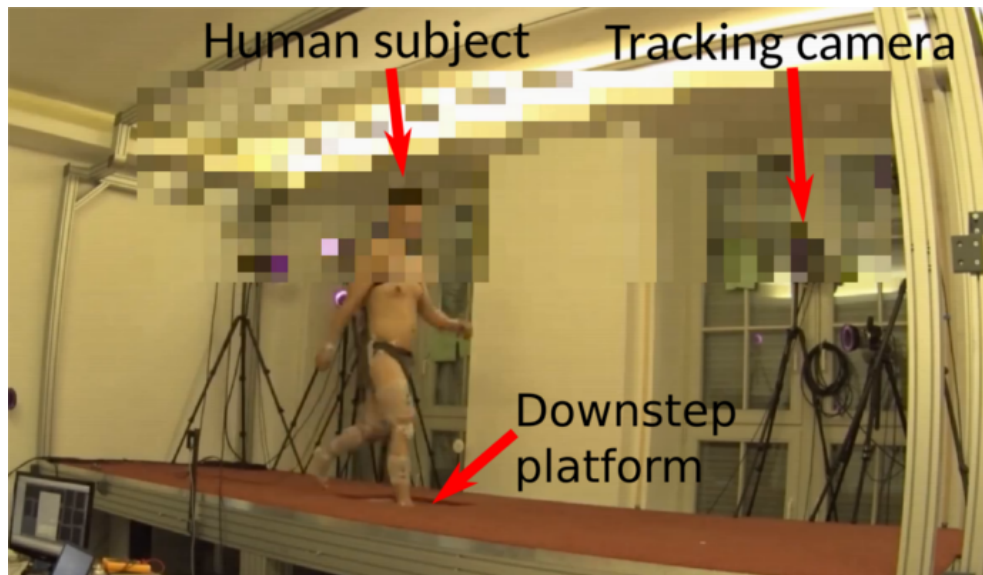


Figure 3.1: The experiment setup for data collection of human walking. Force plates are installed beneath the platform.

Both expected and unexpected downstep trials therefore allow complete vision of the walking platform. The experiment consists of nine experimental conditions: four known downstep heights, four unknown downstep heights, and nominal flat-ground walking. For each experimental conditions, eight trials per subject were performed. The data of 3 subjects were analyzed. Inverse Kinematics (IK) and Inverse Dynamics (ID) optimization was performed in OpenSim [69; 70]. Differences between nominal walking and downstep compensation in the coronal plane were regarded to be small and insufficiently affected by the downsteps. Subsequently, we limit our focus to the results in the sagittal plane.

3.2 KINEMATICS AND KINETICS ANALYSIS

With the Inverse Kinematics, we optimize the pose of the model that best matches the the coordinate data of the markers for each time frame. By assigning weights to the markers and unprescribed coordinates ($Q = SE(3) \times Q^{joints}$), we obtain the flow q and \dot{q} of the coordinates for all time frames. Using the time evolution of the human subject and the approximately correct mass and limb length from a scaled OpenSim musculoskeletal model [38], we can compute the center of mass kinematics. Gait tiles for an expected and unexpected 10 centimeter downstep trial are shown in Figure 3.2 and 3.3, respectively. Unsurprisingly, we observe a larger pelvis angle with respect to the stance leg for the unexpected 10 centimeter downstep compared to the expected 10 centimeter downstep. Additionally, the up-step¹ stepsize is significantly larger, which is caused by the comparatively small down-step stepsize for the unexpected 10 centimeter downstep. These results will be more apparent in the angular momentum analysis around the stance leg. As one of the main objectives of perturbed walking is to keep the whole body upright, it was shown that also the direction of the GRFs from the CoP point slightly upwards of the CoM, which, according to the Virtual Pivot Point model [71], realizes this upper-body stability [4]. It was also shown that this observed principle is not visible during unexpected downsteps due to the stumbling behavior as a result of the small step size.

¹ The complete downstep trial is divided into three steps; down-step: the step from the nominal walking platform upon the downstep platform, over-step: the step from the nominal walking platform upon the

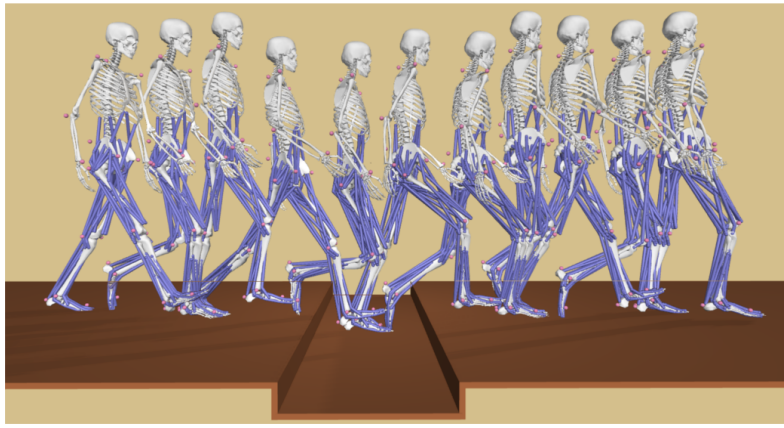


Figure 3.2: Gait tiles of the human subject in OpenSim walking over an **expected** 10 cm downstep.

A powerful abstraction for a full-body analysis of the human gait is the consideration of the CoM kinematics. Although the human subjects have an upper body with arms (which are not present on Cassie), the point-mass dynamics can capture the contributions towards changes in angular momentum. Figure 3.4 shows a polynomial fit to the normalized mean vertical CoM position and the GRFs, normalized by Body-Weight (BW), for the nominal and downstep trials. The analysis is performed from the Vertical Leg Orientation (VLO) before the downstep and ends at the VLO after the downstep. Subsequently, two complete steps are considered in the analysis. For example, if we consider a left stance leg during downstep detection, the analysis is from the moment of the CoM passing the left foot on the raised pre-downstep platform until the moment of the CoM passing the left foot on the raised post-downstep platform.

The within-subject variance is deemed sufficiently low, $\max(\text{std}(z_{CoM})) < 0.018\text{cm}$, to permit polynomial fits for analysis and further application. From Figure 3.4, we observe that the CoM position is significantly lowered for both scenarios. This is more significant for expected downsteps where the lowering of the CoM height starts before the swing leg penetrates the flat-ground platform height. The lowest point of the CoM for an expected 10 centimeter drop is 17% of the CoM height at VLO (0.0074 SD) and 12% (0.0024 SD) for an unexpected 10 centimeter drop. For

nominal walking platform of the stance leg not subjected to the downstep, up-step: the step from the downstep platform upon the nominal walking platform.



Figure 3.3: Gait tiles of the human subject in OpenSim walking over an **unexpected** 10 cm downstep.

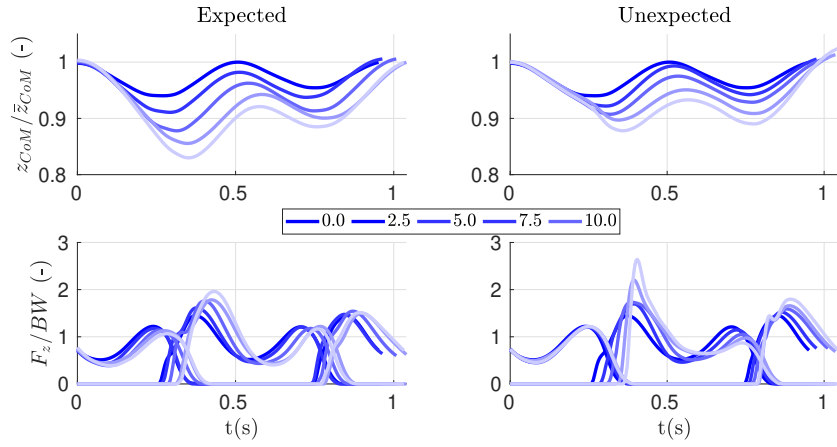


Figure 3.4: Average vertical CoM position and vertical GRF for walking over flat ground, expected, and unexpected downsteps. The GRFs start at the VLO before the downstep, switch to the swing leg experiencing the downstep, and end at the original stance leg when the downstep has been overcome.

the nominal walking condition, the lowering of the CoM height is only 6% which is in accordance with other findings in literature [4].

For these expected downsteps, the lowering of the CoM produces a reduced impact force of the swing leg experiencing the downstep. However, for unexpected downsteps, the change in vertical CoM height during downstep is predominantly caused by the passive pendulum properties of the stance leg, and the peak of the GRF is significantly higher compared to the expected downsteps. With the subjects being instructed to ‘continue’ walking, an essential metric regarding stability is the angular momentum around the stance contact location. This metric culminates human behavior regarding the horizontal and vertical CoM position with the resulting forward walking velocity. The angular momentum around the ground contact of the current stance leg can be computed as

$$L_{st} = \sum_{i=0}^{N_{\text{segments}}} r_i \times m_i \dot{r}_i + I_i \dot{\theta}_i, \quad (3.1)$$

where N_{segments} is the number of body segments, r_i is the position of the CoM of segment i in the stance-foot frame, and m_i , I_i , and $\dot{\theta}_i$ are the mass, inertia, and rotational velocity around its own CoM respectively. The trajectory of the angular

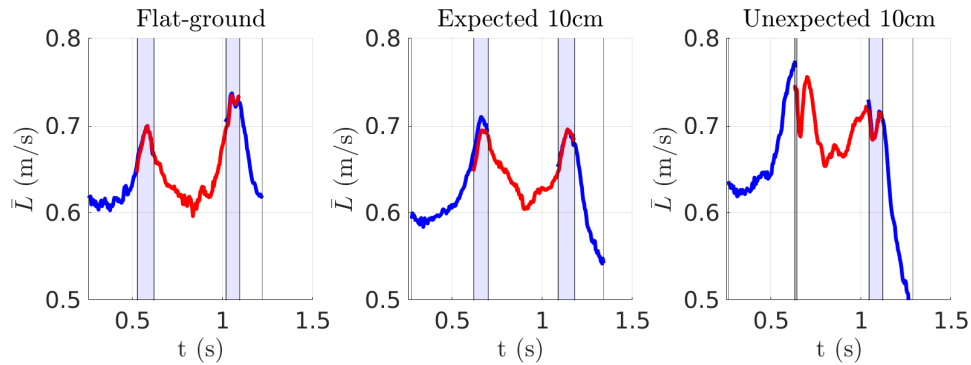


Figure 3.5: Averaged trajectories of the angular momentum around the contact point for walking on flat-ground, expected, and unexpected downsteps (with 10 centimeter depth). Blue boxed regions indicate the DSP.

momentum around the ground contact point of the current stance leg is shown in Fig 3.5. These results indicate that angular momentum is much more constrained towards the flat-ground walking condition for expected trials. This smaller deviation in the angular momentum compared to unexpected downstep trials is caused by the reduced vertical CoM position and the smaller change in horizontal CoM velocity. An increase in down-step stepsize causes changes to the nominal step-lengths in unexpected downstep trials that were governed by the passive dynamics of the swing leg instead active swing leg positioning. We will later see that these differences in step length for expected and unexpected trials can be remedied by the H-LIP walking in Chapter 4.

3.3 HUMAN DATA INTERPOLATION

In order to abstract the human data to a representation that can be used in the Reduced Order Model (RoM) realization in Chapter 4 and 6, we create an interpolated surface. The creation of this surface is supported by the smoothness of the results for different downstep heights (for both expected and unexpected downsteps) which has been made apparent in Figure 3.4. Subsequently, from the measurement data, we create C^1 (continuously differentiable) surfaces for the vertical CoM position and the desired GRFs shown in Figure 3.6 and 3.7. For the vertical CoM position, we pose a Bézier polynomial optimization for the three compensatory steps according to

$$\begin{aligned} \min_{\alpha} \quad & \sum_{i=1}^3 \|z_{\text{CoM},i}^d(\tau) - z_{\text{CoM},i}^{\text{Bézier}}(\tau, \alpha_i)\|^2 & (3.2) \\ \text{s.t.} \quad & z_{\text{CoM},1}^{\text{Bézier}}(0, \alpha_1) = z(0) & (\text{IC}) \\ & \dot{z}_{\text{CoM},1}^{\text{Bézier}}(0, \alpha_1) = 0 \\ & z_{\text{CoM},3}^{\text{Bézier}}(1, \alpha_1) = z(0) & (\text{FC}) \\ & \dot{z}_{\text{CoM},3}^{\text{Bézier}}(1, \alpha_3) = 0 \\ & z_{\text{CoM},i}^{\text{Bézier}}(1, \alpha_i) = z_{\text{CoM},i+1}^{\text{Bézier}}(0, \alpha_{i+1}), k \in \{1, 2\} & (\text{Continuity}) \\ & \dot{z}_{\text{CoM},i}^{\text{Bézier}}(1, \alpha_i) = \dot{z}_{\text{CoM},i+1}^{\text{Bézier}}(0, \alpha_{i+1}), k \in \{1, 2\}, \end{aligned}$$

where α is the set of Bézier polynomial parameters for all three steps, i is the step (1: down-step, 2: over-step, or 3: up-step), τ is the phasing variable $\tau \in [0, 1]$, IC indicates the initial condition at the VLO before the downstep, FC indicates the final condition at the VLO after the downstep, and Continuity indicates the continuity constraints between the steps i and subsequently realizes the C^1 surface. The total step-time or duration is implicitly constrained as the Bézier polynomials are fitted onto the normalized stepping time range $\bar{t} \in [0, 1]$ in the walking implementations in Chapter 4 and 6. The Bézier polynomials are defined as

$$z(\tau, \alpha) = \sum_{j=0}^{N_{\alpha}} \alpha_j \frac{N_{\alpha}!}{j!(N_{\alpha} - j)!} \tau^j (1 - \tau)^{N_{\alpha} - j}, \quad (3.3)$$

where N_{α} is the order of Bézier polynomial. A similar optimization problem is constructed for each curve of the GRFs. The continuity is enforced between Double Support and Single Support Phases of the respective steps i . In our analysis from pre-downstep to post-downstep VLO, three legs are in contact with the ground; the initial stance leg on the nominal walking platform, the initial swing leg that impacts the downstep platform, and the initial stance leg when it impacts the nominal walking platform after the downstep platform impact. Subsequently, three surfaces are created. In Figure 3.6 and 3.7, interpolation surfaces of the vertical CoM trajectory

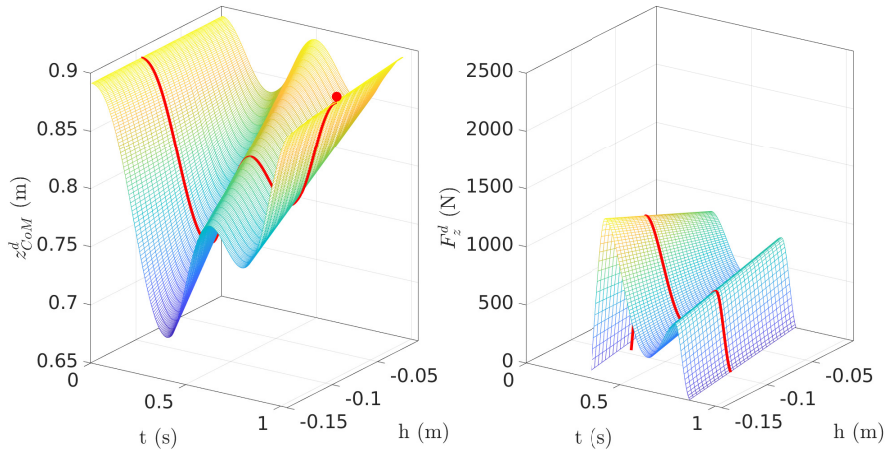


Figure 3.6: The desired vertical CoM trajectory z_{CoM}^d and the GRF in SSP parameterized by time (t) and the downstep height h for **expected** downsteps.

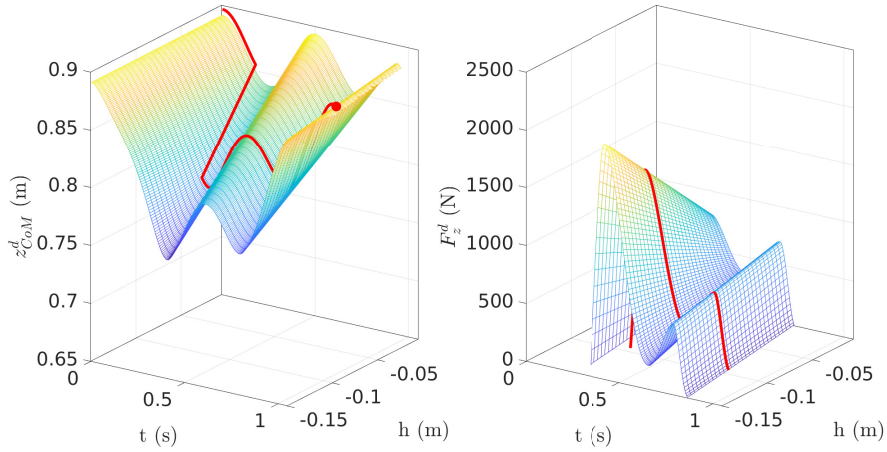


Figure 3.7: The desired vertical CoM trajectory z_{CoM}^d and the GRF in SSP parameterized by time (t) and the downstep height h for **unexpected** downsteps.

and the vertical GRF of the initial swing leg on the downstep platform are shown. These figures also highlight the C^1 curves are traversed during an expected and unexpected downstep. For the expected downstep, the trajectory of the vertical position of the CoM is adapted from the moment of the VLO before the downstep, as it is known that the subsequent step will be subjected to a change in walking height. The vertical CoM and the vertical GRF are equal at the VLO after the downstep and the VLO of nominal walking. This continuity enables the smooth transition from downstep behavior to nominal walking behavior. For the unexpected downsteps, the trajectory may only be adapted when the swing foot detects the downstep (penetrates the virtual ground surface). The red trajectory in Figure 3.7 changes direction after the nominal walking surface penetration. The swing foot travels through the downstep height until it reaches the downstep platform while the position of the vertical CoM is guided to the desired height which corresponds with the currently detected downstep height. After impact, the downstep height is known to the biped (human or robot), and the trajectory of this downstep height h is followed for the remaining compensatory behavior.

The complex underlying principles of locomotion, such as interactions between the biped and the environment, overactuated joint-level motion generation, high-dimensionality, and nonlinear hybrid dynamics, make a full-body analysis of human locomotion a daunting task. However, these principles can often be abstracted towards a simple model that resolves the redundancy by exhibiting the targeted behavior of the walker with the least number of variables and parameters possible [72]. For example, bipedal organisms that differ in overall morphology, such as humans, birds, and even kangaroos, can all be represented by a decoupled spring-mass-damper inverted pendulum model in the sagittal- and coronal plane [73] that exhibit the targeted CoM kinematics and GRFs. Analyzing the motion of the human for application towards morphologically different robots therefore promotes the abstraction towards an equivalent template model (or Reduced Order Model).

The template and anchor framework [72] has been key in developing a thorough understanding of abstraction methods for bipedal locomotion. Although the spring-mass properties in human locomotion has already been known since the 17th century [74], its abstraction remains vital in both the analysis of the human gait and the development [34; 36] and control [75; 17; 76; 77] of bipedal robots. However, it was also observed that the canonical Spring-Loaded Inverted Pendulum (SLIP) model shown in Figure 4.1 could not accurately describe the vertical and horizontal kinematics while simultaneously representing the observed GRFs. The foot-roll phases as addressed in Chapter 2.1.1 necessitates the introduction of actuation and damping into the system. We consider an actuated SLIP model, which has been successful in offline trajectory optimization for Cassie [17; 78], and as the descriptor of the human nominal and compensatory motion. The reason for introducing this aSLIP is threefold;

- Contributions of muscle activation (either intentional, as a reflex, or as a preflex [79]¹) and changes to posture alter the dynamic behavior of the human walking over expected and unexpected downsteps. The subsequent analysis would be high dimensional.
- The raw measurement data presented using IK is noisy and is only to an assumed extent representative of a point-mass model.
- The aSLIP can accurately describe the compliant Cassie model for gait generation.

In order to obtain a tractable analysis of the dynamics, which is a closer representation of the RoM, we abstract the human towards the actuated Spring-Loaded Inverted Pendulum (aSLIP) model from [17; 78] with optimized system parameters using Direct Collocation optimization. We initialize the solution of the optimization with the polynomial fits of the human measurement data and solve using the non-convex solver IPOPT [80].

¹ Muscular reactionary behavior from the passive force-length and force-velocity properties of the muscle.

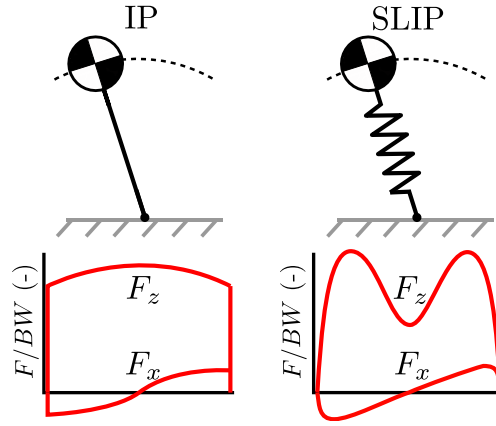


Figure 4.1: Inverted Pendulum (IP) and Spring-Loaded Inverted Pendulum (SLIP) reduced order models and their respective simulated GRFs in the vertical and horizontal direction.

4.1 THE ACTUATED SPRING-LOADED INVERTED PENDULUM MODEL

The dynamics of the aSLIP model are described in Appendix C which contain an SSP and DSP with an impact map from SSP to DSP (the transition from DSP to SSP is smooth). Figure 4.2 presents a schematic overview of the aSLIP model in SSP and DSP. For a polynomial expression of the stiffness and damping of the leg spring, the force in the spring is equal to the GRF. This force is computed as

$$F_s = K(L)s + D(L)\dot{s}, \quad (4.1)$$

where $s = L - r$ is the compression of the leg spring with L as the uncompressed length and r as the compressed or real length as indicated in Figure 4.2. The aSLIP walker is subsequently an underactuated point-foot walker with compliance. During SSP, the inertia of the swing leg is ignored, and the step-length of the nominal and compensatory gait can always be realized. Although Chapter 3 has shown that the ankle torque plays a role in both the nominal and the compensatory downstep gait, this ankle actuation is not introduced in the RoM. The simultaneous control of the CoM kinematics with the leg and ankle actuation would lead to an ill-posed optimization problem where the trade-off between tracking and energy expenditure would lead to vastly different solutions. The contribution of the ankle torque is therefore realized via the control of the uncompressed length of the spring.

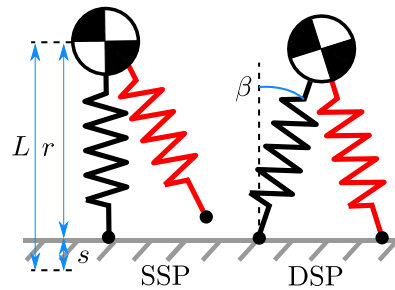


Figure 4.2: aSLIP model in SSP (at VLO) and DSP.

4.2 REDUCED ORDER MODEL FITTING

We construct a non-convex optimization problem for fitting the behavior of the human to the aSLIP model. With the introduction of the actuation, we will jointly optimize a leg-length dependent stiffness and damping for nominal walking and acceleration of the rest-length of the leg spring. The changes to the representative stiffness of the human leg are therefore encapsulated by the change in the physical length and the rest-length of the leg spring. We consider the compensatory behavior to be between the pre- and post-downstep VLO and jointly optimize 5 phases: the initial SSP at VLO, the touch-down on the downstep platform introducing DSP, the over-step during the second SSP, the touch-down on the nominal walking platform of this leg introducing the second DSP, and the lifting of the leg from the downstep platform until the final VLO during the third SSP. We wish to fit the reduced-order model both as an analysis tool and for obtaining the leg-length dependent stiffness of the representative leg from the ground-contact point to the CoM. We are subsequently requiring the model to exhibit the kinematic and kinetic behavior of the human in nominal walking and walking over expected and unexpected downsteps. We pose the optimization problem in which we define the cost by tracking the vertical CoM position and the energy expenditure of both legs. Soft constraints on the duration of the downstep ensure the horizontal CoM kinematics. The Direct Collocation optimization is formulated as

$$\begin{aligned}
 \min \quad & \sum_{i=1}^5 (||z^a - z^d||^2 + w(||\ddot{L}_1||^2 + ||\ddot{L}_2||^2)) & (4.2) \\
 \text{s.t.} \quad & f_{\text{aSLIP}} + g_{\text{aSLIP}}\ddot{L} = 0 & (\text{dynamics constraints}) \\
 & \mathbf{x}_i = \mathbf{x}_{i+1} & (\text{state continuity}) \\
 & \mathbf{x}_0 = \mathbf{x}_5 & (\text{VLO to VLO continuity}) \\
 & F_{z,k}(t) \geq 0, \forall k, \forall t & (\text{positive GRFs}) \\
 & F_{z,sw}(0) = 0 \wedge F_{z,st}(t_f) = 0, \forall k, & (\text{smooth transitions})
 \end{aligned}$$

where

- i indicates a phase of the walking gait,
- $w \in \mathbb{R}$ is a scaling parameter on the cost,
- \ddot{L}_j is the acceleration on the rest-length of leg j ,
- f_{aSLIP} and g_{aSLIP} represent the equations of motion of the aSLIP model in either SSP or DSP,
- \mathbf{x}_i indicates the full state of the system at phase i ,
- $F_{z,k}$ is the vertical GRF at phase k , and
- $F_{z,st}$ and $F_{z,sw}$ are the vertical GRFs of the current stance and new stance leg respectively.

From the optimization, we also obtain the leg length-dependent stiffness, for which we assume a second-degree polynomial as shown in Figure 4.3, and a constant damping coefficient. Higher degrees of parameterizations of the stiffness and damping were evaluated in the same optimization framework, which did not show an improvement on lowering the cost. The optimization is solved using IPOPT [80] with 20 nodes per phase.

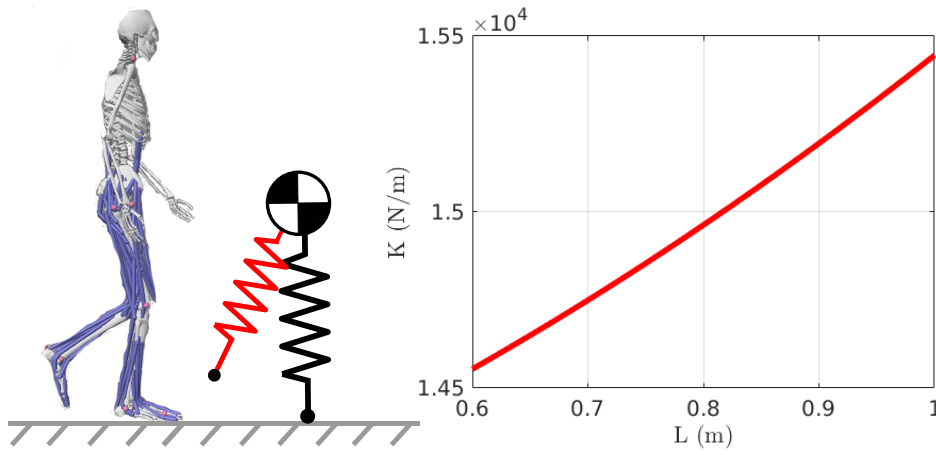


Figure 4.3: Abstraction of the human kinematics and kinetics towards the reduced order aSLIP model of walking. We optimize a quadratic stiffness that minimizes Equation (4.2).

4.3 REDUCED ORDER MODEL WALKING REALIZATION

We wish to realize closed-loop walking that exhibits the observed kinematic and kinetic behavior with the leg stiffness and damping from the optimization. To this end, we employ the Backstepping Barrier Function (BBF) [37] and the Step-to-Step (S2S) dynamics of the Hybrid Linear Inverted Pendulum (H-LIP). The vertical state is tracked using a backstepping controller with CLFs (Chapter 2.3.2) for vertical tracking and realization of the GRFs using Control Barrier Functions [81; 82]. The horizontal state is stabilized using a closed-form stepping formulation using H-LIP RoM, which relies on a constant CoM height that makes the step-to-step S2S dynamics of the model linear [78; 35].

The stiffness and damping of the leg spring from the direct collocation optimization are used as the parameters in the walking model of the aSLIP. The following section closely follows [37].

4.3.1 Vertical CoM Tracking

For the vertical state, we define the control objective to drive the vertical CoM position to follow the desired trajectory from Figures 3.6 and 3.7. These output definitions prescribe the vertical CoM kinematics for flat-ground walking and during expected and unexpected downsteps. The output is defined as

$$\eta = \begin{bmatrix} z_{\text{CoM}} - z_{\text{CoM}}^d(t) \\ \dot{z}_{\text{CoM}} - \dot{z}_{\text{CoM}}^d(t) \end{bmatrix}, \quad (4.3)$$

where superscript d indicates the desired time dependent vertical trajectory from the human data. The output dynamics are

$$\dot{\eta} = \begin{bmatrix} \dot{z}_{\text{CoM}} - \dot{z}_{\text{CoM}}^d(t) \\ \ddot{z}_{\text{CoM}} - \ddot{z}_{\text{CoM}}^d(t) \end{bmatrix} = \underbrace{\begin{bmatrix} \dot{z}_{\text{CoM}} - \dot{z}_{\text{CoM}}^d(t) \\ -g - \ddot{z}_{\text{CoM}}^d(t) \end{bmatrix}}_{f_\eta} + \underbrace{\begin{bmatrix} 0 \\ \frac{1}{m} \end{bmatrix}}_{g_\eta} F_z^P, \quad (4.4)$$

where F_z^P is the net vertical force on the CoM for each domain P (SSP or DSP). The GRF is related from the spring forces in the leg; e.g., during the SSP, the vertical component of the GRF and its first order time derivative is in accordance with Equation (4.1),

$$F_z^{\text{SSP}} = (K(L)s + D\dot{s}) \cos(\beta_{st}), \quad (4.5)$$

$$\begin{aligned} \ddot{F}_z^{\text{SSP}} = & \left(\frac{\partial K(L)}{\partial L} \dot{L}s + K(L)\dot{s} \right) \cos(\beta_{st}) - K(L)s \sin(\beta_{st}) \dot{\beta}_{st} + \\ & D\dot{s} \cos(\beta_{st}) - D\dot{s} \sin(\beta_{st}) \dot{\beta}_{st}, \end{aligned} \quad (4.6)$$

where β_{st} is the stance leg angle from Figure 4.2. The time derivative of the vertical component of the GRF is affine in the control input \dot{L} as $\dot{s} = \dot{L} - \dot{r}$. We can define the affine control system for which the state is the input to the system in Equation (4.4)

$$\dot{\eta} = f_{\eta} + g_{\eta} F_z^P \quad (4.7)$$

$$\dot{F}_z^P = f_z + g_z \dot{L}, \quad (4.8)$$

where \dot{L} is thus the acceleration of the rest-length of the aSLIP. As this system is in *strict-feedback form*, we can apply a control Lyapunov function version of the canonical backstepping to stabilize the dynamics of both systems. For the system in (4.7), a feedback linearizing controller can be synthesized

$$\bar{F}_z = \frac{1}{g_{\eta,2}} (-f_{\eta,2} + K_{FL}\eta), \quad (4.9)$$

where $K_{FL} = [K_P, K_D]$ is the feedback gain matrix, and subscript 2 indicates the second element of the vector. The closed-loop stable system is rendered

$$\dot{\eta} = f_{\eta} + g_{\eta} \bar{F}_z^P = A_{cl}\eta. \quad (4.10)$$

We can define a Lyapunov function on the closed-loop dynamics to realize τ_z that stabilizes η with the augmented Lyapunov equation [66] according to

$$V(\eta, F_z) = \eta^T P \eta + \frac{1}{2} (F_z - \bar{F}_z)^2. \quad (4.11)$$

More details can be seen in [37]. Given that we want to supply the controller with additional constraints concerning the GRFs, we use a CLF-QP from Chapter 2.3.2 which states that as long as the CLF constraint is satisfied, the controller guarantees exponential convergence of η (the vertical CoM kinematics) to 0.

4.3.2 Contact Force Embedding

We also want to enforce the desired GRF from human walking to ensure dynamic similarity between the human and the RoM. Since the time derivative of F_z is affine in the control input \dot{L} we can realize contact force embedding with Control Barrier Functions (CBF) [82; 81] based on the constraint

$$(1 - c)F_z^d + \Delta_F \leq F_z^a \leq (1 + c)F_z^d - \Delta_F, \quad (4.12)$$

where $c \in (0, 1)$ is a relaxation parameter and Δ_F is an additional bound such that the permissible set at the boundary of DSP is nontrivial [37]. A schematic representation of this constraint is shown in Figure 4.4. This force-embedding is included in both the SSP and the DSP as linear constraints in the CLF-QP. In *SSP*, we define a single CBF that ensures the GRF of the robot remains in a relaxed tube. In *DSP* the former stance foot has a GRF that goes to zero while the former swing foot has a GRF that goes from zero to the initial GRF of the following SSP. During the downstep, we use the interpreted GRF trajectories from Figure 3.6 and 3.7 as the desired F_z^d . The CLF-QP is formulated as

$$\min_{\dot{L}_{st/sw}, \delta} \quad \ddot{L}_{st/sw}^2 + p\delta^2 \quad (4.13)$$

$$\text{s.t.} \quad L_f V(x) + L_g V(x) \dot{L}_{st/sw} + \lambda V(x) \leq \delta \quad (\text{ES-CLF})$$

$$L_f h(x) + L_g h(x) \dot{L}_{st/sw} \geq -\alpha(h(x)). \quad (\text{CBF})$$

Friction cone constraints are subsequently not explicitly considered but the embedding of the vertical GRF ensures that the horizontal components are reasonable and not expected to exceed the constraints from Equation (2.5).

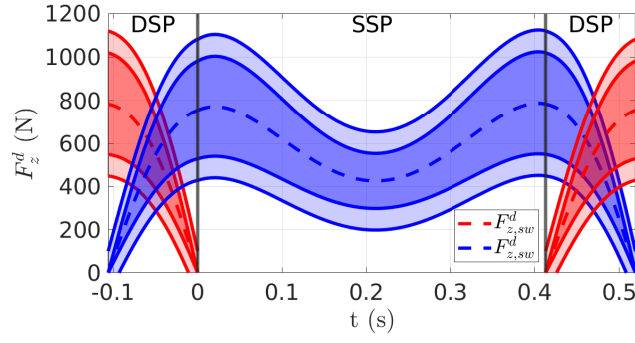


Figure 4.4: Force embedding representation for DSP and SSP indicating the relaxation $(1+c)$ and the additional bound Δ_F according to Equation (4.12). Notice that $F_{z,sw}^d$ is a slice of the desired GRF in Figure 3.6 or 3.7 at $h=0$.

4.3.3 Horizontal stabilization

The horizontal state is stabilized using the S2S dynamics approximation via the Hybrid Linear Inverted Pendulum (H-LIP) [78; 35]. Using a constant height assumption on the vertical CoM during SSP and DSP (which is an approximation due to the tracking of the human vertical CoM behavior), the S2S dynamics of the system can be described in closed-form. The horizontal dynamics of the H-LIP model are described by

$$\ddot{p} \begin{cases} \ddot{p} = \lambda^2 p & \text{if SSP} \\ \ddot{p} = 0 & \text{if DSP} \end{cases} \quad (4.14)$$

where p is the horizontal position of the CoM with respect to the stance foot and $\lambda = \sqrt{g/z_0}$ with g being the gravity constant and z_0 being the nominal walking height. The S2S dynamics (from the end of SSP of step k to the end of SSP of step $k+1$) of the H-LIP are step-size and step-time dependent according to

$$\mathbf{x}_{\text{SSP}k+1}^- = \underbrace{e^{A_{\text{SSP}}T_{\text{SSP}}}}_A \begin{bmatrix} 1 & T_{\text{DSP}} \\ 0 & 1 \end{bmatrix} \mathbf{x}_{\text{SSP}k}^- + \underbrace{e^{A_{\text{SSP}}T_{\text{SSP}}}}_B \begin{bmatrix} -1 \\ 0 \end{bmatrix} u_k, \quad (4.15)$$

where u_k is the step-size, T_{SSP} and T_{DSP} are the duration of the SSP and DSP respectively, and A_{SSP} originates from the state-space representation of the SSP dynamics

$$\frac{d}{dt} \begin{bmatrix} p \\ \dot{p} \end{bmatrix} = \underbrace{\begin{bmatrix} 0 & 1 \\ \lambda^2 & 0 \end{bmatrix}}_{A_{\text{SSP}}} \begin{bmatrix} p \\ \dot{p} \end{bmatrix}. \quad (4.16)$$

As mentioned previously, in reality we have a non-constant vertical CoM position from the aSLIP nominal gait and compensation optimization $\dot{p} = \lambda^2 p = gp/z_{\text{CoM}}(t)$, yet the contribution of this deviation contributes to model difference between the H-LIP and the system (human or robot) according to

$$x_{k+1} = Ax_k + Bu_k + w, \quad (4.17)$$

where the disturbance w represents the model difference between the H-LIP and the aSLIP RoM walker. The stepsize for flat-ground walking is determined by

$$u_k^d = u_k^{\text{H-LIP}} + K(x^{\text{aSLIP}} - x^{\text{H-LIP}}), \quad (4.18)$$

where $u_k^{\text{H-LIP}}$ is the nominal step-size of the H-LIP, K is the deadbeat gain (i.e. $(A+BK)^2 = 0$) which stabilizes the H-LIP model to the desired post-impact state in

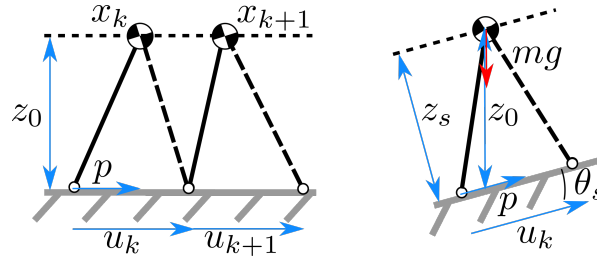


Figure 4.5: H-LIP walking on flat terrain and on a slope of θ_s radians.

one step, and x^{aSLIP} is the horizontal state of the aSLIP walker. More details of the H-LIP stepping can be found in [35]. For the downstep scenarios, the H-LIP is taking the *slope* of the walking surface into account. For the expected downstep, the slope is altered at the VLO before the downstep based on the previous step-size and the known downstep height. For the unexpected downstep, the slope is altered continuously based on the current step-size and the penetration of the swing foot. In accordance with Figure 4.5, θ_s is defined as

$$\begin{aligned} \text{expected} & \begin{cases} \theta_s = \arctan\left(\frac{-h}{u_{k-1}}\right) & \text{if step = down-step} \\ \theta_s = \arctan\left(\frac{h}{u_{k-1}}\right) & \text{if step = over-step} \\ \theta_s = 0 & \text{if step = up-step} \end{cases} \\ \text{unexpected} & \begin{cases} \theta_s = \arctan\left(\frac{-z_{\text{sw}}}{u_{k-1}}\right) & \text{if step = down-step} \\ \theta_s = \arctan\left(\frac{h}{u_{k-1}}\right) & \text{if step = over-step} \\ \theta_s = 0 & \text{if step = up-step} \end{cases} \end{aligned} \quad (4.19)$$

where z_{sw} is the vertical position of the swing foot with respect to the stance foot, u_{k-1} is the step-size before the VLO of the initial down-step, and h is the downstep height. The desired post-impact state of the H-LIP is therefore stated as

$$x_{\text{H-LIP}}^d = \frac{\dot{x}_{\text{H-LIP}}^d}{\sigma} + z_0 \sin(\theta_s), \quad (4.20)$$

where $\dot{x}_{\text{H-LIP}}$ is the desired walking velocity, σ is the orbital slope of the periodic orbits for a specific SSP duration according to

$$\sigma := \lambda \coth\left(\frac{T_{\text{SSP}}}{2} \lambda\right), \quad (4.21)$$

where T_{SSP} is the predefined SSP duration. The desired post-impact state adaptation negates the influence of the vertical CoM deviation from the H-LIP nominal height z_0 when the walker is walking over the downsteps. Details on the orbit characterization of the H-LIP, including Period-1 and Period-2 orbits for sagittal walking and coronal stabilization respectively, can be found in [35].

4.3.4 Control Structure

The RoM walking realization is able to simultaneously traverse expected and unexpected downsteps. Both scenarios consist of three steps; the partial step from either VLO before the downstep or the virtual ground penetration until the downstep platform impact, the full step from original stance leg take-off until original stance-leg impact on the recovery platform, and the partial step from the downstep swing leg take-off until the VLO after the downstep. As such, a count keeps track of the number of steps that have been taken during the compensatory behavior. The offline generated surfaces from Figure 3.6 and 3.7 are applied in an online feedback motion planning methodology. The H-LIP stepping directly determines the swing leg position and the human CoM

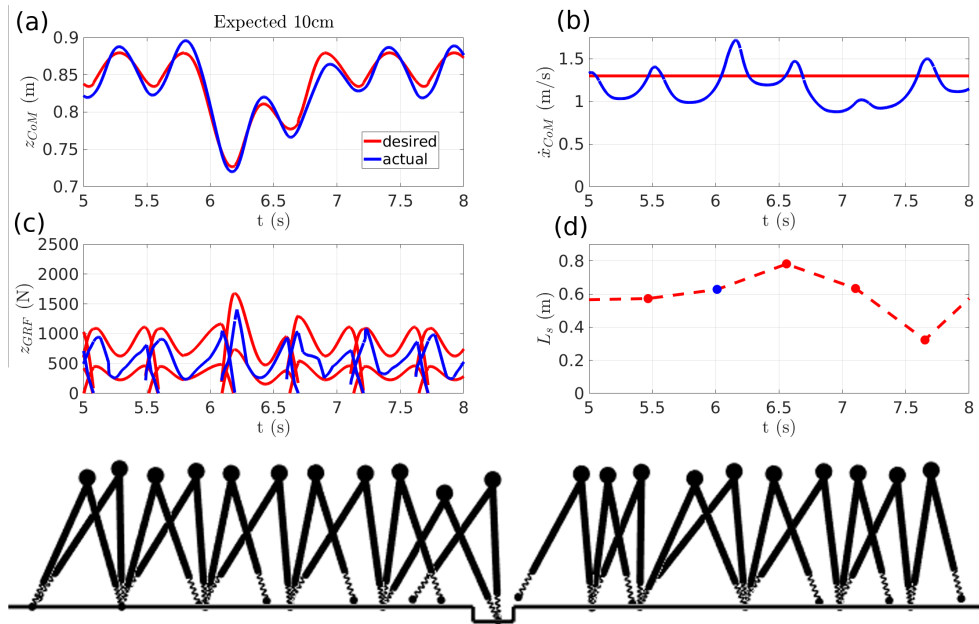


Figure 4.6: Simulation results of the aSLIP walking over the **expected** downstep with 10 centimeter depth: (a) the vertical mass trajectories of the desired ones and the actual ones, (b) the horizontal velocity of the mass, (c) the GRF profile with its bounds, and (d) the step-lengths

4.4 RESULTS

Figures 4.6 and 4.7 show the simulation results of the aSLIP walker for expected and unexpected downsteps for a 10 centimeter downstep height respectively. The gait tiles of the aSLIP walker for these conditions are shown at the bottom of the respective figures with a capture interval of 0.2 seconds. Figure 4.8 shows the coupling of the trajectory generation and the BBF control structure.

We observe that both scenarios track the vertical CoM position to a desirable accuracy. For the unexpected downstep, the descent according to the surface in Figure 3.7 is clearly visible. The post-VLO trajectory is equal to the nominal walking trajectory until the swing foot penetrates the ground (and the DSP would begin under nominal walking conditions). This realizes a desirable lowering of the vertical CoM position in the limited duration of swing foot travel and the first half of the DSP. The forward walking velocity expectantly oscillates around the desired velocity. For the expected downstep scenario, the compensatory behavior minimally affects the forward walking velocity. This aligns with our observations from the human experiments in Figure 3.5. The forward walking velocity significantly decreases during the unexpected downstep, predominantly during the up-step. The reason for this is the mass-less swing leg which can instantaneously be set to the desired position during the penetration swing phase. The stabilization of the forward walking velocity is additionally affected by the deviation of the vertical CoM position from the H-LIP nominal walking height.

For the expected downstep scenario, for which the vertical CoM position is lowered more significantly than for the unexpected downstep scenario, the difference between the H-LIP RoM and the aSLIP walker is amplified. This results in a less conservative step length. Regardless, the H-LIP on flat ground and under the down-, over-, and up-step conditions from Equation (4.19) excellently stabilizes towards the desired walking velocity post-downstep. From Figures 4.6 and 4.7 it can also be

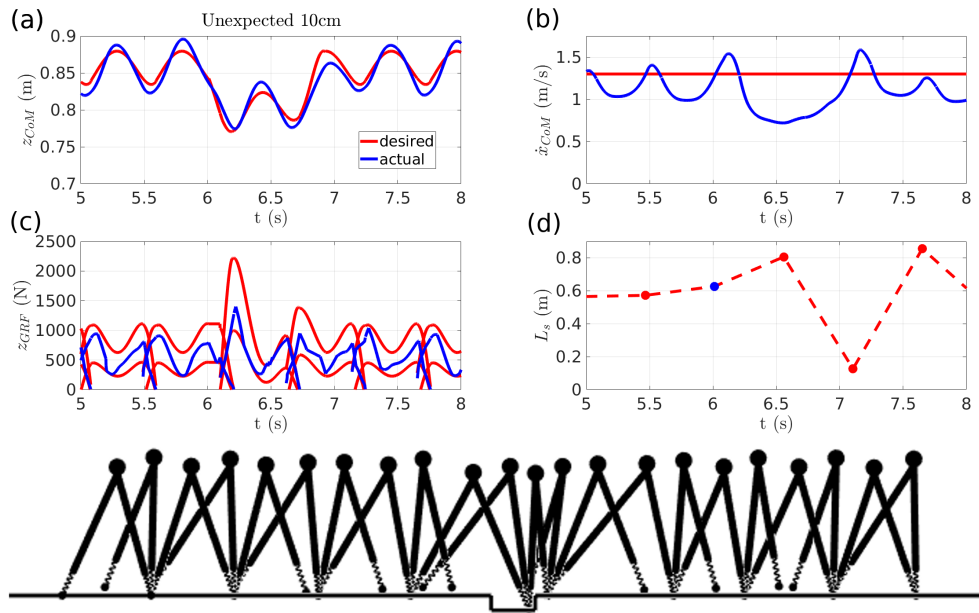


Figure 4.7: Simulation results of the aSLIP walking over the **unexpected** downstep with 10 centimeter depth: (a) the vertical mass trajectories of the desired ones and the actual ones, (b) the horizontal velocity of the mass, (c) the GRF profile with its bounds, and (d) the step-lengths

seen that the vertical GRFs lay within the relaxed tube of the force-embedding. The BBF realization requires a relaxation factor of 0.4 during downstep behavior. For nominal walking, this factor can be reduced to 0.2. An additional difficulty in realizing human-like behavior in the forward walking direction is the coupling of the control of the horizontal and vertical CoM position. Under a non-zero leg angle β , the horizontal position of the CoM is also affected by the vertical stabilization with the CLF-QP. This affects the horizontal velocity of the CoM and therefore affects the step size.

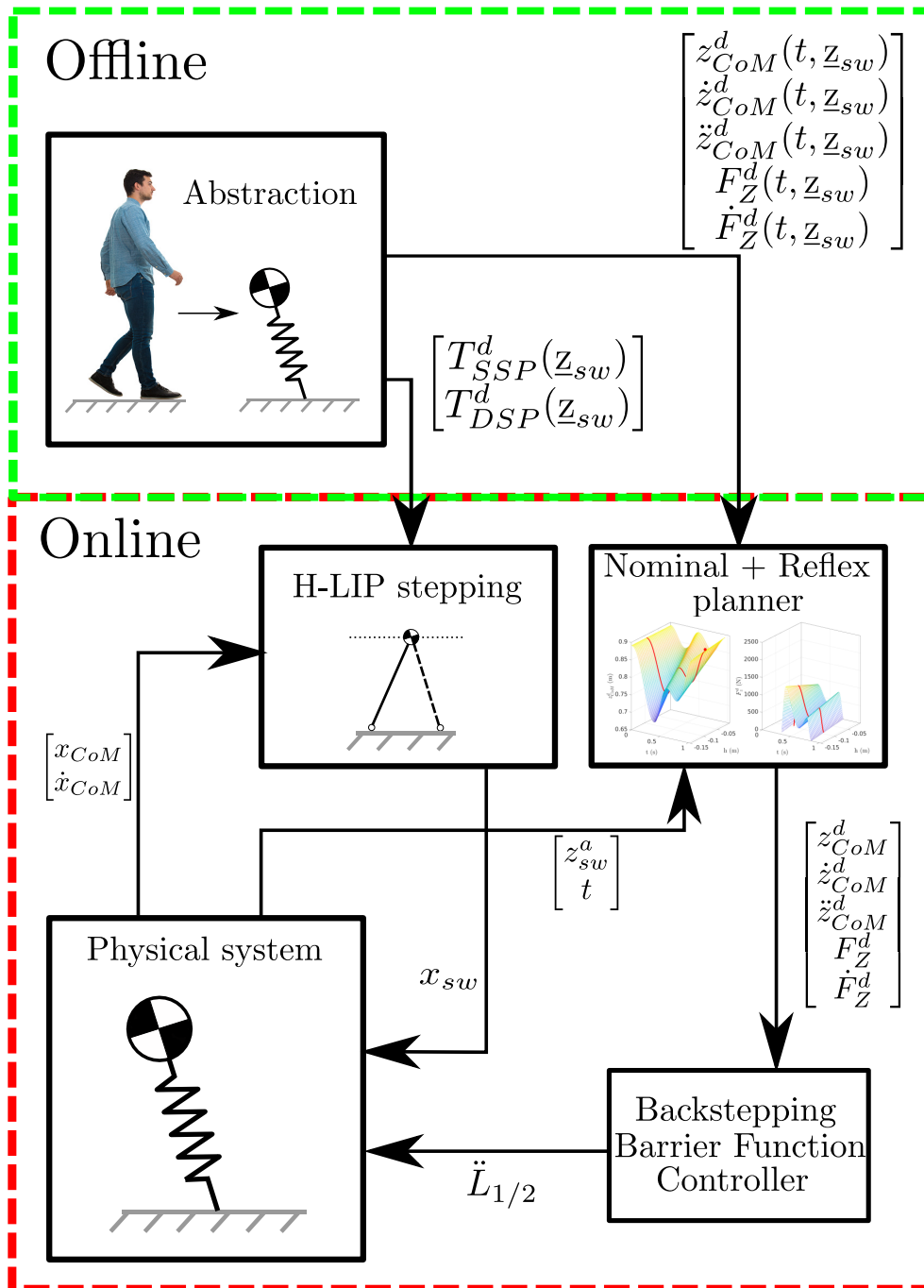


Figure 4.8: Trajectory generation based on the reduced-order model analysis and the feedback control structure of the Backstepping Barrier Function walking realization on the aSLIP model.

5

ROBOT WALKING SYNTHESIS

The outputs from the human, such as the desired vertical CoM kinematics, the desired GRFs, the step-time, and the forward walking velocity, cannot be applied to morphologically different bipeds as it will not necessarily result in realizable walking on a robot with different natural dynamics. As we wish to ensure dynamic similarity between the robot and the human, this walking behavior and these parameters should be scaled towards the representative aSLIP of Cassie from [78]. In this chapter, we present our human-to-robot walking synthesis for Cassie [36], with significant morphological differences compared to humans.

5.1 OUTPUT DEFINITIONS

Initial work was conducted on a representation of Cassie, which was fully actuated in the sagittal plane (with the use of ankle torque actuation). Full actuation requires a forward walking output for which the forward CoM velocity \dot{x}_{CoM} was chosen (an RD1 output). The outputs were phased with the forward CoM position with respect to the stance leg x_{CoM} . The step-sizes of the biped were determined offline. Although this proved to be successful in 2D walking in MATLAB, it proved to be difficult in realization in 3D (in a physics-based simulator as opposed to forward integrating and directly controlling the equations of motion of Cassie in Equation (2.2)). Later improvements for underactuated walking with the H-LIP stepping controller from Chapter 4.3.3 removed this requirement to phase with the horizontal CoM position and instead allowed us to determine a mean (or nominal) walking velocity and phase the outputs with time.

Additionally, initial work on the deviation of the vertical CoM kinematics was based on findings of human walking in literature for which relationships between vertical CoM oscillation, step-size, and walking velocity were determined [83; 84; 85]. These relationships were then applied to scale the trajectories from the human to Cassie. This resulted in a less robust walking realization. Furthermore, the human relationships were based on a full-order model instead of our assumed RoM, which convinced us to state a different walking synthesis. The results of that are presented in the next section.

5.2 HUMAN INSPIRED TRAJECTORY SYNTHESIS

Before we translate the observed motion and dynamics of the human to a bipedal robot, we first emphasize several differences between the two systems; the human and the robot.

- Cassie has a different mass distribution and does not have an upper body or arms. The abstraction towards the CoM assumes whole-body behavior during walking is primarily captured by the CoM dynamics.
- Cassie has an overall lower CoM position during nominal walking.

- Cassie has different [78] or no leg compliance compared to the human test subject for which the representative leg stiffness was determined from the aSLIP direct collocation optimization in Chapter 4.2.
- Cassie is assumed to have point feet, limiting the realizable behaviors such as the foot rolling motion on humans.

To be general, we do not consider the compliance in the robot or complex foot rolling behaviors on the robot for the walking synthesis. Cassie has only been employed as a flat-footed walker and as such, the foot roll phases apparent in the human gait have not been realized.

Based on the RoM characterization of the human walking, we want to transfer the CoM kinematics and the GRF profile from the human to the robot Cassie. Firstly, the nominal *virtual* leg length of Cassie (as defined by the distance between the ground contact point and the CoM instead of the ankle and the hip) is a decision variable that determines the scaling of the other gait parameters. For a chosen averaged leg length over a step, we assume the SSP duration of Cassie is related to that of the human by the passive pendulum properties of the swing phase in nominal walking

$$T_{S,C} = \frac{\sqrt{\bar{L}_C/g}}{\sqrt{\bar{L}_H/g}} T_{S,H}, \quad (5.1)$$

where $T_{S,C}$ and $T_{S,H}$ are the SSP durations of Cassie and human respectively, and \bar{L}_C and \bar{L}_H are the averaged leg length of Cassie and the human respectively. This results in an observed SSP duration from the measurement data of 0.39 seconds and a scaled SSP duration for Cassie of 0.34 seconds approximately. For realizing flat-footed walking on Cassie, we remove the horizontal displacement of the CoM caused by the foot-roll phases in the human gait

$$x_{\text{CoM},C} = \frac{1 - x_{\text{roll}}}{L_{s,H}} x_{\text{CoM},H}, \quad (5.2)$$

where $x_{\text{CoM},C}$ is the scaled horizontal displacement of the CoM for Cassie, x_{roll} is the horizontal displacement of the CoM during the heel and toe roll phases from the human nominal walking trial, $L_{s,H}$ is the leg length of the human, and $x_{\text{CoM},H}$ is the horizontal displacement of the CoM of the human. The DSP duration of Cassie, $T_{D,C}$, is based on the relative duration of the SSP and DSP of the human after removing the duration of the roll-phase. Combining the total step-time, $T_C = T_{S,C} + T_{D,C}$, with the horizontal displacement allows us to redefine the nominal walking velocity for Cassie as

$$\dot{x}_{\text{CoM},C} = \frac{x_{\text{CoM},C}(t_f) - x_{\text{CoM},C}(t_0)}{T_C}, \quad (5.3)$$

where t_0 and t_f are the start and end-time of a step. This significantly reduces the nominal walking velocity for Cassie from 1.22 to 0.82 meters per second. This change is necessitated by the smaller CoM height and the lack of foot roll phases of Cassie with respect to the human. An identical *Froude* number [86; 87] $Fr = \dot{x}_{\text{CoM}} / \sqrt{g\bar{L}}$ theoretically ensures dynamic similarity between walkers, yet the differences in the walking phases prevents the application of this dimensionless quantity.

The desired ground reaction forces are scaled with the mass fraction of the robot and the human according to

$$F_{z,C} = \frac{m_C}{m_H} F_{z,H}, \quad (5.4)$$

where $F_{z,C}$ and $F_{z,H}$ are the vertical GRFs of Cassie and the human respectively and m_C and m_H are the total masses of Cassie and the human respectively. The vertical

Parameter	Human	Cassie
Mass (kg)	66.5	33.0
Mean CoM height (m)	0.87	0.79
Step time SSP (s)	0.41	0.39
Step time DSP (s)	0.10	0.08
Forward walking velocity (m/s)	1.67	0.82

Table 5.1: Walking parameters from human data and Cassie from the human-to-robot walking synthesis.

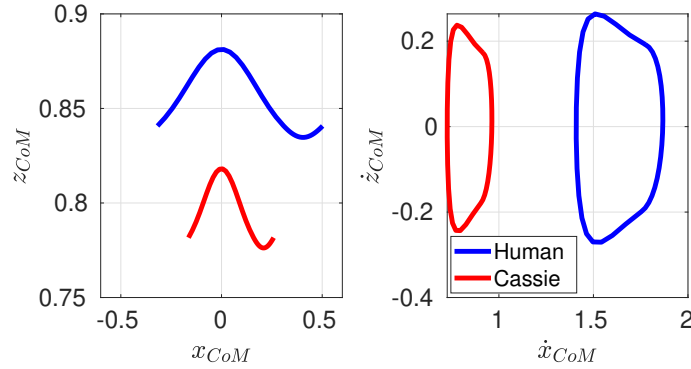


Figure 5.1: Phase portraits of the center-of-mass kinematics of the human and Cassie from the human-to-robot walking synthesis.

CoM trajectory is scaled by the fractional change in virtual leg length of the human and removing the contribution of the roll phases to the stance leg angle. First we define the horizontal and vertical CoM position in a polar coordinate system in accordance to Figure 4.2

$$L_C = \frac{\bar{L}_C}{\bar{L}_H} L_H, \quad (5.5)$$

$$z_{CoM,C} = L_C \cos(\beta_H). \quad (5.6)$$

The phase portraits of the human from observation and of Cassie from scaling are shown in Figure 5.1. The resulting outputs can be embedded onto the aSLIP representation obtained in [17]. For the scaled data, similar multi-parameterized surfaces as shown in Figure 3.6 and 3.7 are available for Cassie. RoM walking results for an expected and unexpected 10cm downstep are shown in Figure D.3 and D.4 in Appendix D.

The nominal and downstep step-times, the vertical CoM kinematics, the forward walking velocity, and the vertical GRFs are employed in the next chapter to realize 3D underactuated walking on Cassie.

6 | 3D ROBOTIC WALKING REALIZATION

In this chapter, we will present the autonomous 3D bipedal walking for nominal and downstep compensation via human-to-robot motion synthesis. We will first present Cassie in more detail and comment on prototyping of the 2D implementation, in which we have considered fully actuated and compliant walking realizations. We will then present details on the walking implementation with Task-Space Control.

6.1 THE BIPEDAL ROBOT CASSIE

The bipedal robot under consideration, as both a representative RoM in Chapter 5 and a full-order 3D walker, is Agility Robotics' Cassie [36] as shown in Figure 6.1. This full-scale biped and its predecessors MABEL [88], and ATRIAS [34], is modeled to closely resemble the SLIP model with the mass mostly concentrated at the pelvis, compliance, and agile lightweight legs. These legs are designed as closed kinematic chains with stiff leaf springs at the knee and the tarsus, as shown in Figure 6.2. This figure also indicates the passive, compliant, and actuated joints. The change in leg length is realized via changing the shape of the compliant kinematic chain.

Each leg of Cassie has five conventional torque actuators. Three actuators are located at the hip, which realize the pitch (flexion/extension), roll (abduction/adduction), and yaw (lateral/medial rotation) of each leg. One actuator is located at the knee, which realizes the change in leg length, and one actuator is located at the ankle, which realizes ankle flexion and dorsiflexion. The ankle toe actuator is located at the tarsus to ensure a low inertia of the swing leg. The compliance in the kinematic chain is relatively low with a joint stiffness of 2300 and 2000 Newton-meters per radian for the knee and the tarsus springs, respectively. Cassie can have underactuation in different ways; firstly, no ankle torque can be exerted on the ground around the forward axis, making Cassie underactuated in the coronal plane, secondly, the compliance of Cassie introduces underactuation in the control

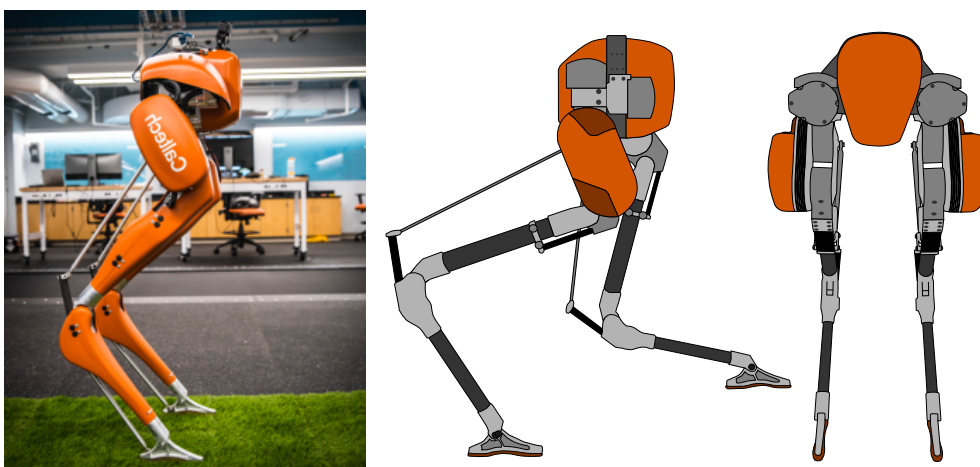


Figure 6.1: The underactuated and compliant Cassie biped with a schematic representation of the side- and front-view.

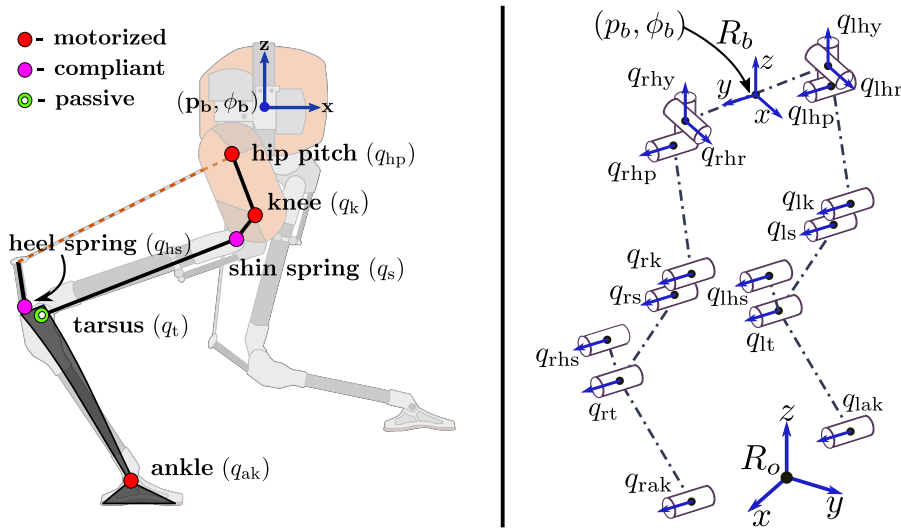


Figure 6.2: The compliant and actuated sagittal joints (left) and the degrees of freedom (right) of the Cassie biped.. Figures in courtesy of Jenna Reher [89].

of the leg length. Lastly, the ankle torque can be disregarded [17; 60; 15; 16] due to the generalization of the resulting walking method.

Although the compliance is present in the RoM walking via the abstraction towards a representative SLIP leg stiffness from the contact point to the CoM position [78], in this chapter, we will see how both a compliant and a rigid Cassie is considered where the leaf springs at the knee and tarsus are considered compliant and non-compliant respectively.

6.2 2D PROTOTYPING

Initial work was conducted on a compliant 2D walking simulation in MATLAB with a corresponding Task-Space Controller. For a compliant model, the joint torques at the compliant joints can be computed as

$$\begin{cases} \tau_{\text{shin}} = K_s q_s + D_s \dot{q}_s \\ \tau_{\text{tarsus}} = K_t q_t + D_t \dot{q}_t \end{cases} \quad (6.1)$$

where K_t and D_t are the joint stiffness and damping of the compliant tarsus joint. The stiffness parameters are provided by the manufacturer [36], the damping is an informed decision variable based on the fiberglass material of the leaf springs. This is in contrast to the rigid model assumption which would introduce the joint-level holonomic constraints on the shin- and heel spring and the tarsus- and knee joint according to

$$\begin{cases} q_s = 0 \\ q_t + q_k = 13 \text{ deg} , \\ q_{hs} = 0 \end{cases} \quad (6.2)$$

which removes the compliance from Figure 6.2; the shin and heel-spring angle are enforced to be zero radians, and the kinematic chain (the tarsus and knee joints) is enforced to be a rigid. The Jacobian of the holonomic constraints is

$$J_h = \begin{bmatrix} J_{st} \\ J_{achilles} \end{bmatrix}, \quad (6.3)$$

where J_{st} represents the Jacobian of the ground contact modelling and $J_{achilles}$ is the Jacobian of the holonomic constraint representation of the achilles rod from Figure 6.2. The rigid model holonomic Jacobian, J_s , is considered separately for clarity. The TSC can be constructed where, building upon the definition in Chapter 2.3.3, we introduce additional cost terms of a slack variable, and the difference between the desired (from joint properties) and actual (from the optimization) joint forces.

$$\begin{aligned}
\min_{u, F_h, F_s, \dot{q}, \delta} \quad & \|\dot{y}^a - \dot{y}^d - \dot{y}^t\|^2 + \|\delta\|^2 + \|F_s - F_s^*\|^2 & (6.4) \\
\text{s.t.} \quad & D\ddot{q} + C = J_h^T F_h + B\tau & \text{(EOM)} \\
& J_h \ddot{q} + \dot{J}_h \dot{q} = 0 & \text{(holonomic)} \\
& J_s \ddot{q} + \dot{J}_s \dot{q} = \delta & \text{(compliant model)} \\
& \tau_{\min} \leq \tau \leq \tau_{\max} & \text{(torque limit)} \\
& A_{GRF} F_{GRF} \leq 0 & \text{(friction cone)} \\
& (1-c)F_z^d - \Delta_F \leq F_{FE} \leq (1+c)F_z^d + \Delta_F, & \text{(force embedding)}
\end{aligned}$$

where

- F_s^* are the torques in the compliant joints from Equation (6.1),
- δ is a vector of slack variables $\delta \in \mathcal{R}^4$ for relaxation of the holonomic constraints to realize compliance (two compliant joints per leg),
- F_{FE} are the vertical components of the contact forces to realize force embedding according to Figure 4.4,
- y^d is the desired output,
- y^a is the actual output, and
- $\dot{y}^t = -K_p(y^a - y^d) - K_d(\dot{y}^a - \dot{y}^d)$ where K_p, K_d are the feedback PD gain matrices.

The compliant TSC realizes the structural compliance in the controller by forcing the holonomic forces in the tarsus and heel spring in the optimization towards the estimated forces from the joint stiffness and damping. The slack variables in δ therefore allow the deviation of the rigid model holonomic constraint to the extent that the estimated joint torques require. The resulting TSC is used to realize nominal walking with human-inspired trajectories and force-embedding in 2D MATLAB simulation. However, it was not able to reliably realize downstep behavior to the extent that the human could (downsteps of up to 10 centimeter). As such, a rigid description of Cassie with a corresponding rigid TSC was considered for embedding the downstep behavior. The joint-level holonomic constraints are now explicitly satisfied as mentioned in Chapter 2. The rigid TSC is stated as

$$\begin{aligned}
\min_{u, F_h, \dot{q}, \delta} \quad & \|\dot{y}^a - \dot{y}^d - \dot{y}^t\|^2 & (6.5) \\
\text{s.t.} \quad & D\ddot{q} + C = J_h^T F_h + B\tau & \text{(EOM)} \\
& J_h \ddot{q} + \dot{J}_h \dot{q} = 0 & \text{(holonomic)} \\
& J_s \ddot{q} + \dot{J}_s \dot{q} = 0 & \text{(rigid model)} \\
& \tau_{\min} \leq \tau \leq \tau_{\max} & \text{(torque limit)} \\
& A_{GRF} F_{GRF} \leq 0 & \text{(friction cone)} \\
& (1-c)F_z^d - \Delta_F \leq F_{FE} \leq (1+c)F_z^d + \Delta_F, & \text{(force embedding)}
\end{aligned}$$

The TSC-QP is solved using *quadprog* in MATLAB. With this QP description, we realized expected and unexpected downstep behavior via a translation of the output definitions from Chapter 4 via the motion synthesis in Chapter 5. The 3D walking realization is also realized on a rigid model of Cassie.

6.3 ROBOT WALKING OUTPUT CONSTRUCTION

As we want to control the full-order dynamics of Cassie, we are not only concerned with vertical CoM tracking with force-embedding and horizontal stabilization, we also need to control the additional degrees of freedom of Cassie. Subsequently, the outputs of the three-dimensional Cassie model in SSP are defined as

$$y_{SSP}^d = \begin{bmatrix} \alpha_{\text{pelvis}} \\ \beta_{\text{pelvis}} \\ \gamma_{\text{st}} \\ \gamma_{\text{sw}} \\ z_{\text{CoM}}^d(t, z_{\text{sw}}, n_{ds}) \\ x_{\text{sw}}(t, \theta) \\ y_{\text{sw}}(t, \theta) \\ z_{\text{sw}}(t, n_{ds}) \\ \alpha_{\text{sw}} \end{bmatrix}, \quad (6.6)$$

where

- $\alpha_{\text{pelvis}}, \beta_{\text{pelvis}}$ indicate the pitch and roll of the pelvis,
- γ_{st} and γ_{sw} indicate the yaw of the stance and swing leg respectively,
- n_{ds} indicates the downstep step; the down-step, the over-step, and the up-step, and
- α_{sw} indicates the pitch of the swing foot toe.

All the desired pitch, roll, and yaw angles are represented by a Bézier polynomial smoothly guiding the current angle to zero radians. The swing foot positions in the horizontal plane originate from a decoupling of a Period-1 H-LIP for the sagittal plane and a Period-2 H-LIP for the coronal plane [14]. The vertical position of the swing foot tracks a pre-defined Bézier spline with unique formulations for the over-step and up-step for the downsteps scenarios, addressed in the next section. In DSP, the swing leg outputs are not tracked which allows us to state the effective outputs as

$$y_{DSP}^d = \begin{bmatrix} \alpha_{\text{pelvis}} \\ \beta_{\text{pelvis}} \\ \gamma_{\text{st}} \\ \gamma_{\text{sw}} \\ z_{\text{CoM}}^d(t, z_{\text{sw}}, n_{ds}) \end{bmatrix}, \quad (6.7)$$

In the implementation, the SSP output from Equation (6.6) is used for both SSP and DSP. During DSP the desired swing leg outputs are set equal to the actual swing leg outputs. The foot contact constraints ensure that neither foot slips, rotates around its edges, or prematurely lifts from the walking surface.

6.3.1 Force Embedding

In contrast to the aSLIP representation of Cassie, in which the complex leg structure from Figure 6.1 is replaced by a single spring, the ground reaction forces of the rigid 3D model of Cassie are not equal to the forces in the compliant joints. The representation from Equation (2.9), in which the ground contact is modeled as a holonomic constraint, is used for the approximation of the ground reaction forces. The force-embedding can therefore be realized as a linear constraint in the TSC-QP

$$(1 - c)F_{z,SSP/DSP}^d - \Delta_F \leq F_{FE} \leq (1 + c)F_{z,SSP/DSP}^d + \Delta_F, \quad (6.8)$$

	Bézier for	Bézier polynomial coefficients
\mathcal{B}	smooth transition	$[0, 0, 1, 1, 1]$
$\mathcal{B}_{z,nw}$	nominal walking	$[0, z_{sw}^{\max} \mathbf{I}_4, 0, z_{sw}^{\text{neg}}]$
$\mathcal{B}_{z,os}$	over-step	$[h, z_{sw}^{\max} + h \mathbf{I}_4, 0, z_{sw}^{\text{neg}} + h]$
$\mathcal{B}_{z,us}$	up-step	$[-h, z_{sw}^{\max} \mathbf{I}_4, 0, z_{sw}^{\text{neg}}]$

Table 6.1: Bézier polynomial coefficients for nominal walking and compensatory steps. \mathbf{I}_4 indicates a four-column row vector of ones. The Bézier polynomials are shown in Figure 6.3.

where F_{FE} is the selection of vertical components of the ground contact wrench of the legs that are in contact with the ground via Equation (2.9). The desired GRFs are parameterized similarly to the vertical CoM trajectories

$$F_{z,SSP/DSP}^d = F_{SSP/DSP}^d(t, z_{sw}, n_{ds}). \quad (6.9)$$

6.3.2 Swing Foot Trajectory Construction

The desired swing foot trajectory is decomposed in the x , y , and z direction. For 3D walking, the forward swing leg trajectory x_{sw} is governed by the H-LIP stepping controller of the sagittal plane, the side-ward swing leg trajectory y_{sw} is governed by the H-LIP stepping controller of the coronal plane, and the vertical swing leg trajectory z_{sw} is governed by a constructed Bézier polynomial that realizes a desired maximum swing foot height and ensures a foot penetration of the nominal walking platform. Based on the H-LIP step-sizes and step-velocities for Period-1 and Period-2 orbits for the sagittal and coronal stepping respectively, the desired swing foot position, velocity, and acceleration can be constructed as

$$\begin{cases} \{x, y\}_{sw}^d = (1 - \mathcal{B}(t))\{x, y\}_{sw}^a + \mathcal{B}(t)\{x, y\}_{H-LIP}^d \\ \{\dot{x}, \dot{y}\}_{sw}^d = -\dot{\mathcal{B}}(t)\{x, y\}_{sw}^a + \dot{\mathcal{B}}(t)\{x, y\}_{H-LIP}^d + \mathcal{B}(t)\{\dot{x}, \dot{y}\}_{H-LIP}^d \\ \{\ddot{x}, \ddot{y}\}_{sw}^d = -\ddot{\mathcal{B}}(t)\{x, y\}_{sw}^a + \ddot{\mathcal{B}}(t)\{\dot{x}, \dot{y}\}_{H-LIP}^d + 2\dot{\mathcal{B}}(t)\{\dot{x}, \dot{y}\}_{H-LIP}^d \end{cases}, \quad (6.10)$$

where $\mathcal{B}(t)$ is a Bézier polynomial that smoothly transitions from zero to one over the course of the SSP duration ($t = 0 \rightarrow t = T_{SSP}$). The vertical swing foot trajectory is differently constructed for nominal walking, the over-step, and the up-step (the downstep is equal to the nominal walking trajectory).

$$\begin{cases} z_{sw}^d = \mathcal{B}_z(t) \\ \dot{z}_{sw}^d = \dot{\mathcal{B}}_z(t) \\ \ddot{z}_{sw}^d = \ddot{\mathcal{B}}_z(t) \end{cases}, \quad (6.11)$$

where the Bézier coefficients are shown in Table 6.1. The resulting Bézier polynomials of the smooth transition from Equation (6.10) and the vertical swing foot trajectories are shown in Figure 6.3.

6.4 CONTACT FORCE EMBEDDED TASK SPACE CONTROL

To realize the proposed trajectory synthesis on the bipedal robot, we apply the task space controller (TSC) for output tracking. The force embedding can be realized via a linear constraint on the holonomic forces, which are optimization variables in the TSC. We directly specify a linear constraint on the vertical GRF to realize the force-embedding.

$$(1 - c)F^d + \Delta_F \leq SF_h \leq (1 + c)F^d - \Delta_F, \quad (6.12)$$

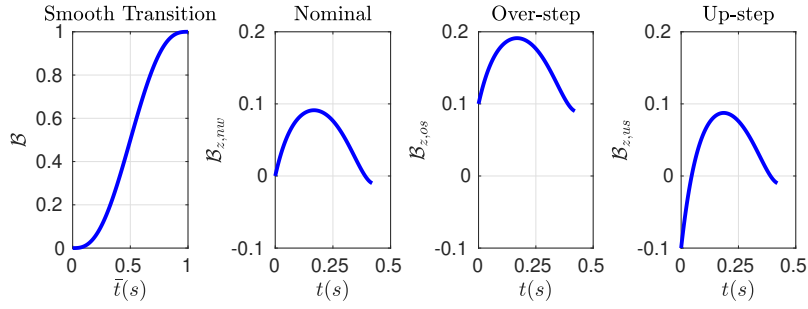


Figure 6.3: Bézier polynomials of the smooth transition to guide actual to desired trajectories and nominal and compensatory vertical swing foot trajectories. Notice that the maximum swing foot height with respect to the height of the impact surface remains approximately equal.

where $F^d = F^d(t, z_{sw}, n_{ds})$ and S is a selection matrix to select the vertical component of the ground contact wrench in Equation (2.4).

The final quadratic program with the equation of motion (EOM) constraint, holonomic constraints, contact force constraints is formulated as:

$$\begin{aligned}
 \min_{u, F_h, \dot{q}} & (\dot{y}^a - \dot{y}^d - \dot{y}^t)^T W (\dot{y}^a - \dot{y}^d - \dot{y}^t) + u^T W_{\text{reg}} u & (6.13) \\
 \text{s.t.} & D\dot{q} + C = J_h^T F_h + B\tau & (\text{EOM}) \\
 & J_h \dot{q} + \dot{J}_h q = 0 & (\text{holonomic}) \\
 & J_s \dot{q} + \dot{J}_s q = 0 & (\text{rigid model}) \\
 & \tau_{\min} \leq \tau \leq \tau_{\max} & (\text{torque limit}) \\
 & A_{\text{GRF}} F_{\text{GRF}} \leq 0 & (\text{friction cone}) \\
 & (1 - c)F^d + \Delta_F \leq S F_h \leq (1 + c)F^d + \Delta_F, & (\text{force embedding})
 \end{aligned}$$

where y^d is the desired output, y^a is the actual output, $\dot{y}^t = -K_p(y^a - y^d) - K_d(\dot{y}^a - \dot{y}^d)$ with K_p, K_d being the feedback PD gain matrices, W is the weight matrix and W_{reg} is the regularization matrix for the control inputs. The QP is solved using OSQP [90] at 2 KHz in the Mujoco physics simulator [91]. During SSP and DSP, each constraint in the QP considers one or two feet in contact with the ground respectively. A time-based domain switching determines the number of feet in contact with the ground. When the QP fails in the DSP due to early lift-off or late ground contact, a SSP controller is used as a backup controller. Additionally, if the foot penetration does not suffice to bring the swing foot to the downstep height in the duration of the SSP, a DSP controller is used instead and the swing foot follows a passive trajectory. To prevent hitting the walking platform during the up-step, we ensure the horizontal position of the swing foot x_{sw} remains constant for the first 0.1 seconds of the up-step swing phase while the vertical position z_{sw} is unaffected.

The control structure, including the abstraction of the human towards a RoM, the offline gait trajectory generation, and the TSC feedback loops, are shown in Figure 6.4. Appendix E present the PD gain matrices, the output weights, and the control loop algorithms. These algorithms present how the downstep detection, the step count, and the synthesis of the desired outputs are realized for the expected and the unexpected downsteps separately. These algorithms can straightforwardly be combined to realize the human-to-robot synthesized locomotion on Cassie. In the next chapter, we will present and analyze results of the nominal walking and walking over downsteps.

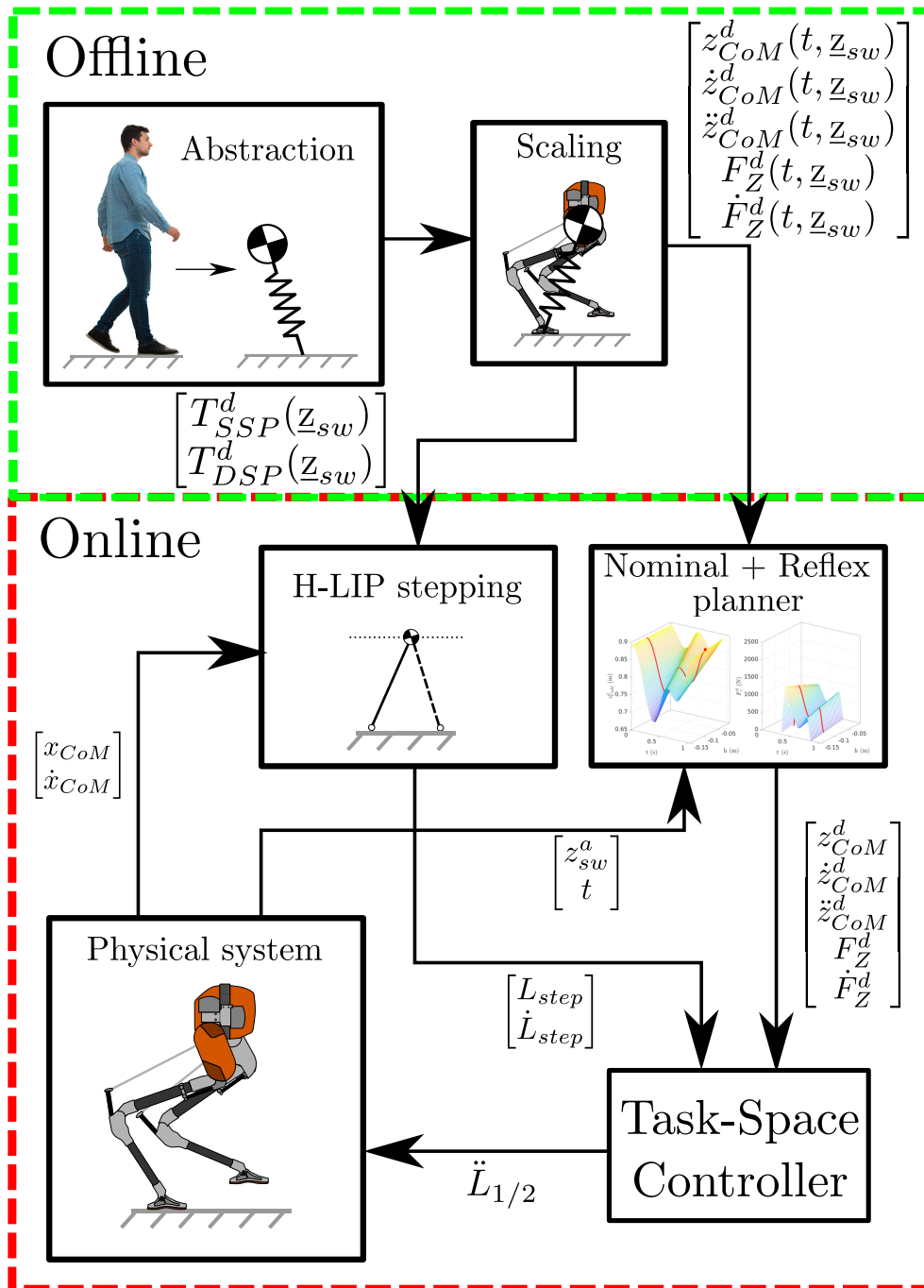


Figure 6.4: Trajectory generation based on the reduced-order model analysis and human-to-robot motion synthesis, and the feedback control structure of the 3D walking realization on Cassie with a Task-Space Controller.

7 | RESULTS

The methodology presented in this thesis, and specifically the RoM trajectory synthesis from human data, was applied to the aSLIP model and the robot Cassie to walk over expected and unexpected downsteps. The results of the realization on the aSLIP model were addressed in Chapter 4. This section will focus on the presentation and analysis of the 3D walking realization.

7.1 3D CASSIE DOWNSTEP NAVIGATION

Expected and unexpected 10 centimeter downstep results are presented in Figure 7.2 and 7.3. The gait tiles of Cassie for these conditions are shown at the bottom of the respective figures with a capture interval of approximately 0.2 seconds.

The simulation results demonstrate the successful translation of human RoM data to the realization of downstep behaviors on Cassie in 3D simulation. The 10 centimeter downstep on Cassie is an even more significant disturbance compared to the human. The mean desired CoM height is lower for Cassie and as such, the downstep height is a larger percentage of the overall *virtual* leg length. The accurate tracking, combined with the force-embedding with a relaxation factor of $c = 0.3$, ensures the dynamic similarity between the robot and the human on a reduced-order model level. In work on fully actuated walking in Chapter 6, it was already highlighted that it was challenging to realize locomotion as tuning becomes a trade-off between tracking the horizontal and vertical CoM kinematics. This issue permeates to the underactuated walking. Now, the tracking of the vertical CoM when the walker is not at VLO (the stance leg is not perpendicular to the ground) affects the horizontal CoM kinematics. A critical observation between the results for expected and unexpected downstep navigation is that the increased oscillation of the vertical CoM position for expected downsteps increasingly affects the horizontal CoM velocity (shown in Figure 7.2.b), which in turn results in significant deviations in the step-sizes during the compensatory behavior. This is supported by the periodic orbits of the expected and unexpected 10cm downstep in Figure 7.1 which portray the phase portrait of the CoM kinematics in the sagittal (Period-1 H-LIP stabilization)

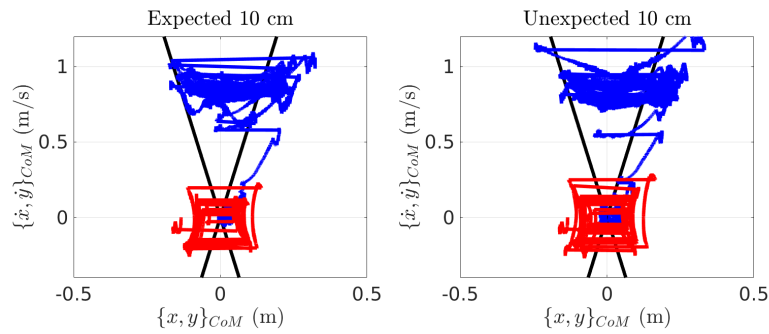


Figure 7.1: Period-1 and Period-2 orbits of 3D walking for expected and unexpected downsteps with 10cm depth. Blue and red indicate the Period-1 and Period-2 orbits respectively.

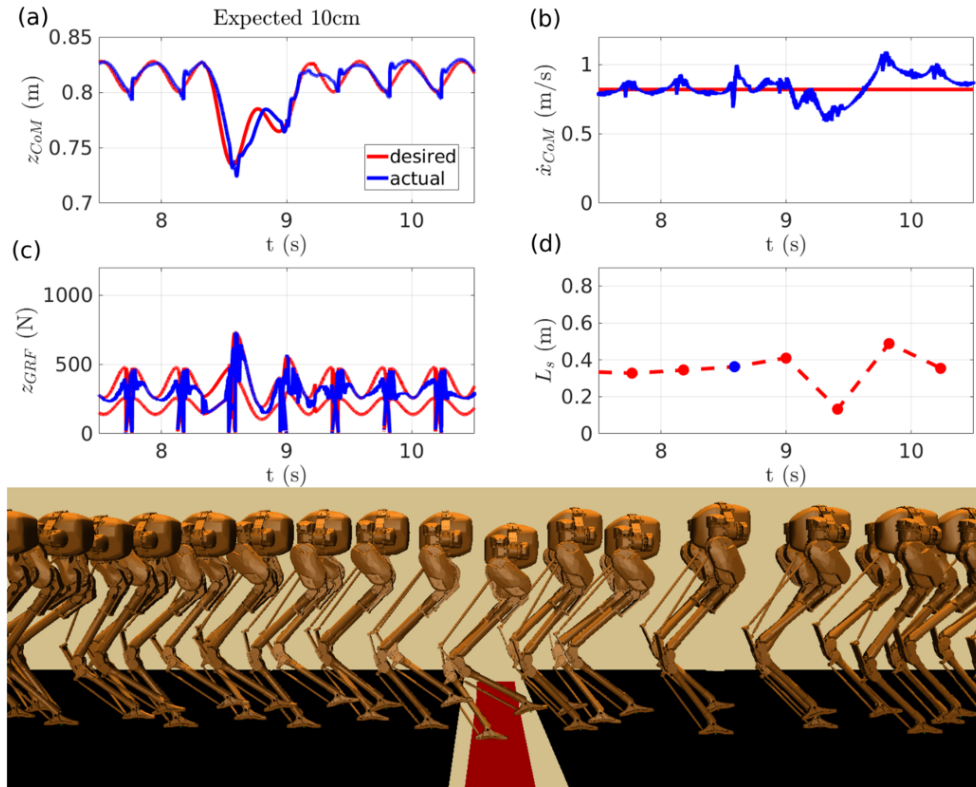


Figure 7.2: Simulation results of 3D walking for Cassie over the **expected** downstep with 10cm depth: (a) the vertical mass trajectories of the desired ones and the actual ones, (b) the horizontal velocity of the mass, (c) the GRF profile with its bounds, and (d) the step-lengths. The blue dot indicates the down-step step.

and coronal (Period-2 H-LIP stabilization), respectively. The successful navigation of downsteps is concluded from the return of the deviation in horizontal velocity to the nominal walking velocity. The more significant deviation from the nominal periodic orbits in Figure 7.1 makes apparent that the stability of the horizontal CoM dynamics (in both the sagittal and the coronal plane) is more affected under the unexpected downstep conditions.

An additional difficulty in achieving great tracking performance is the trade-off between tracking the vertical CoM kinematics and force embedding. In Figures 7.2 and 7.3 we see decreased tracking performance for the unexpected downstep scenario as the recovery behavior exceeds the one step required for the expected scenario. This becomes especially apparent for the unexpected downstep scenario, in which the vertical CoM position of the step after the up-step is tracked to a desirable accuracy. We argue that this is predominantly due to inaccuracies in the desired GRFs from the human measurements with regards to the changes in the horizontal CoM velocity. From the TSC-QP formulation in Equation (6.13) it is apparent that the tracking of the vertical CoM kinematics is enforced in the cost of the optimization while the force-embedding is realized as an explicit, although relaxed, constraint. Further relaxing the force-embedding constraint does not necessarily improve the tracking of the vertical CoM kinematics. The relaxation allows the GRF to persist in a region that is only locally optimal in realizing desired tracking behavior. As such, continuing the accurate tracking performance might become infeasible as the GRFs that realize this are not achievable due to the underlying dynamics of the system.

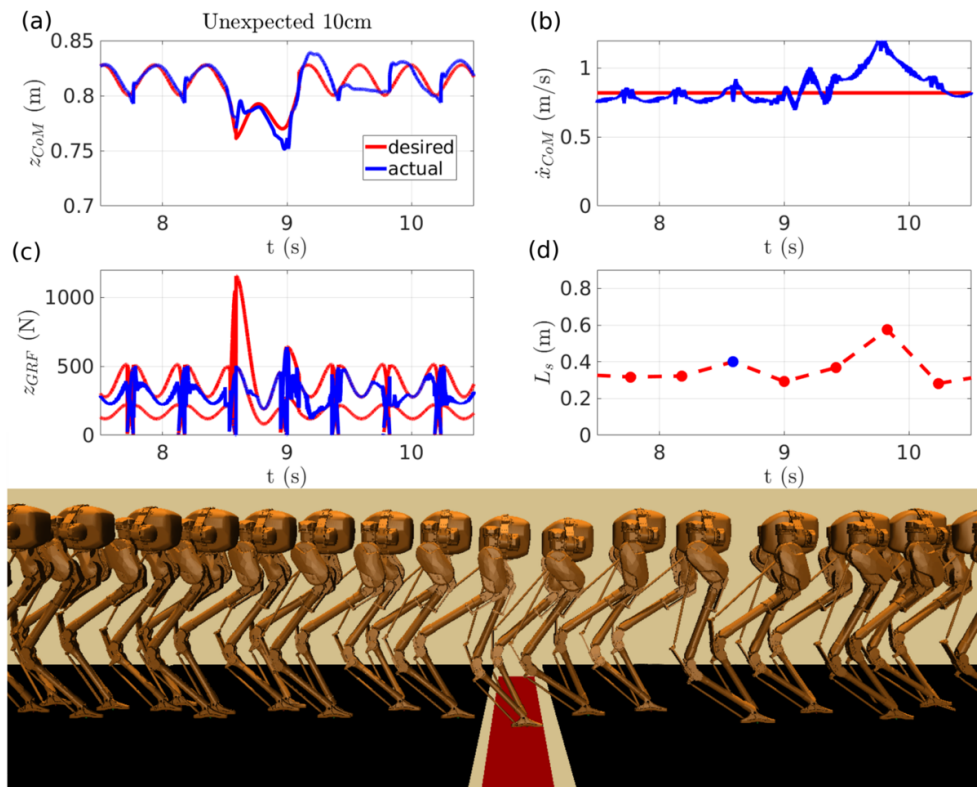


Figure 7.3: Simulation results of 3D walking for Cassie over the **unexpected** downstep with 10cm depth: (a) the vertical mass trajectories of the desired ones and the actual ones, (b) the horizontal velocity of the mass, (c) the GRF profile with its bounds, and (d) the step-lengths. The blue dot indicates the down-step step.

The control of the swing leg and vertical CoM for humans is mostly governed by the passive dynamics of the system when experiencing unexpected downsteps. For the robot, the vertical swing foot behavior is explicitly controlled at all times according to Figure 6.3, which prevents an immediate impact velocity and, with the requirement of lowering the CoM, results in a decreased GRF during the downstep. This lies at the core of the human-to-robot translation of desired dynamics. The accuracy of the robot in portraying the desired kinematics and kinetics may only be as good as the underlying assumption of the equivalent reduced-order model representation of the human and the robot, coupled with the realized step-sizes.

The improved controllability of Cassie with respect to the human means that in both scenarios—expected and unexpected downsteps—the increase of the forward CoM velocity is significantly reduced. Thus, both downstep scenarios can be traversed more effectively, and motion planning based on the sensing of the environment via the kinematics (the foot penetration of the walking platform) can help traverse unexpected changes in walking height and explicitly plan motion when exceeding the nominal step-time.

7.2 ENERGY EFFICIENCY

The human to robot synthesised trajectory also have effect on the energy efficiency during nominal walking. Compared to *state-of-the-art* approaches [35] in which the vertical CoM position is explicitly being kept constant, we compare canonical H-LIP

	Unit	Canonical H-LIP	Human Synthesized SLIP
P_t	Nm/s	536.98	388.45
P_p	Nm/s	1256.10	799.42
P_{pn}	Nm/s	1975.23	1210.39
$CoT_{mt,t}$	–	1.25	0.97
$CoT_{mt,p}$	–	2.94	1.99
$CoT_{mt,pn}$	–	4.61	3.02

Table 7.1: Supplied power and the mechanical Cost of Transport of the canonical H-LIP walking [35] and the human synthesized SLIP walking presented in this thesis. A walking duration of 15 seconds is considered with a forward walking velocity of approximately 0.81 meters per second.

walking with human synthesised SLIP walking. In bipedalism, the energy efficiency can be quantified with the *Cost of Transport* metric

$$CoT = \frac{Power}{Weight \cdot Distance} \quad (7.1)$$

However, to distinguish between efficiency of the mechanical system and actuators, and the control system the specific *energetic cost of transport* CoT_{et} , which considers the total energy consumed by the system, and the specific *mechanical cost of transport* CoT_{mt} which considers only the positive mechanical work of the actuators [55] can be used. In simulation, the overall energy supplied by the *virtual* battery, the current through, and the voltage over the individual motors is not known. As such, the mechanical cost of transport is considered in Table 7.1. For the supplied power actuator, we consider [92; 93]

- the total power $P_t = \text{regen}(u\dot{q})$ where the regeneration function $\text{regen}(u\dot{q}) = [u\dot{q}]^+ - C[u\dot{q}]^+$ accounts for the regeneration loss when the supplied torque and the rotation of the joint are in opposite direction,
- the positive-only power $P_p = [u\dot{q}]^+$, and
- the positive and negative power $P_{pn} = |u\dot{q}|$

where u and \dot{q} are the joint torque and rotational velocity for an actuated joint respectively. In theory, without frictional- and impact losses and joint- and linkage damping, locomotion is energy conservative if all energy supplied by the braking is regenerated. The total power P_t therefore assumes the negative power is perfectly regenerated if $C = 1$. The positive-only power P_p disregards any energy generation during breaking and the positive and negative power P_{pn} considers the *harvested* energy as a supplied energy.

The results shown a decrease in energy consumption and a subsequent decrease in the CoT for all the power consumption definitions. The actuation is realized by brushless DC servo motors that do not have perfect regenerative properties assumed by P_t . However, the positive and negative power definition P_{pn} assumes no regeneration at all. As such, all presented results are an approximation of the real system.

The main contribution to the decrease in the CoT is the pendulum-like stance phase, in line with the *inverted pendulum* theory [40; 41] from Chapter 2. This theory, which is realized by the human-to-robot motion synthesis, keeps the length of the leg approximately constant and as such requires less knee torque. The constant height assumption of the H-LIP does not use this advantageous property apparent in biological bipedalism. The CoT metrics of different autonomous bipedal robots are reported in [60; 53] yet the simulation-only nature of the metrics in this thesis prevent a one-to-one comparison.

8

DISCUSSION

The presented human-to-robot motion synthesis successfully allows Cassie to overcome similar scenarios to those observed from human experiments. The translation of motion capture data to a musculoskeletal model for abstracting center of mass (CoM) kinematics allows the fitting of a reduced-order model. The resulting reduced-order model not only allows walking realization on the aSLIP for nominal walking and (un)expected downstep behavior, it also substantiates the dynamic scaling of the human towards the robot. The successful realization of walking highlights the power of scaling output kinematics and kinetics when the underlying they can be represented by equivalent reduced-order models.

8.1 HUMAN WALKING

The analysis of the human motion capture and ground reaction force (GRF) measurement data has given insight into the whole-body compensatory behavior of the human walking over expected and unexpected downsteps from 2.5 to 10 cm. We have observed that for the unexpected downsteps, the changes in vertical CoM height only occur after the swing leg impacts the down-step surface. In addition, we have observed that the passive trajectory of the swing leg, and its resulting step-size, in the unexpected downstep scenario causes a significant increase in horizontal CoM velocity after the ground impact.

8.2 REDUCED ORDER MODEL WALKING

The abstraction of the human CoM kinematics and ground contact kinetics in Chapter 3 and 4 have given us insight into the reflexive, reflexive, and active compensation of the human walking over downsteps. We have shown that the unexpected downstep requires more overall actuation of the leg in order to stabilize towards the nominal gait compared to the expected downstep. The realization of walking on the aSLIP model has proven to be an excellent tool in better understanding the human gait on a reduced-order model abstracted level. A shortcoming is that the step-sizes of the Hybrid Linear Inverted Pendulum (H-LIP) stepping stabilization can directly be realized (as we neglect swing leg inertia), and subsequently, the horizontal stabilization behavior is *too accurate* compared to the human. Especially in the case of the unexpected downstep scenario, where we have seen that the step size is mainly governed by the passive dynamics of the swing leg, the step-sizes are not necessarily representative of the human compensatory gait. This shortcoming and potential future work to remedy this effect are mentioned in the next chapter.

8.3 3D ROBOTIC WALKING

The robot walking synthesis in Chapter 5 scales the walking outputs of the human to a reduced-order model representation of the considered bipedal robot. The 3D walking realization highlights the power of abstracting key human motion charac-

teristics and can subsequently embed active and passive reactive behavior of the human onto a morphologically different bipedal robot. The results in Figure 7.2 and 7.3 have shown this successful downstep navigation with approximately equivalent dynamics as those observed in the human. It has highlighted that the principled abstraction of motion characteristics could further improve the *state-of-the-art* of bipedal robot robustness and agility in which human compensation is explicitly embedded in an online motion parameterization by the swing leg platform penetration. Additionally, improvements in efficiency are highlighted in comparison to the constant walking height thus far realized in the implementations of H-LIP stepping. Although the constant walking height decreases the error between the robot and the H-LIP reduced-order model, it leads to an inefficient nominal walking gait. The human-to-robot walking synthesis therefore already has advantages for this nominal walking behavior.

It is clear that the deviation of the CoM height from the assumed nominal walking height of the H-LIP affects the stabilization in the compensatory gait. The increased deviation under expected downsteps, as shown in Figure 3.4, amplifies the difference between the robot and the H-LIP RoM and subsequently affects the stepping optimal stepping behavior. The indication of the step sizes affecting the forward walking velocity in nominal walking and walking over downsteps in Figure 7.2 and 7.3 support this conclusion. The effect of this approach to stepping stabilization with human-to-robot tracking and force embedding can be seen in the supplementary video of this thesis [94]. Existing realizations of traversing unexpected downsteps either rely on the underlying robustness of the controller or on more heuristic approaches to the swing-leg and vertical CoM trajectories. The human-to-robot motion synthesis facilitates a more principled approach to the downstep behavior that could be readily applicable to other walking behavior such as stair walking. Lastly, it is the current hypothesis that the principled abstraction of the key human motion characteristics realize explicit compensatory behavior which allows the state of the system to be in a more robust region of the state-space.

We have demonstrated that the specific walking responses of humans to the changes in the environment can be embedded in morphologically and dynamically different robotic bipedal systems. By scaling the outputs of the human in the motion synthesis and embedding the contact forces in the low-level control, the dynamic similarity between models is realized on the closed-loop systems. The proposed method has been successfully realized on the actuated Spring-Loaded Inverted Pendulum (aSLIP) and 3D simulated Cassie to overcome expected and unexpected downsteps with similar responses to those found in the human gait.

The presented framework expands upon state-of-the-art approaches for realizing flat-ground walking [78; 35] on bipedal robots and reduced-order model abstractions [11; 1] from observations in biology. A connection between observations and application in robotics has been established, and human-to-robot motion synthesis is presented with an approach to integrate the morphological differences between the human and the robot. This builds upon concepts of dynamic similarity in bipedal locomotion [29; 25].

Although the presented framework has enabled Cassie to successfully navigate expected and unexpected downstep scenarios in a dynamically similar manner as the human, the considered model of Cassie, the motion synthesis, and the controller structure are subjected to shortcomings in accurately portraying a reduced-order model representation of the human walker. Together with the assumption on the equivalent reduced-order model representation of the human and the robot, this prevents true dynamic similarity of the generated trajectories and ground reaction force profiles.

9.1 FUTURE WORK

We present concrete improvements to achieving dynamic similarity and to further establish the underlying framework of employing human data in the motion synthesis of morphologically different bipedal robots.

9.1.1 Vertical Center Of Mass Dynamics

Firstly, the oscillation of the vertical Center of Mass position affects the horizontal stabilization capabilities of the H-LIP stepping as mentioned in Chapter 8. The power of the H-LIP stepping method is its closed-form step-to-step dynamics, which ensure a closed-form step size solution on the full-order robot. Small oscillations, such as those present in the nominal walking gait, can accurately be stabilized by the H-LIP without any tedious gain- and parameter tuning. However, the significant lowering of the Center of Mass, especially for the expected downstep scenario, significantly affects the stabilization. As such, a better understanding of the effect of these deviations on the H-LIP step-to-step dynamics could allow the realization of more agile behavior without the loss of the closed-form strengths of the current stepping implementation.

9.1.2 Systems With Non-Trivial Compliance

Secondly, the current 3D model of Cassie is assumed rigid. The human musculoskeletal system contains significant compliance and uses this to its advantage to increase efficiency and robustness. Although compliant bipedal robots have successfully been controlled, the translation of these advantageous properties is not yet well-understood. However, it could significantly improve general bipedal robotic walking and the current framework to more closely dynamically mimic the active and passive compensatory behavior of the human.

9.1.3 3D Fully Actuated Walking

The 3D walking implementation in Chapter 7 is underactuated in the sagittal plane, yet, the observations from human data in Chapter 3 indicates that the ankle is an important stabiliser in the compensatory gait. Work was conducted on fully actuated walking in 2D and 3D with pre-determined step-sizes scaled from human data. It was deemed that this method could not reliably reproduce the downstep compensation observed in the human. A promising direction could be to consider the ankle actuation in the sagittal plane with the current 3D implementation with H-LIP stepping stabilization. This requires dynamically scaled trajectories of the forward CoM kinematics, which we already obtained in Chapter 5, and include the forward CoM velocity as a Relative Degree 1 output in the Task-Space Controller in Equation 6.13.

9.1.4 Follow-The-Leader

The presented work currently focuses on a specific downstep scenario. Future work will consider a general framework of transferring versatile human locomotion to dynamic bipedal robot behaviors, which could lead to impressive feats such as *follow-the-leader* traversal of stepping stones and walking over stairs. In these scenarios, the robot could monitor the human, abstract the observed joint kinematics to a representative reduced-order model, and traverse the stepping stones or stairs in a dynamically similar fashion with desired kinematics and kinetics that apply to the reduced-order model representation of the robot in question. To achieve this provable applicability of the observed kinematics and kinetics, a deeper understanding of the closed-loop dynamics of walking is required. Future work will focus on this generalized human motion abstraction.

A | CONTRIBUTIONS

This section presents the contributions to the literature in the form of an abstract submitted and accepted to be presented at the World Conference on Biomechanics (WCB 2022, Taipei) and a conference paper submitted (still under review) to the International Conference on Intelligent Robots and Systems (IROS 2022, Tokyo).

An Activated SLIP Model of Human Walking Captures the Response to Expected and Unexpected Downsteps

Joris Verhagen, Guoping Zhao, Ajay Seth

1 Introduction

How animals and humans handle unexpected changes in terrain during locomotion is not yet fully understood. While spring-loaded inverted pendulum (SLIP) models are used to explain the dynamics of downsteps during running, their extension to downsteps for human walking has not been explored. We hypothesize that an activated, aSLIP, model [1] can capture how humans successfully negotiate downsteps and provide an intuitive and more applicable understanding.

2 Methods

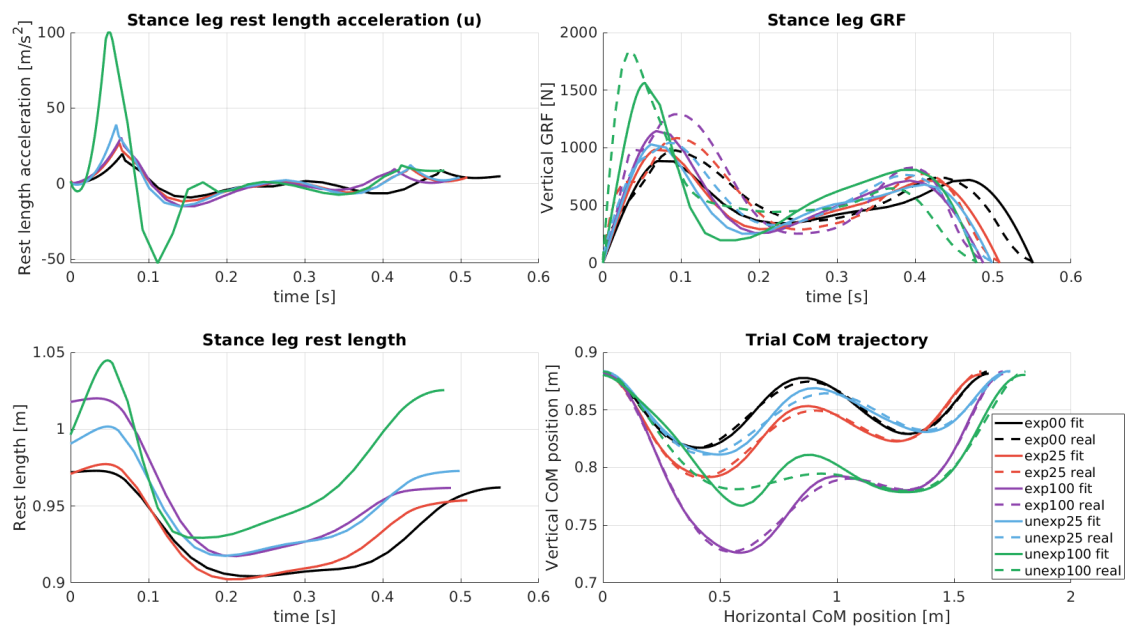
We measured human kinematics and kinetics walking over flat ground with expected and unexpected downsteps using optical motion capture and force-plates where only one leg experienced a downstep. Both conditions considered 2.5, 5.0, 7.5, and 10.0 cm downsteps. We computed the center of mass (CoM) kinematics. We fit the aSLIP model from [1] with quadratic stiffness (with respect to leg length) and damping obtained from nominal gait and specified the activation as the acceleration of the rest length. This activation relates to leg length and muscle forces according to the equilibrium point hypothesis [2]. We formulated a direct collocation problem where the cost function consists of energy expenditure and the error between simulated and experimental CoM position. We included continuity constraints and soft bounds on the duration of the phases and on GRF peaks. For each of the eight trials with experimental conditions, we optimized over two strides, starting from vertical leg orientation (VLO) before the downstep until the first VLO afterward, using IPOPT [3]. The process was considered successful if the activated SLIP model could track the experimental CoM trajectory under 1 cm RMS.

3 Results

The resultant aSLIP models matched experimental CoM trajectories within 8mm RMS. Stance leg rest length actuation, rest length, CoM position, and GRFs for selected experimental conditions are presented in Figure 1.

4 Discussion

Our activated SLIP model accurately captures the kinematics and kinetics of human walking over expected and unexpected downsteps. The increased actuation for unexpected downsteps indicates that the effective stiffness of the leg increases after impact and that this effect also increases with larger downsteps. The results from our aSLIP model reveal that humans are more compliant when the downstep is known and make more effective use of passive dynamics, as seen by the decrease



in actuation. We have shown that the simple actuated SLIP model provides insight into active and passive changes of the leg when subjected to expected and unexpected downsteps. These findings could be applied to bipedal robotics to negotiate downsteps in a way similar to humans.

Acknowledgments

We thank Xiaobin Xiong (AMBER Lab, Caltech) for his advice and help with the actuated SLIP model.

References

- [1] Xiong, X., Ames, A. D. (2018, October). Bipedal hopping: Reduced-order model embedding via optimization-based control. In 2018 IEEE/RSJ International Conference on Intelligent Robots and Systems (IROS) (pp. 3821-3828). IEEE.
- [2] Feldman, A. G., Levin, M. F. (2009). The equilibrium-point hypothesis—past, present and future. *Progress in motor control*, 699-726.
- [3] Wächter, A., Biegler, L. T. (2006). On the implementation of an interior-point filter line-search algorithm for large-scale nonlinear programming. *Mathematical programming*, 106(1), 25-57.

From Human Walking to Bipedal Robot Locomotion: Reflex Inspired Compensation on Planned and Unplanned Downsteps

Joris Verhagen¹, Xiaobin Xiong², Aaron D. Ames² and Ajay Seth¹

Abstract—Humans are able to negotiate downstep behaviors—both planned and unplanned—with remarkable agility and ease. The goal of this paper is to systematically study the translation of this human behavior to bipedal walking robots, even if the morphology is inherently different. Concretely, we begin with human data wherein expected and unexpected downsteps are taken. We analyze this data from the perspective of a reduced-order template model representation of the human, encoding the center of mass (CoM) and contact forces, which allows for the translation of these behaviors into the corresponding reduced-order model of a bipedal robot. We embed the resulting behaviors into the full-order dynamics of a bipedal robot via nonlinear optimization-based controllers. The end result is the demonstration of planned and unplanned downsteps in simulation on an underactuated walking robot.

I. INTRODUCTION

Bipedal robotics has experienced tremendous progress in the last decades. Yet, even in fully known environments, the agility and robustness of mechanical bipeds has yet to match their biological counterparts. We argue that this is due to a lack of online motion planning, an absence of reflex-like control, and non-advantageous passive dynamics, which biological systems employ to overcome disturbances. This can most notably be seen when considering significant unexpected changes in stepping height. For example, [1] describes the behavior of guinea fowls subjected to an unexpected downstep in a running gait. Similarly, these (un)expected downstep scenarios have been the focus in human running [2], [3] and walking [4], [5]. While there has been efforts to achieve similar behaviors in the context of robotic running [6], [7], they have yet to be realized on robots with different morphologies. The goal of this paper, therefore, is to translate the reflex behavior present in humans negotiating both planned and unplanned downstep behaviors to morphologically different bipedal robots.

The nonlinear control and biomechanics communities have traditionally pursued the study of bipedal robot locomotion from different perspectives. The control theorist approach is mainly concerned with realizing stable and robust locomotion with formal guarantees—even if the resulting walking does not directly share commonality with human walking. Methods such as offline trajectory optimization with Hybrid Zero Dynamics [8], [9], closed-form template-model stepping methods [10] require a varying degree of model

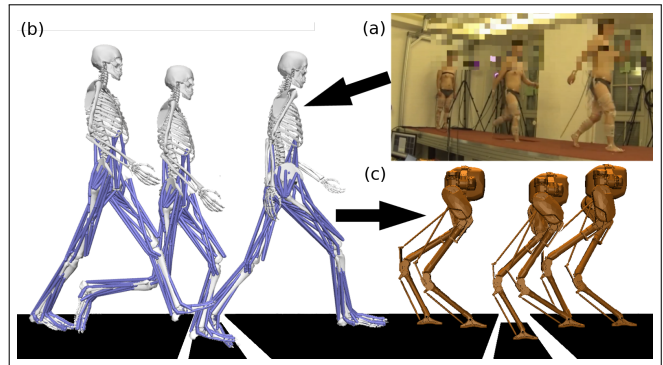


Fig. 1. The human measurement data in OpenSim mapped to a representative skeletal model of the test subject, compared to 3D Cassie subjected to the same downstep height. Changes occur in step-time, step-length, forward walking velocity, desired contact forces, and vertical CoM trajectories.

knowledge, but have been successfully utilized to achieve dynamic walking behaviors experimentally on underactuated robots. The biomechanist approach typically focuses on the methods of actuation, human morphology, and activation. Although formal notions of ‘biologically-inspired walking’ exist [11], the intersection of these distinct fields has received less focus than one might expect from the significant similarities between analyzing biological bipedal locomotion and realizing robotic bipedal locomotion. Additionally, while there have been approaches to benchmarking human likeness [12] this does not address how to achieve human-like behaviors on walking robots. In this work, we identify similarity between human and robotic walking via *reduced-order models (RoMs)* and use this to embed human walking behaviors—and specifically downstepping—on walking robots.

This paper presents a method for translating downstep behaviors—both planned and unplanned—from humans to walking robots. Specifically, the 3D bipedal robot Cassie [13] which is substantially morphologically different from a human. To achieve this goal, we first collect data from human walking downstep experiments and abstract this behavior to a reduced-order model (RoM) that captures the essential components of this behavior: the kinematics of the center of mass (CoM) and the ground reaction forces. We then consider the dynamics associated with this RoM via the Spring-Loaded Inverted Pendulum (SLIP) model and generated nominal downstep compensation. We stabilize the vertical state and realize force-embedding with the Backstepping-Barrier Function framework developed in [14] and stabilize the horizontal state via step-size adaptation of the Hybrid Linear Inverted Pendulum (H-LIP) via the linear Step-to-Step

¹Authors are with the Faculty of Mechanical, Maritime, and Materials Engineering (3ME) and with the faculty of Biomechanical Engineering, Delft University of Technology, 2628 CD Delft, The Netherlands j.p.m.verhagen@student.tudelft.nl

²Authors are with the Faculty of Civil and Mechanical Engineering, California Institute of Technology, Pasadena, CA 91125, USA

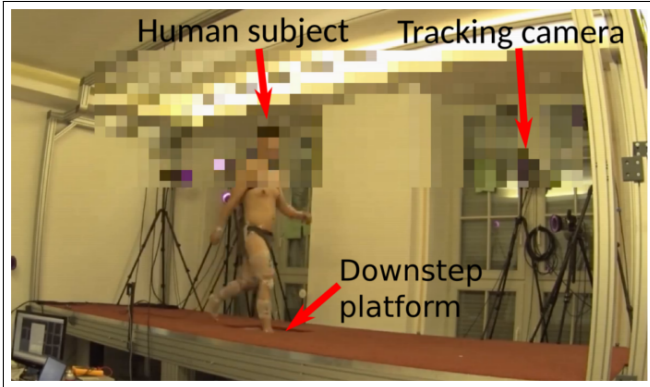


Fig. 2. The experiment setup for data collection of human walking. Force plates are installed beneath the platform.

(S2S) dynamics. For the 3D implementation, a rigid model is assumed where the output dynamics are stabilized towards the desired trajectories using a Task-Space Controller (TSC) and force-embedding is realized as a linear constraint. The end result of this approach is the ability to generate downstep behaviors in simulation on the 3D model of Cassie. We, therefore, are able to start from human data for downstepping and, through a principled abstraction of the key elements of locomotion, arrive at robotic downstepping even when the morphologies of the human and robot differ dramatically.

The structure of this paper is as follows. In Section II we describe the human walking on downsteps and corresponding data analysis; specifically related to the CoM and ground reaction forces. Section III uses the collected human walking data, coupled with RoMs of locomotion, to generate walking on SLIP like models. This walking on reduced-order models is embedded into the full-order dynamics of the 3D robot in Section IV. Finally, the results of the paper are described in Section V wherein the 3D walking achieved on Cassie for downstep behaviors—both planned and unplanned—is described.

II. HUMAN WALKING ON DOWNSTEPS

A. Data Collection

To understand (un)expected downsteps in humans we analyzed experiments conducted at the Lauflabor lab at Technische Universität Darmstadt. Human subjects were instructed to walk on a platform 2 meter wide and 6 meters long shown in Fig. 2. At the center of the platform, a variable height walking platform is located. Three force plates are present, before, on, and after the variable height platform, which record the ground reaction forces at 1 kHz. Full body movement was recorded by a motion capture system consisting of 26 markers and 16 cameras at 240 Hz. Eight trials were conducted for each downstep height at 0.0 cm, -2.5 cm, -5.0 cm, -7.5 cm, and -10.0 cm for both expected and unexpected situations¹. A total of nine

¹All trials allow full vision of the walking platform. Unexpected trials are performed by suddenly lowering the walking platform when the swing foot approaches the ground

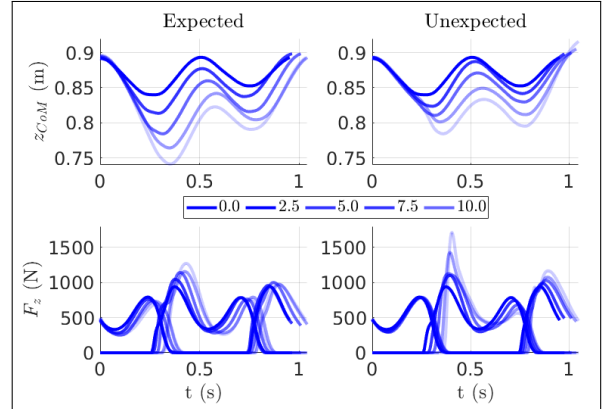


Fig. 3. Average vertical CoM position and vertical GRF for flat-ground, expected, and unexpected downsteps. The GRFs start at the VLO before the downstep, switch to the swing leg experiencing the downstep, and ends at the original stance leg when the downstep has been overcome.

experimental conditions were tested; four known downstep heights, four unknown downstep heights, and nominal flat-ground walking.

Inverse Kinematics (IK) optimization was performed in OpenSim [15], [16] to obtain the joint angles and Center of Mass (CoM) positions and velocities of the human. Differences in behavior in the coronal plane were to be small and insufficiently affected by the downsteps. Subsequently, we limit our focus to the results in the sagittal plane.

B. Kinematics and Kinetics Analysis

A powerful abstraction for a full-body analysis of the human gait is the consideration of the CoM behavior. Although the human subjects have an upper body with arms (which are not present on Cassie), the contributions towards changes in angular momentum can be captured by the point-mass dynamics. Fig 3 shows a polynomial fit to the mean vertical CoM position for the nominal and downstep trials and the GRFs. The analysis is performed from the Vertical Leg Orientation (VLO) before the downstep and ends at the VLO after the downstep². The within-subject variance is low. From Fig 3, we observe that the CoM position is significantly lowered both before swing foot impact which is especially the case for expected downsteps. For these expected downsteps, the lowering of the CoM is accompanied with a reduced impact force of the swing leg experiencing the downstep. For unexpected downsteps, the change in vertical CoM height during downstep is predominantly caused by the passive pendulum properties of the stance leg and the peak of the GRF is significantly higher compared to the expected downsteps. From the measurement data, we create C^1 surfaces for the vertical CoM position and the desired GRFs shown in Fig. 4. With the subjects being instructed to ‘continue’ their gait, an important metric with regards to stability is the angular momentum around the stance leg.

²Two full steps are considered. If we consider a left stance leg during downstep detection, the analysis is from the moment of the CoM passing the left foot on the raised pre-downstep platform until the moment of the CoM passing the left foot on the raised post-downstep platform.

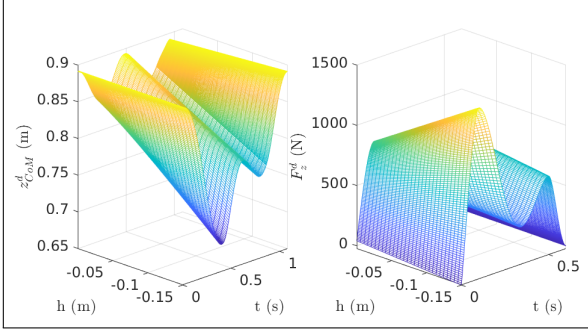


Fig. 4. The desired vertical CoM trajectory z_{CoM}^d and the GRF in SSP parameterized by time (t) and the downstep height h for expected downsteps. Similar regressions are applied for the walking on unexpected downsteps

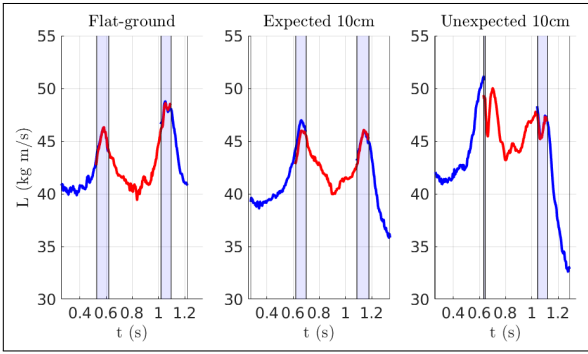


Fig. 5. Averaged trajectories of the angular momentum around the contact point for walking on flat-ground, expected, and unexpected downsteps (with 10cm depth). Blue boxed regions indicate the DSP.

The stance-foot angular momentum is shown in Fig 5. These results indicate that the angular momentum is much more contained towards the flat-ground walking condition for expected trials. This is caused both by the reduced vertical CoM position and the smaller change in horizontal CoM velocity. The latter is caused by an increase in step-size as it was noticed that changes to the nominal step-lengths in unexpected downstep trials were governed by the passive dynamics of the swing leg.

C. Human Walking Model Reduction

The contributions of muscle activation (either deliberate or reflexive) and changes to posture alter the dynamic behavior of the human when subjected to expected and unexpected downsteps. The subsequent analysis would be high dimensional. Additionally, our results from the raw measurement data using IK are noisy, do not explicitly contain the acceleration, and are only to an assumed extend representative of a point-mass model. In order to obtain a tractable analysis of the dynamics which is a closer representative of the RoM, we abstract the human towards the actuated Spring Loaded Inverted Pendulum (aSLIP) model from [17], [14] which contains actuation on the rest-length of the spring.

We construct a non-convex optimization problem of fitting the behavior of the human to the aSLIP model. With the introduction of the actuation, we will jointly optimize a

leg-length dependent stiffness and a damping for nominal walking, and acceleration of the rest-length of the spring. The changes to the representative stiffness of the human leg are therefore captured by the change in the physical length and the rest-length of the spring. The optimization is formulated as:

$$\begin{aligned} \min \sum_{i=1}^5 (& \|z^a - z^d\|^2 + w(\|\ddot{L}_1\| + \|\ddot{L}_2\|^2)) & (1) \\ \text{s.t. } & f_{aSLIP} + g_{aSLIP}\ddot{L} = 0 & (\text{dynamics constraints}) \\ & \mathbf{x}_i = \mathbf{x}_{i+1} & (\text{state continuity}) \\ & \mathbf{x}_0 = \mathbf{x}_5 & (\text{VLO}) \\ & F_{z,k}(t) \geq 0, \forall k, \forall t \\ & F_{z,sw}(0) = 0 \wedge F_{z,st}(t_f) = 0, \forall k \end{aligned}$$

where i indicates a phase of the walking gait, $w \in \mathbb{R}$ is a scaling parameter on the cost, \ddot{L}_j is the acceleration on the rest-length of leg j , f_{aSLIP} and g_{aSLIP} represent the equations of motion of the aSLIP model in either SSP or DSP, \mathbf{x}_i indicates the full state of the system at phase i , $F_{z,k}$ is the vertical GRF at phase k , and $F_{z,st}$ and $F_{z,sw}$ are the vertical GRFs of the current stance and new stance leg respectively. As we consider the analysis from pre-downstep VLO to post-downstep VLO, we jointly optimize 5 phases². Agreement in the horizontal velocities is enforced with soft bounds on the step duration as to not over-constrain the dynamics of the RoM. From the optimization, we also obtain the leg length-dependent stiffness, for which we assume a second degree polynomial as shown in Fig. 6, and the damping, which is assumed constant. Higher degrees of parameterizations of the stiffness and damping were evaluated in the same optimization framework, which is not showing significant improvement on lowering the cost.

III. WALKING REGENERATION ON A REDUCED-ORDER MODEL OF HUMANS

Given the kinematics and kinetics data of human walking, we first want to re-generate the motion via feedback control on the optimized aSLIP model that represents human walking dynamics. We apply the Backstepping-Barrier Function (BBF) controller with the step-to-step (S2S) dynamics approximation approach developed in [14]. The backstepping component in the BBF based quadratic program (BBF-QP) allows the tracking of the vertical state of the point mass, which is underactuated due to the spring in the leg; the control Barrier function in the BBF-QP allows the GRF stays in a range of desired GRF profile of human walking. The S2S dynamics approximation provides stepping stabilization that addresses the point-foot underactuation of walking.

A. Vertical CoM Tracking

For the vertical state, we define the objective as driving the vertical CoM position to follow a desired trajectory during nominal walking and during (un)expected downsteps. The output is defined as:

$$\eta = \begin{bmatrix} z_{CoM} - z_{CoM}^d(t) \\ \dot{z}_{CoM} - \dot{z}_{CoM}^d(t) \end{bmatrix}, \quad (2)$$

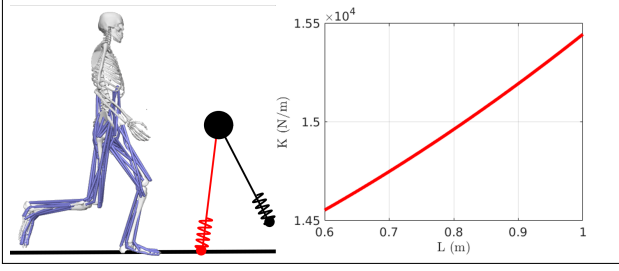


Fig. 6. Abstraction of the human kinematics and kinetics towards the reduced order aSLIP model of walking. We optimize a quadratic stiffness which minimizes Eq. (1)

where superscript d indicates the desired time dependent vertical trajectory from the human data. The output dynamics is:

$$\dot{\eta} = \begin{bmatrix} \dot{z}_{\text{CoM}} - \dot{z}_{\text{CoM}}^d(t) \\ -g - \ddot{z}_{\text{CoM}}^d(t) \end{bmatrix} + \begin{bmatrix} 0 \\ \frac{1}{m} \end{bmatrix} F_z^P = f_\eta + g_\eta F_z^P, \quad (3)$$

where F_z^P is the net vertical force on the CoM for each domain P (SSP or DSP). The GRF is related from the spring forces in the leg; e.g., during the SSP, the vertical component of the GRF is:

$$F_z^{\text{SSP}} = (K(L)s + D(L)\dot{s}) \cos \theta_{st},$$

where θ_{st} is the stance leg angle, and $s = L - L_0$ is the spring deformation. Taking the derivative of the vertical GRF w.r.t. time results in the affine control system for which the state is the input to the system Eq. (3):

$$\dot{\eta} = f_\eta + g_\eta F_z^P \quad (4)$$

$$\dot{F}_z^P = f_z + g_z \tau_z \quad (5)$$

where $\tau = \ddot{L}$ is the acceleration of the rest-length of the aSLIP. As this system is in *strict-feedback form*, we can apply a control Lyapunov function version of the canonical backstepping approach to stabilize the dynamics of both systems with the augmented Lyapunov equation $V(\eta, F_z) = \eta^T P \eta + \frac{1}{2}(F_z - \bar{F}_z)$. More details can be seen in [14].

We also want to enforce the desired GRF from the human walking in the controller. Since the time derivative of F_z is affine in the control input \ddot{L} which allows contact force embedding with Control Barrier Functions (CBF) based on the constraint

$$(1 - c)F_z^d + \Delta_F \leq F_z^a \leq (1 + c)F_z^d - \Delta_F, \quad (6)$$

where $c \in (0, 1)$ is a relaxation parameter and Δ_F is an additional bound such that the permissible set at the boundary of DSP is nontrivial [18]. This can be included in both the SSP and the DSP as linear constraints in the CLF-QP. In SSP, we define a single CBF which ensures the robot's GRF remains in a relaxed tube. In DSP the former stance foot has a GRF that goes to zero while the former swing foot has a GRF that goes from zero to the initial GRF of the following SSP. During the downstep, we use the interpreted GRF trajectory from Fig. 4 as the desired F_z^d .

B. Horizontal stabilization

The horizontal state is stabilized using the S2S dynamics approximation via the Hybrid Linear Inverted Pendulum (H-LIP). Using a constant height assumption on the vertical CoM during SSP and DSP (which is relaxed due to the tracking of the human vertical CoM behavior), the S2S dynamics of the system can be described in closed-form. In SSP, the horizontal dynamics of the H-LIP model are described by $\ddot{p} = \lambda^2 p$, where p is the horizontal position of the CoM w.r.t. the stance foot and $\lambda = \sqrt{g/z_0}$ with g being the gravity constant and z_0 being the nominal walking height. In DSP, we assume a constant horizontal CoM velocity. The S2S dynamics (from the end of SSP of step k to the end of SSP of step $k+1$) of the H-LIP are step-size and step-time dependent according to

$$\mathbf{x}_{\text{SSP}k+1}^- = e^{A_{\text{SSP}}T_{\text{SSP}}} \begin{bmatrix} 1 & T_{\text{DSP}} \\ 0 & 1 \end{bmatrix} \mathbf{x}_{\text{SSP}k}^- + e^{A_{\text{SSP}}T_{\text{SSP}}} \begin{bmatrix} -1 \\ 0 \end{bmatrix} u_k, \quad (7)$$

where u_k is the step-size, T_{SSP} and T_{DSP} are the duration of the SSP and DSP respectively, and A_{SSP} originates from the state-space representation of the SSP dynamics

$$\frac{d}{dt} \begin{bmatrix} p \\ \dot{p} \end{bmatrix} = \begin{bmatrix} 0 & 1 \\ \lambda^2 & 0 \end{bmatrix} \begin{bmatrix} p \\ \dot{p} \end{bmatrix} := A_{\text{SSP}} \begin{bmatrix} p \\ \dot{p} \end{bmatrix}. \quad (8)$$

As mentioned previously, in reality we have a non-constant vertical CoM position from the aSLIP nominal gait and compensation optimization $\ddot{p} = \lambda^2 p = gp/z_{\text{CoM}}(t)$, yet the contribution of this deviation contributes to model difference between the H-LIP and the system (human or robot) according to

$$x_{k+1} = Ax_k + Bu_k + w \quad (9)$$

The stepsize for flat-ground walking is determined by

$$u_k^d = u_k^{\text{H-LIP}} + K(x^{\text{aSLIP}} - x^{\text{H-LIP}}) \quad (10)$$

where $u_k^{\text{H-LIP}}$ is the nominal step-size of the H-LIP, K is the deadbeat gain (i.e. $(A + BK)^2 = 0$), and x^{aSLIP} is the horizontal state of the aSLIP walker. More details of the H-LIP stepping can be found in [14], [10]. For the downstep scenario's, the H-LIP is taking the *slope* of the walking surface into account. For the expected downstep, the slope is altered at the VLO before the downstep based on the previous step-size and the known downstep height. For the unexpected downstep, the slope is altered continuously based on the current step-size and the penetration of the swing foot.

IV. 3D ROBOTIC WALKING REALIZATION

We now present our human inspired walking synthesis on a 3D bipedal robot. We use the robot Cassie as an example, which is a bipedal walking system with significant morphological differences compared to human.

A. Human Inspired Trajectory Synthesis

Before we translate the observed motion and dynamics of the human to a bipedal robot, we first emphasize several potential differences between the two systems. A robot may have a different distribution of mass and it may not have an upper body or arms. The robot Cassie has a much lower CoM. The abstraction towards the CoM assumes whole-body behavior during walking is primarily captured by the CoM dynamics. A robot may have different or no leg compliance compared to the human test subject. The robot may not have actuated feet or may have point feet, which limits the realizable behaviors such the foot rolling motion on human. To be general, we do not consider the compliance in the robot or complex foot rolling behaviors on the robot.

Based on the RoM characterization of the human walking, we want to transfer the CoM trajectory and the GRF profile from the human to the robot Cassie. Firstly, the nominal leg length of Cassie (as defined by the distance between the contact pivot and the CoM rather than the hip) is a decision variable which determines the scaling of the other gait parameters. For a chosen averaged leg length over a step, we assume the step SSP duration of Cassie is related to that of the human by the passive pendulum properties of the swing phase in nominal walking

$$T_{S,C} = \frac{\sqrt{\bar{L}_C/g}}{\sqrt{\bar{L}_H/g}} T_{S,H}, \quad (11)$$

where $T_{S,C}$ and $T_{S,H}$ are the walking period of Cassie and human respectively, and \bar{L}_C and \bar{L}_H are the averaged leg length of Cassie and the human respectively. For the flat-footed walking, we remove the horizontal displacement of the CoM caused by the foot-roll phases

$$x_{\text{CoM},C} = \frac{1 - x_{\text{roll}}}{L_{s,H}} x_{\text{CoM},H} \quad (12)$$

where $x_{\text{CoM},C}$ is the scaled horizontal displacement of the CoM for Cassie, x_{roll} is the horizontal displacement of the CoM during the heel and toe roll phases, $L_{s,H}$ is the leg length of the human, and $x_{\text{CoM},H}$ is the horizontal displacement of the CoM of the human. This allows us to redefine the nominal walking velocity for Cassie as

$$\dot{x}_{\text{CoM},C} = (x_{\text{CoM},C}(t_f) - x_{\text{CoM},C}(t_0))/T_{S,C}, \quad (13)$$

where t_0 and t_f are the start and end-time of a step. The desired ground reaction forces are scaled with the mass fraction according to

$$F_{z,C} = \frac{m_C}{m_H} F_{z,H}, \quad (14)$$

where $F_{z,C}$ and $F_{z,H}$ are the vertical GRFs of Cassie and the human respectively and m_C and m_H are the total masses of Cassie and the human respectively. The vertical CoM trajectory is scaled by the fractional change in virtual leg length of the human and removing the contribution of the roll phases to the stance leg angle. The resulting outputs can be embedded onto the aSLIP representation obtained in [17].

For the scaled data, similar multi-parameterized surfaces as shown in Fig. 4 are available for Cassie.

As we want to control the full-order dynamics of Cassie, we are not only concerned with vertical CoM tracking with force-embedding and horizontal stabilization, we also need to control the additional degrees of freedom of Cassie. Subsequently, the outputs of the walking are defined as

$$y^d = \begin{bmatrix} [\alpha_{\text{pelvis}} \quad \beta_{\text{pelvis}} \quad \gamma_{st} \quad \gamma_{sw}]^T \\ z_{\text{CoM}}^d(t, z_{sw}, n_{ds}) \\ x_{sw}(t, \theta) \\ y_{sw}(t, \theta) \\ z_{sw}(t, n_{ds}) \\ \alpha_{sw} \end{bmatrix}, \quad (15)$$

where α , β , and γ indicate pitch, roll, and yaw respectively which are represented by Bézier splines guiding the trajectory to 0 angle, and n_{ds} indicates the downstep step. The swing foot positions in the horizontal plane originate from a decoupling of a Period-1 H-LIP for the sagittal plane and a Period-2 H-LIP for the coronal plane as shown in [10]. The vertical position of the swing foot tracks a pre-defined Bézier spline with unique formulations for the over-step and up-step for the downsteps scenarios. The desired GRFs are parameterized similarly to the vertical CoM trajectories $F^d(t, z_{sw}, n_{ds})$.

B. Contact Force Embedded Task Space Control

To realize the proposed trajectory synthesis on the bipedal robot, we apply the task space controller (TSC) for output tracking. The force embedding can be realized via a linear constraint on the holonomic forces, which are optimization variables in the TSC. We directly specify a linear constraint on the vertical GRF to realize the force-embedding.

$$(1 - c)F^d + \Delta_F \leq SF_h \leq (1 + c)F^d - \Delta_F, \quad (16)$$

where $F^d = F^d(t, z_{sw}, n_{ds})$ and S is a selection matrix to select the vertical component of the GRF from F_h (the vector of all the holonomic forces).

The final quadratic program with the equation of motion (EOM) constraint, holonomic constraints, contact force constraints is formulated as:

$$\begin{aligned} \min_{u, F_h, \dot{q}} \quad & \|\dot{y}^a - \dot{y}^d - \dot{y}^t\|^2 & (17) \\ \text{s.t.} \quad & D\ddot{q} + C = J_h^T F_h + B\tau & (\text{EOM}) \\ & J_h \ddot{q} + \dot{J}_h \dot{q} = 0 & (\text{holonomic}) \\ & \tau_{\min} \leq \tau \leq \tau_{\max} & (\text{torque limit}) \\ & A_{\text{GRF}} F_{\text{GRF}} \leq 0 & (\text{friction cone}) \\ & (1 - c)F^d + \Delta_F \leq SF_h \leq (1 + c)F^d + \Delta_F \end{aligned}$$

where q is the configuration, D is the mass matrix, C is the Coriolis and gravitation term, J_h is the Jacobian of the holonomic constraints, B is the actuation matrix, τ is the input torque, and A_{GRF} is a constant matrix that specifies the friction cone constraints. y^a is the actual output, and $\ddot{y}^t = -K_p(y^a - y^d) - K_d(\dot{y}^a - \dot{y}^d)$ with K_p, K_d being the feedback PD gain matrices.

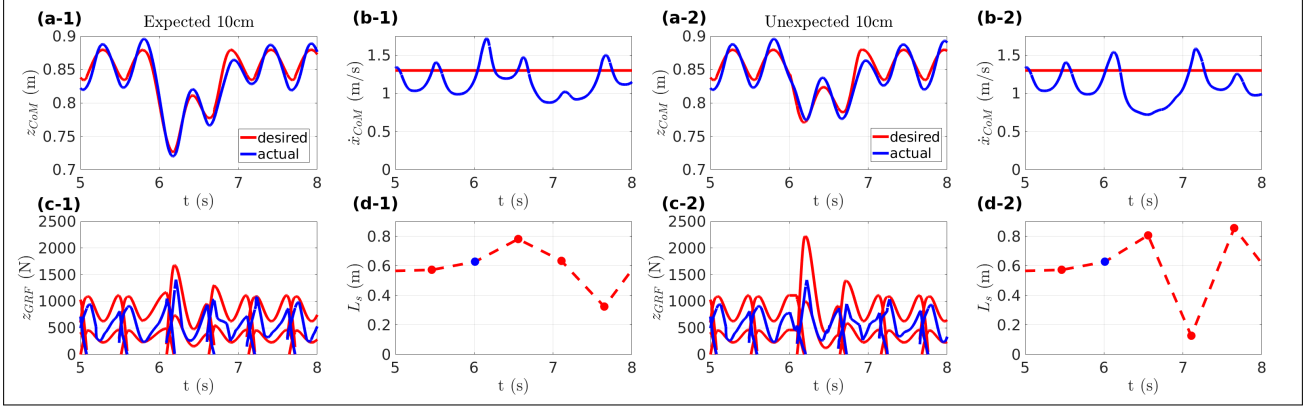


Fig. 7. Simulation results of the aSLIP walking over the expected (1) and unexpected (2) downstep with 10cm depth: (a) the vertical mass trajectories of the desired ones and the actual ones, (b) the horizontal velocity of the mass, (c) the GRF profile with its bounds, and (d) the step-lengths

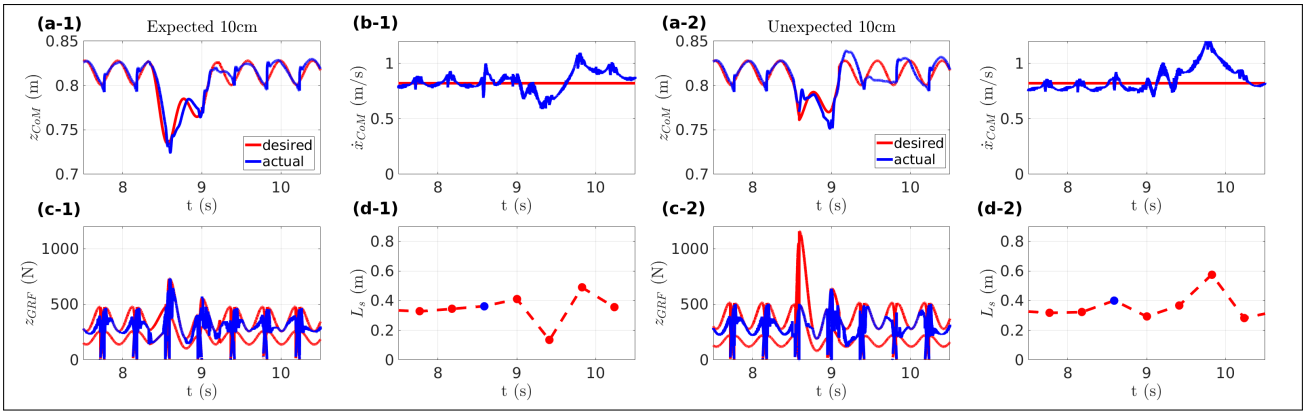


Fig. 8. Simulation results of Cassie walking over the expected and unexpected downsteps with 10cm depth. Individual subfigures are explained in Fig. 7.

The QP is solved using OSQP [19] at 2 KHz in the Mujoco physics simulator [20]. During SSP and DSP, each constraint in the QP considers one or two feet in contact with the ground respectively. A time-based domain switching determines the number of feet in contact with the ground. In case when the QP fails in the DSP due to early lift-off, a SSP controller is used as a backup controller.

V. RESULTS

The methodology presented in the paper, and specifically the RoM trajectory synthesis from human data, was applied to the aSLIP model and the robot Cassie to walking over expected and unexpected downsteps.

A. aSLIP Walking

We first apply the proposed approach to the aSLIP model. As the aSLIP model assumes a massless swing leg, the desired swing-leg behavior can directly be set and does not affect the dynamics of the system. Subsequently, the H-LIP step adaptation from Fig. 1 does not affect the difference step-sizes between the expected and unexpected downsteps. Although the vertical CoM behavior and the GRFs obtained from the human are successfully embedded onto the aSLIP walker, this fact prevents an accurate representation of the step-sizes of the human. We do see that due to the changes in

vertical CoM position, the periodic orbits occur outside the orbital lines. For the expected case, this seems to increase the walking velocity during downstep while for the unexpected case, this leads to a decrease. This is contrary to what we observe in the human data.

B. 3D Cassie Walking

The main simulation results of the paper demonstrate the successful translation of human RoM data to the realization of downstep behaviors on Cassie (illustrated in Fig. 9). To achieve 3D walking, we are additionally concerned with stabilizing the coronal plane which is successfully achieved with P2 orbits of the H-LIP regardless of the deviations to the nominal walking height. Here tracking becomes more difficult and the trade-off between tracking and force embedding becomes apparent. In Fig. 8 we see decreased tracking performance for the unexpected downstep scenario as the recovery behavior exceeds the one step required for the expected scenario. We argue that this is predominantly due to inaccurate desired GRFs from the human measurements. The control of the swing leg and vertical CoM for humans is mostly governed by the passive dynamics of the system when experiencing the unexpected downstep. For the robot, the vertical swing foot behavior is explicitly controlled at all times which prevents a fast impact velocity and, with



Fig. 9. Gait tiles (associated with the plots in Fig. 8) of Cassie walking down an expected downstep (left) and an unexpected downstep (right).

the requirement of lowering the CoM, results in a minimum GRF during the downstep.

The improved controllability of Cassie w.r.t. the human means that in both scenarios—known and unknown downsteps—the increase of the forward CoM velocity is significantly reduced. Thus both known downsteps and unknown downsteps can be traversed more effectively, and controllers based on foot penetration can help traverse unexpected changes in walking height and can explicitly plan motion when exceeding the nominal step-time.

VI. CONCLUSION AND FUTURE WORK

We have successfully shown that the walking responses of human to the environment can be embedded on morphologically and dynamically different robotic bipedal systems. By scaling the outputs of the human in the motion synthesis and embedding the contact forces in the low-level control, dynamic similarity between models is realized on the closed-loop systems. The proposed method has been successfully realized on the aSLIP and 3D simulated Cassie to overcome expected and unexpected downsteps with similar responses to those found in the human gait. The presented work currently focuses on a specific downstep scenario. Future work will consider a general framework of transferring versatile human locomotion to dynamic bipedal robot behaviors.

VII. ACKNOWLEDGEMENT

The authors would like to thank Guoping Zhao from the Lauflabor lab at Technische Universität Darmstadt for sharing measurement data and advising on its processing.

REFERENCES

- [1] M. A. Daley, J. R. Usherwood, G. Felix, and A. A. Biewener, "Running over rough terrain: guinea fowl maintain dynamic stability despite a large unexpected change in substrate height," *Journal of experimental biology*, vol. 209, no. 1, pp. 171–187, 2006.
- [2] Ö. Drama, J. Vielemeyer, A. Badri-Spröwitz, and R. Müller, "Postural stability in human running with step-down perturbations: an experimental and numerical study," *Royal Society open science*, vol. 7, no. 11, p. 200570, 2020.
- [3] M. Ernst, M. Götzke, R. Müller, and R. Blickhan, "Vertical adaptation of the center of mass in human running on uneven ground," *Human movement science*, vol. 38, pp. 293–304, 2014.
- [4] J. Vielemeyer, E. Griebbach, and R. Müller, "Ground reaction forces intersect above the center of mass even when walking down visible and camouflaged curbs," *Journal of experimental biology*, vol. 222, no. 14, p. jeb204305, 2019.
- [5] M. H. van der Linden, H. T. Hendricks, B. R. Bloem, and J. Duysens, "Hitting a support surface at unexpected height during walking induces loading transients," *Gait & posture*, vol. 29, no. 2, pp. 255–260, 2009.
- [6] K. Green, R. L. Hatton, and J. Hurst, "Planning for the unexpected: Explicitly optimizing motions for ground uncertainty in running," in *2020 IEEE International Conference on Robotics and Automation (ICRA)*. IEEE, 2020, pp. 1445–1451.
- [7] H. Vejdani, Y. Blum, M. Daley, and J. Hurst, "Bio-inspired swing leg control for spring-mass robots running on ground with unexpected height disturbance," *Bioinspiration & biomimetics*, vol. 8, no. 4, p. 046006, 2013.
- [8] E. R. Westervelt, J. W. Grizzle, and D. E. Koditschek, "Hybrid zero dynamics of planar biped walkers," *IEEE transactions on automatic control*, vol. 48, no. 1, pp. 42–56, 2003.
- [9] K. Sreenath, H.-W. Park, I. Poulakakis, and J. W. Grizzle, "A compliant hybrid zero dynamics controller for stable, efficient and fast bipedal walking on mabel," *The International Journal of Robotics Research*, vol. 30, no. 9, pp. 1170–1193, 2011.
- [10] X. Xiong and A. Ames, "3d underactuated bipedal walking via h-hip based gait synthesis and stepping stabilization," *arXiv preprint arXiv:2101.09588*, 2021.
- [11] A. D. Ames, "Human-inspired control of bipedal walking robots," *IEEE Transactions on Automatic Control*, vol. 59, no. 5, pp. 1115–1130, 2014.
- [12] D. Torricelli, R. S. Mizanoor, V. Lippi, M. Weckx, G. Mathijssen, B. Vanderborght, T. Mergner, D. Lefeber, and J. L. Pons, "Benchmarking human likeness of bipedal robot locomotion: State of the art and future trends," *Metrics of Sensory Motor Coordination and Integration in Robots and Animals*, pp. 147–166, 2020.
- [13] Agility Robotics: <http://www.agilityrobotics.com>.
- [14] X. Xiong and A. Ames, "Slip walking over rough terrain via h-hip stepping and backstepping-barrier function inspired quadratic program," *IEEE Robot. Autom. Lett.*, vol. 6, no. 2, pp. 2122–2129, 2021.
- [15] S. L. Delp, F. C. Anderson, A. S. Arnold, P. Loan, A. Habib, C. T. John, E. Guendelman, and D. G. Thelen, "Opensim: open-source software to create and analyze dynamic simulations of movement," *IEEE transactions on biomedical engineering*, vol. 54, no. 11, pp. 1940–1950, 2007.
- [16] A. Seth, J. L. Hicks, T. K. Uchida, A. Habib, C. L. Dembia, J. J. Dunne, C. F. Ong, M. S. DeMers, A. Rajagopal, M. Millard *et al.*, "Opensim: Simulating musculoskeletal dynamics and neuromuscular control to study human and animal movement," *PLoS computational biology*, vol. 14, no. 7, p. e1006223, 2018.
- [17] X. Xiong and A. D. Ames, "Bipedal hopping: Reduced-order model embedding via optimization-based control," in *2018 IEEE/RSJ International Conference on Intelligent Robots and Systems (IROS)*. IEEE, 2018, pp. 3821–3828.
- [18] X. Xiong, J. Reher, and A. D. Ames, "Global position control on underactuated bipedal robots: Step-to-step dynamics approximation for step planning," in *2021 IEEE International Conference on Robotics and Automation (ICRA)*, 2021, pp. 2825–2831.
- [19] B. Stellato, G. Banjac, P. Goulart, A. Bemporad, and S. Boyd, "Osqp: An operator splitting solver for quadratic programs," *Mathematical Programming Computation*, vol. 12, no. 4, pp. 637–672, 2020.
- [20] E. Todorov, T. Erez, and Y. Tassa, "Mujoco: A physics engine for model-based control," in *2012 IEEE/RSJ international conference on intelligent robots and systems*. IEEE, 2012, pp. 5026–5033.

B | HUMAN EXPERIMENTS

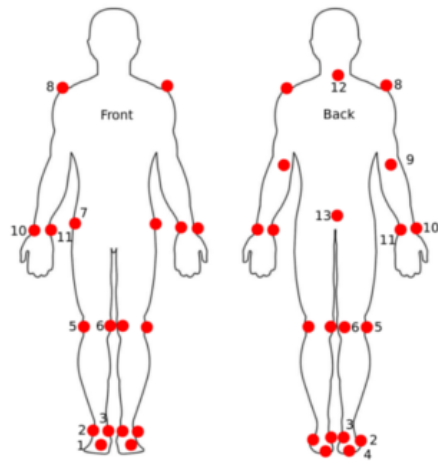


Figure B.1: Motion capture markers on the human subject. 1: Right toe tip, 2: Right ankle lateral, 3: Right ankle medial, 4: Right heel, 5: Right knee lateral, 6: Right knee medial, 7: Anterior superior iliac spine, 8: Right Acromium, 9: Right elbow, 10: Right wrist lateral, 11: Right wrist medial, 12: C7, 13: Sacral. On the right is the perturbation platform.

C

ACTUATED SPRING LOADED INVERTED PENDULUM MODEL

the aSLIP model [17; 78] describes the equations of motion of a point-mass model with stiffness and damping. The actuation is on the second time derivative of the rest-length of the spring. The equations for the SSP and DSP are respectively

$$\begin{aligned}
 \text{SSP: } & \begin{cases} \ddot{r}_{st} = \frac{F_{st}}{m} - g \cos(\beta_{st}) + r_{st} \dot{\beta}_{st}^2 \\ \ddot{\beta}_{st} = \frac{1}{r_{st}} (-2\dot{\beta}_{st} \dot{r}_{st} + g \sin(\beta_{st})) \\ \ddot{s}_{st} = \ddot{L}_{st} - \ddot{r}_{st} \end{cases} \\
 \text{DSP: } & \begin{cases} \ddot{r}_{st} = \frac{F_{st} + F_{sw} \cos(\delta_q)}{m} - g \cos(\beta_{st}) + r_{st} \dot{\beta}_{st}^2 \\ \ddot{\beta}_{st} = \frac{-2\dot{\beta}_{st} \dot{r}_{st} + g \sin(\beta_{st}) - \frac{F_{sw}}{m} \sin(\delta_q)}{r_{st}} \\ \ddot{s}_{st} = \ddot{L}_{st} - \ddot{r}_{st} \\ \ddot{r}_{sw} = \frac{F_{sw} + F_{st} \cos(\delta_q)}{m} - g \cos(\beta_{sw}) + r_{sw} \dot{\beta}_{sw}^2 \\ \ddot{\beta}_{sw} = \frac{-2\dot{\beta}_{sw} \dot{r}_{sw} + g \sin(\beta_{sw}) - \frac{F_{st}}{m} \sin(\delta_q)}{r_{sw}} \\ \ddot{s}_{sw} = \ddot{L}_{sw} - \ddot{r}_{sw} \end{cases} \quad (\text{C.1})
 \end{aligned}$$

where $\delta_q = \beta_1 - \beta_2$ and $\ddot{L}_{1/2}$ are the inputs and the second derivatives of the leg length of the springs.

D | BACKSTEPPING BARRIER FUNCTION RESULTS

The multi-parameterized vertical CoM and GRF surfaces for Cassie, as presented for the human in Figure 3.6 and 3.7, are shown in Figure D.1 and D.2. The surfaces have great similarities but differences in the deviation of the vertical CoM position, the mean vertical CoM position, the total step-time, and the height of the GRF surface as explained in Section 5.

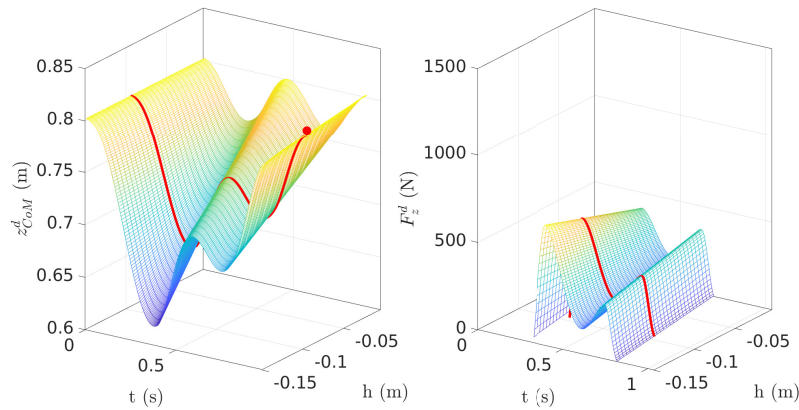


Figure D.1: The desired vertical CoM trajectory z_{CoM}^d and the GRF in SSP parameterized by time (t) and the downstep height h for **expected** downsteps for Cassie.

Reduced-order Model walking results of the aSLIP representative of Cassie with the outputs scaled in accordance with Section 5 are shown in Figure D.3 and D.4. The results of RoM walking for Cassie are similar to those of RoM walking for the human which substantiate the claim of permissible scaling with the goal of dynamic similarity.

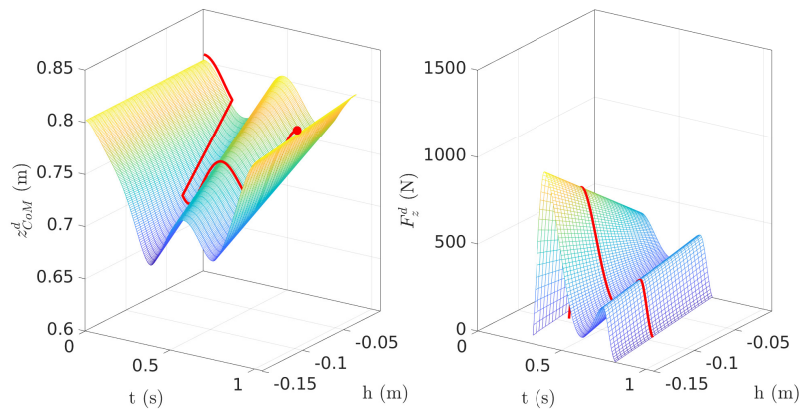


Figure D.2: The desired vertical CoM trajectory z_{CoM}^d and the GRF in SSP parameterized by time (t) and the downstep height h for **unexpected** downsteps for Cassie.

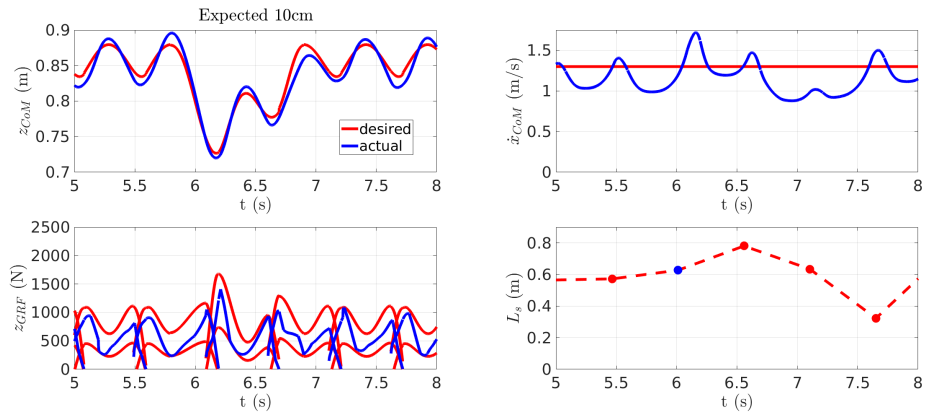


Figure D.3: Simulation results of the aSLIP walking over the **expected** downstep with 10cm depth: (a) the vertical mass trajectories of the desired ones and the actual ones, (b) the horizontal velocity of the mass, (c) the GRF profile with its bounds, and (d) the step-lengths

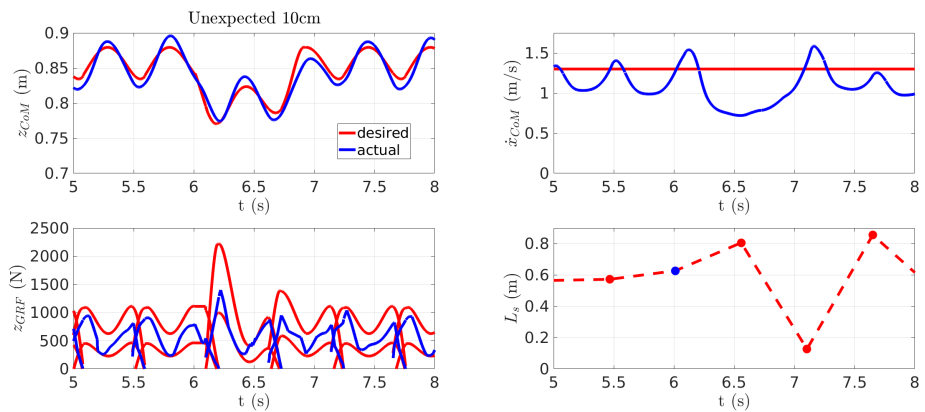


Figure D.4: Simulation results of the aSLIP walking over the **unexpected** downstep with 10cm depth: (a) the vertical mass trajectories of the desired ones and the actual ones, (b) the horizontal velocity of the mass, (c) the GRF profile with its bounds, and (d) the step-lengths

E | 3D ROBOT WALKING CONTROL

For the 3D implementation, the PD gain matrices and the weights for the outputs

$$y_{SSP}^d = \begin{bmatrix} [\alpha_{\text{pelvis}} \quad \beta_{\text{pelvis}} \quad \gamma_{st} \quad \gamma_{\text{sw}}]^T \\ z_{CoM}^d(t, z_{\text{sw}}, n_{ds}) \\ x_{\text{sw}}(t, \theta) \\ y_{\text{sw}}(t, \theta) \\ z_{\text{sw}}(t, n_{ds}) \\ \alpha_{\text{sw}} \end{bmatrix}, \quad (\text{E.1})$$

are given as

$$K_P = \text{diag}([1000 \quad 1000 \quad 1000 \quad 1500 \quad 3000 \quad 1000 \quad 4000 \quad 4000 \quad 5000 \quad 4000]) \quad (\text{E.2})$$

$$K_D = \text{diag}([50 \quad 50 \quad 100 \quad 200 \quad 50 \quad 250 \quad 50 \quad 250 \quad 250 \quad 50]) \quad (\text{E.3})$$

$$W = [150 \quad 100 \quad 400 \quad 1000 \quad 1000 \quad 50000 \quad 1000 \quad 4000 \quad 1000 \quad 4500] \quad (\text{E.4})$$

where we notice a relatively large weight on the swing foot trajectories in order to guarantee close tracking of the swing foot. The next page presents the algorithms for the expected and the unexpected downsteps in Algorithm 1 and 2 respectively.

Algorithm 1 Human-to-robot TSC-QP controller for **expected** downsteps

Require: Behavior: $z_{\text{CoM}}(t, h, n_{ds}), F_z(t, h, n_{ds}), T_{\text{SSP}}, T_{\text{DSP}}, n_{ds} = 0, h$ Control: $K_P, K_D, W, W_{\text{reg}}$ **while** Simulation **do** **if** new step **then** **if** VLO and step=downstepStep **then** $n_{ds} \leftarrow 1$ **else if** $n_{ds} = 1$ or $n_{ds} = 2$ **then** $n_{ds} \leftarrow n_{ds} + 1$ **else** $n_{ds} \leftarrow 0$ **end if** **end if** $z_{\text{CoM}}^d \leftarrow z_{\text{CoM}}(t, h, n_{ds})$ $F_z^d \leftarrow F_z(t, h, n_{ds})$ **if** SSP **then** Desired step size \leftarrow H-LIP in Eq. (4.18) Desired horizontal swing foot position \leftarrow Eq. (6.10) Desired vertical swing foot position \leftarrow Eq. (6.11) $y^d \leftarrow$ Eq. (6.6) **else** $y^d \leftarrow$ Eq. (6.7) **end if** $u \leftarrow$ TSC-QP in Eq. (6.13)**end while**

Algorithm 2 Human-to-robot TSC-QP controller for **unexpected** downsteps

Require: Behavior: $z_{\text{CoM}}(t, z_{\text{sw}}, n_{ds}), F_z(t, z_{\text{sw}}, n_{ds}), T_{\text{SSP}}, T_{\text{DSP}}, n_{ds} = 0$ Control: $K_P, K_D, W, W_{\text{reg}}$ **while** Simulation **do** **if** new step **then** **if** $z_{\text{sw}} < 0$ and isDownstep = *false* **then** $h \leftarrow z_{\text{sw}}$ $n_{ds} \leftarrow 1$ isDownstep \leftarrow true **else if** $n_{ds} = 1$ or $n_{ds} = 2$ **then** $n_{ds} \leftarrow n_{ds} + 1$ **else** $n_{ds} \leftarrow 0$ **end if** **end if** $z_{\text{CoM}}^d \leftarrow z_{\text{CoM}}(t, h, n_{ds})$ $F_z^d \leftarrow F_z(t, h, n_{ds})$ **if** SSP **then** Desired step size \leftarrow H-LIP in Eq. (4.18) Desired horizontal swing foot position \leftarrow Eq. (6.10) Desired vertical swing foot position \leftarrow Eq. (6.11) $y^d \leftarrow$ Eq. (6.6) **else** $y^d \leftarrow$ Eq. (6.7) **end if** $u \leftarrow$ TSC-QP in Eq. (6.13)**end while**

BIBLIOGRAPHY

- [1] M. A. Daley, J. R. Usherwood, G. Felix, and A. A. Biewener, "Running over rough terrain: guinea fowl maintain dynamic stability despite a large unexpected change in substrate height," *Journal of experimental biology*, vol. 209, no. 1, pp. 171–187, 2006.
- [2] Ö. Drama, J. Vielemeyer, A. Badri-Spröwitz, and R. Müller, "Postural stability in human running with step-down perturbations: an experimental and numerical study," *Royal Society open science*, vol. 7, no. 11, p. 200570, 2020.
- [3] M. Ernst, M. Götze, R. Müller, and R. Blickhan, "Vertical adaptation of the center of mass in human running on uneven ground," *Human movement science*, vol. 38, pp. 293–304, 2014.
- [4] J. Vielemeyer, E. Griesbach, and R. Müller, "Ground reaction forces intersect above the center of mass even when walking down visible and camouflaged curbs," *Journal of experimental biology*, vol. 222, no. 14, p. jeb204305, 2019.
- [5] M. H. van der Linden, D. S. Marigold, F. J. Gabreëls, and J. Duysens, "Muscle reflexes and synergies triggered by an unexpected support surface height during walking," *Journal of neurophysiology*, 2007.
- [6] M. Shinya, S. Fujii, and S. Oda, "Corrective postural responses evoked by completely unexpected loss of ground support during human walking," *Gait & posture*, vol. 29, no. 3, pp. 483–487, 2009.
- [7] S. Masahiro and O. Shingo, "Fast muscle responses to an unexpected foot-in-hole scenario, evoked in the context of prior knowledge of the potential perturbation," *Experimental brain research*, vol. 203, no. 2, pp. 437–446, 2010.
- [8] S. Aminiaghdam, R. Blickhan, R. Müller, and C. Rode, "Posture alteration as a measure to accommodate uneven ground in able-bodied gait," *PloS one*, vol. 12, no. 12, p. e0190135, 2017.
- [9] S. Aminiaghdam, R. Müller, and R. Blickhan, "Locomotor stability in able-bodied trunk-flexed gait across uneven ground," *Human Movement Science*, vol. 62, pp. 176–183, 2018.
- [10] K. Green, R. L. Hatton, and J. Hurst, "Planning for the unexpected: Explicitly optimizing motions for ground uncertainty in running," in *2020 IEEE International Conference on Robotics and Automation (ICRA)*, pp. 1445–1451, IEEE, 2020.
- [11] H. Vejdani, Y. Blum, M. Daley, and J. Hurst, "Bio-inspired swing leg control for spring-mass robots running on ground with unexpected height disturbance," *Bioinspiration & biomimetics*, vol. 8, no. 4, p. 046006, 2013.
- [12] E. R. Westervelt, J. W. Grizzle, and D. E. Koditschek, "Hybrid zero dynamics of planar biped walkers," *IEEE transactions on automatic control*, vol. 48, no. 1, pp. 42–56, 2003.
- [13] K. Sreenath, H.-W. Park, I. Poulakakis, and J. W. Grizzle, "A compliant hybrid zero dynamics controller for stable, efficient and fast bipedal walking on marble," *The International Journal of Robotics Research*, vol. 30, no. 9, pp. 1170–1193, 2011.
- [14] X. Xiong and A. Ames, "3d underactuated bipedal walking via h-lip based gait synthesis and stepping stabilization," *arXiv preprint arXiv:2101.09588*, 2021.

- [15] M. Dai, X. Xiong, and A. Ames, "Bipedal walking on constrained footholds: Momentum regulation via vertical com control," *arXiv preprint arXiv:2104.10367*, 2021.
- [16] Y. Gong and J. Grizzle, "One-step ahead prediction of angular momentum about the contact point for control of bipedal locomotion: Validation in a lip-inspired controller," in *2021 IEEE International Conference on Robotics and Automation (ICRA)*, pp. 2832–2838, IEEE, 2021.
- [17] X. Xiong and A. D. Ames, "Bipedal hopping: Reduced-order model embedding via optimization-based control," in *2018 IEEE/RSJ International Conference on Intelligent Robots and Systems (IROS)*, pp. 3821–3828, IEEE, 2018.
- [18] H. Diedam, D. Dimitrov, P.-B. Wieber, K. Mombaur, and M. Diehl, "Online walking gait generation with adaptive foot positioning through linear model predictive control," in *2008 IEEE/RSJ International Conference on Intelligent Robots and Systems*, pp. 1121–1126, IEEE, 2008.
- [19] S. Faraji, S. Pouya, C. G. Atkeson, and A. J. Ijspeert, "Versatile and robust 3d walking with a simulated humanoid robot (atlas): A model predictive control approach," in *2014 IEEE International Conference on Robotics and Automation (ICRA)*, pp. 1943–1950, IEEE, 2014.
- [20] M. J. Powell, E. A. Cousineau, and A. D. Ames, "Model predictive control of underactuated bipedal robotic walking," in *2015 IEEE International Conference on Robotics and Automation (ICRA)*, pp. 5121–5126, IEEE, 2015.
- [21] R. Niiyama, S. Nishikawa, and Y. Kuniyoshi, "Athlete robot with applied human muscle activation patterns for bipedal running," in *2010 10th IEEE-RAS International Conference on Humanoid Robots*, pp. 498–503, IEEE, 2010.
- [22] D. G. Caldwell, G. A. Medrano-Cerda, and C. J. Bowler, "Investigation of bipedal robot locomotion using pneumatic muscle actuators," in *Proceedings of International Conference on Robotics and Automation*, vol. 1, pp. 799–804, IEEE, 1997.
- [23] T. Luksch *et al.*, *Human-like control of dynamically walking bipedal robots*. Citeseer, 2010.
- [24] D. Tlalolini, C. Chevallereau, and Y. Aoustin, "Human-like walking: Optimal motion of a bipedal robot with toe-rotation motion," *IEEE/ASME Transactions on Mechatronics*, vol. 16, no. 2, pp. 310–320, 2010.
- [25] D. Torricelli, R. S. Mizanoor, V. Lippi, M. Weckx, G. Mathijssen, B. Vanderborght, T. Mergner, D. Lefeber, and J. L. Pons, "Benchmarking human likeness of bipedal robot locomotion: State of the art and future trends," *Metrics of Sensory Motor Coordination and Integration in Robots and Animals*, pp. 147–166, 2020.
- [26] R. W. Sinnet, M. J. Powell, R. P. Shah, and A. D. Ames, "A human-inspired hybrid control approach to bipedal robotic walking," *IFAC Proceedings Volumes*, vol. 44, no. 1, pp. 6904–6911, 2011.
- [27] A. D. Ames, "Human-inspired control of bipedal walking robots," *IEEE Transactions on Automatic Control*, vol. 59, no. 5, pp. 1115–1130, 2014.
- [28] K. Hu, C. Ott, and D. Lee, "Online human walking imitation in task and joint space based on quadratic programming," in *2014 IEEE International Conference on Robotics and Automation (ICRA)*, pp. 3458–3464, IEEE, 2014.
- [29] E. Andrada and R. Blickhan, "Only the groucho number ensures dynamic similarity during walking,"

- [30] H.-W. Park, A. Ramezani, and J. W. Grizzle, "A finite-state machine for accommodating unexpected large ground-height variations in bipedal robot walking," *IEEE Transactions on Robotics*, vol. 29, no. 2, pp. 331–345, 2012.
- [31] C. O. Saglam and K. Byl, "Robust policies via meshing for metastable rough terrain walking," in *Robotics: Science and Systems*, Citeseer, 2014.
- [32] Y. Liu, P. M. Wensing, J. P. Schmiedeler, and D. E. Orin, "Terrain-blind humanoid walking based on a 3-d actuated dual-slip model," *IEEE Robotics and Automation Letters*, vol. 1, no. 2, pp. 1073–1080, 2016.
- [33] M. Fevre, B. Goodwine, and J. P. Schmiedeler, "Terrain-blind walking of planar underactuated bipeds via velocity decomposition-enhanced control," *The International Journal of Robotics Research*, vol. 38, no. 10-11, pp. 1307–1323, 2019.
- [34] S. Rezazadeh, C. Hubicki, M. Jones, A. Peekema, J. Van Why, A. Abate, and J. Hurst, "Spring-mass walking with atrias in 3d: Robust gait control spanning zero to 4.3 kph on a heavily underactuated bipedal robot," in *Dynamic Systems and Control Conference*, vol. 57243, p. V001T04A003, American Society of Mechanical Engineers, 2015.
- [35] X. Xiong and A. Ames, "3-d underactuated bipedal walking via h-lip based gait synthesis and stepping stabilization," *IEEE Transactions on Robotics*, 2022.
- [36] Agility Robotics: <http://www.agilityrobotics.com>.
- [37] X. Xiong and A. Ames, "Slip walking over rough terrain via h-lip stepping and backstepping-barrier function inspired quadratic program," *IEEE Robot. Autom. Lett.*, vol. 6, no. 2, pp. 2122–2129, 2021.
- [38] A. Rajagopal, C. L. Dembia, M. S. DeMers, D. D. Delp, J. L. Hicks, and S. L. Delp, "Full-body musculoskeletal model for muscle-driven simulation of human gait," *IEEE transactions on biomedical engineering*, vol. 63, no. 10, pp. 2068–2079, 2016.
- [39] V. T. Inman, H. D. Eberhart, *et al.*, "The major determinants in normal and pathological gait," *JBJS*, vol. 35, no. 3, pp. 543–558, 1953.
- [40] G. Cavagna and R. Margaria, "Mechanics of walking," *Journal of applied physiology*, vol. 21, no. 1, pp. 271–278, 1966.
- [41] G. A. Cavagna, F. P. Saibene, and R. Margaria, "External work in walking," *Journal of applied physiology*, vol. 18, no. 1, pp. 1–9, 1963.
- [42] A. D. Kuo, "The six determinants of gait and the inverted pendulum analogy: A dynamic walking perspective," *Human movement science*, vol. 26, no. 4, pp. 617–656, 2007.
- [43] X. Chen, Z. Yu, W. Zhang, Y. Zheng, Q. Huang, and A. Ming, "Bioinspired control of walking with toe-off, heel-strike, and disturbance rejection for a biped robot," *IEEE Transactions on Industrial Electronics*, vol. 64, no. 10, pp. 7962–7971, 2017.
- [44] J. P. Reher, A. Hereid, S. Kolathaya, C. M. Hubicki, and A. D. Ames, "Algorithmic foundations of realizing multi-contact locomotion on the humanoid robot durus," in *Algorithmic Foundations of Robotics XII*, pp. 400–415, Springer, 2020.
- [45] E. Ambrose, W.-L. Ma, C. Hubicki, and A. D. Ames, "Toward benchmarking locomotion economy across design configurations on the modular robot: Amber-3m," in *2017 IEEE Conference on Control Technology and Applications (CCTA)*, pp. 1270–1276, IEEE, 2017.

- [46] T. McGeer *et al.*, “Passive dynamic walking,” *Int. J. Robotics Res.*, vol. 9, no. 2, pp. 62–82, 1990.
- [47] S. H. Collins, M. Wisse, and A. Ruina, “A three-dimensional passive-dynamic walking robot with two legs and knees,” *The International Journal of Robotics Research*, vol. 20, no. 7, pp. 607–615, 2001.
- [48] M. Wisse, “Three additions to passive dynamic walking; actuation, an upper body, and 3d stability,” in *4th IEEE/RAS International Conference on Humanoid Robots, 2004.*, vol. 1, pp. 113–132, IEEE, 2004.
- [49] M. Wisse, G. Keliksdal, J. Van Frankenhyyzen, and B. Moyer, “Passive-based walking robot,” *IEEE Robotics & Automation Magazine*, vol. 14, no. 2, pp. 52–62, 2007.
- [50] K. Hirai, M. Hirose, Y. Haikawa, and T. Takenaka, “The development of honda humanoid robot,” in *Proceedings. 1998 IEEE International Conference on Robotics and Automation (Cat. No. 98CH36146)*, vol. 2, pp. 1321–1326, IEEE, 1998.
- [51] Boston Dynamics: <https://www.bostondynamics.com>.
- [52] K. Narioka, T. Homma, and K. Hosoda, “Humanlike ankle-foot complex for a biped robot,” in *2012 12th IEEE-RAS International Conference on Humanoid Robots (Humanoids 2012)*, pp. 15–20, IEEE, 2012.
- [53] J. Verhagen and A. Seth, “A review on biologically inspired leg design in autonomous bipedal robotics,” 2021.
- [54] H. Miura and I. Shimoyama, “Dynamic walk of a biped,” *The International Journal of Robotics Research*, vol. 3, no. 2, pp. 60–74, 1984.
- [55] S. Collins, A. Ruina, R. Tedrake, and M. Wisse, “Efficient bipedal robots based on passive-dynamic walkers,” *Science*, vol. 307, no. 5712, pp. 1082–1085, 2005.
- [56] N. A. Radford, P. Strawser, K. Hambuchen, J. S. Mehling, W. K. Verdeyen, A. S. Donnan, J. Holley, J. Sanchez, V. Nguyen, L. Bridgwater, *et al.*, “Valkyrie: Nasa’s first bipedal humanoid robot,” *Journal of Field Robotics*, vol. 32, no. 3, pp. 397–419, 2015.
- [57] M. Vukobratović and B. Borovac, “Zero-moment point—thirty five years of its life,” *International journal of humanoid robotics*, vol. 1, no. 01, pp. 157–173, 2004.
- [58] Y. Hurmuzlu and D. B. Marghitu, “Rigid body collisions of planar kinematic chains with multiple contact points,” *The international journal of robotics research*, vol. 13, no. 1, pp. 82–92, 1994.
- [59] J. W. Grizzle, C. Chevallereau, R. W. Sinnet, and A. D. Ames, “Models, feedback control, and open problems of 3d bipedal robotic walking,” *Automatica*, vol. 50, no. 8, pp. 1955–1988, 2014.
- [60] J. Reher, W.-L. Ma, and A. D. Ames, “Dynamic walking with compliance on a cassie bipedal robot,” in *2019 18th European Control Conference (ECC)*, pp. 2589–2595, IEEE, 2019.
- [61] H.-H. Zhao, W.-L. Ma, A. D. Ames, and M. B. Zeagler, “Human-inspired multi-contact locomotion with amber2,” in *2014 ACM/IEEE International Conference on Cyber-Physical Systems (ICCPS)*, pp. 199–210, IEEE, 2014.
- [62] A. D. Ames, K. Galloway, and J. W. Grizzle, “Control lyapunov functions and hybrid zero dynamics,” in *2012 IEEE 51st IEEE Conference on Decision and Control (CDC)*, pp. 6837–6842, IEEE, 2012.

- [63] A. D. Ames, K. Galloway, K. Sreenath, and J. W. Grizzle, "Rapidly exponentially stabilizing control Lyapunov functions and hybrid zero dynamics," *IEEE Transactions on Automatic Control*, vol. 59, no. 4, pp. 876–891, 2014.
- [64] N. Van der Noot, A. J. Ijspeert, and R. Ronsse, "Bio-inspired controller achieving forward speed modulation with a 3d bipedal walker," *The International Journal of Robotics Research*, vol. 37, no. 1, pp. 168–196, 2018.
- [65] F. Heremans, N. Van der Noot, A. J. Ijspeert, and R. Ronsse, "Bio-inspired balance controller for a humanoid robot," in *2016 6th IEEE international conference on biomedical robotics and biomechatronics (BioRob)*, pp. 441–448, IEEE, 2016.
- [66] H. K. Khalil, "Nonlinear systems third edition," *Patience Hall*, vol. 115, 2002.
- [67] J. H. van Dieën, M. Spanjaard, R. Konemann, L. Bron, and M. Pijnappels, "Balance control in stepping down expected and unexpected level changes," *Journal of biomechanics*, vol. 40, no. 16, pp. 3641–3649, 2007.
- [68] M. H. van der Linden, H. T. Hendricks, B. R. Bloem, and J. Duysens, "Hitting a support surface at unexpected height during walking induces loading transients," *Gait & posture*, vol. 29, no. 2, pp. 255–260, 2009.
- [69] S. L. Delp, F. C. Anderson, A. S. Arnold, P. Loan, A. Habib, C. T. John, E. Guendelman, and D. G. Thelen, "Opensim: open-source software to create and analyze dynamic simulations of movement," *IEEE transactions on biomedical engineering*, vol. 54, no. 11, pp. 1940–1950, 2007.
- [70] A. Seth, J. L. Hicks, T. K. Uchida, A. Habib, C. L. Dembia, J. J. Dunne, C. F. Ong, M. S. DeMers, A. Rajagopal, M. Millard, *et al.*, "Opensim: Simulating musculoskeletal dynamics and neuromuscular control to study human and animal movement," *PLoS computational biology*, vol. 14, no. 7, p. e1006223, 2018.
- [71] H.-M. Maus, S. Lipfert, M. Gross, J. Rummel, and A. Seyfarth, "Upright human gait did not provide a major mechanical challenge for our ancestors," *Nature communications*, vol. 1, no. 1, pp. 1–6, 2010.
- [72] R. J. Full and D. E. Koditschek, "Templates and anchors: neuromechanical hypotheses of legged locomotion on land," *Journal of experimental biology*, vol. 202, no. 23, pp. 3325–3332, 1999.
- [73] R. Blickhan and R. Full, "Similarity in multilegged locomotion: bouncing like a monopode," *Journal of Comparative Physiology A*, vol. 173, no. 5, pp. 509–517, 1993.
- [74] G. Borelli, "1685. de motu animalium. lugduni in batavis (1989, maquet p, translator. on the movements of animals)," 1685.
- [75] J. Pratt, T. Koolen, T. De Boer, J. Rebula, S. Cotton, J. Carff, M. Johnson, and P. Neuhaus, "Capturability-based analysis and control of legged locomotion, part 2: Application to m2v2, a lower-body humanoid," *The international journal of robotics research*, vol. 31, no. 10, pp. 1117–1133, 2012.
- [76] B. Dadashzadeh, H. R. Vejdani, and J. Hurst, "From template to anchor: A novel control strategy for spring-mass running of bipedal robots," in *2014 IEEE/RSJ International Conference on Intelligent Robots and Systems*, pp. 2566–2571, IEEE, 2014.
- [77] W. C. Martin, A. Wu, and H. Geyer, "Robust spring mass model running for a physical bipedal robot," in *2015 IEEE International Conference on Robotics and Automation (ICRA)*, pp. 6307–6312, IEEE, 2015.

- [78] X. Xiong and A. D. Ames, "Coupling reduced order models via feedback control for 3d underactuated bipedal robotic walking," in *2018 IEEE-RAS 18th International Conference on Humanoid Robots (Humanoids)*, pp. 1–9, IEEE, 2018.
- [79] I. E. Brown and G. E. Loeb, "A reductionist approach to creating and using neuromusculoskeletal models," in *Biomechanics and neural control of posture and movement*, pp. 148–163, Springer, 2000.
- [80] L. T. Biegler and V. M. Zavala, "Large-scale nonlinear programming using ipopt: An integrating framework for enterprise-wide dynamic optimization," *Computers & Chemical Engineering*, vol. 33, no. 3, pp. 575–582, 2009.
- [81] A. D. Ames, S. Coogan, M. Egerstedt, G. Notomista, K. Sreenath, and P. Tabuada, "Control barrier functions: Theory and applications," in *2019 18th European control conference (ECC)*, pp. 3420–3431, IEEE, 2019.
- [82] S.-C. Hsu, X. Xu, and A. D. Ames, "Control barrier function based quadratic programs with application to bipedal robotic walking," in *2015 American Control Conference (ACC)*, pp. 4542–4548, IEEE, 2015.
- [83] C. R. Lee and C. T. Farley, "Determinants of the center of mass trajectory in human walking and running.," *The Journal of experimental biology*, vol. 201, no. 21, pp. 2935–2944, 1998.
- [84] M. S. Orendurff, A. D. Segal, G. K. Klute, J. S. Berge, E. S. Rohr, and N. J. Kadel, "The effect of walking speed on center of mass displacement.," *Journal of Rehabilitation Research & Development*, vol. 41, no. 6, 2004.
- [85] L. Tesio and V. Rota, "The motion of body center of mass during walking: a review oriented to clinical applications," *Frontiers in neurology*, p. 999, 2019.
- [86] R. M. Alexander, "Walking and running," *The Mathematical Gazette*, vol. 80, no. 488, pp. 262–266, 1996.
- [87] D. G. Hobbelen and M. Wisse, *Limit cycle walking*. Citeseer, 2007.
- [88] J. W. Grizzle, J. Hurst, B. Morris, H.-W. Park, and K. Sreenath, "Mabel, a new robotic bipedal walker and runner," in *2009 American Control Conference*, pp. 2030–2036, IEEE, 2009.
- [89] J. Reher, *Dynamic Bipedal Locomotion: From Hybrid Zero Dynamics to Control Lyapunov Functions via Experimentally Realizable Methods*. PhD thesis, California Institute of Technology, 2021.
- [90] B. Stellato, G. Banjac, P. Goulart, A. Bemporad, and S. Boyd, "Osqp: An operator splitting solver for quadratic programs," *Mathematical Programming Computation*, vol. 12, no. 4, pp. 637–672, 2020.
- [91] E. Todorov, T. Erez, and Y. Tassa, "Mujoco: A physics engine for model-based control," in *2012 IEEE/RSJ international conference on intelligent robots and systems*, pp. 5026–5033, IEEE, 2012.
- [92] R. Jafari, L. L. Flynn, A. Hellum, and R. Mukherjee, "Energy-conserving gaits for point-foot planar bipeds: A five-dof case study," in *Dynamic Systems and Control Conference*, vol. 56123, p. V001T10A001, American Society of Mechanical Engineers, 2013.
- [93] E. Cousineau and A. D. Ames, "Realizing underactuated bipedal walking with torque controllers via the ideal model resolved motion method," in *2015 IEEE International Conference on Robotics and Automation (ICRA)*, pp. 5747–5753, IEEE, 2015.
- [94] J. Verhagen, "Iros 2022: Reflex inspired compensation on planned and unplanned downsteps." <https://youtu.be/sZljPB5ChfQ>, 2022.